Electrochemical Energy Reviews (2024) 7:34
https://doi.org/10.1007/s41918-024-00234-9

REVIEW ARTICLE

The Origin, Characterization, and Precise Design and Regulation of Diverse Hard Carbon Structures for Targeted Applications in Lithium-/Sodium-/Potassium-Ion Batteries

Junjie Liu[1] · Ling Huang[1] · Huiqun Wang[1] · Liyuan Sha[1] · Miao Liu[1] · Zhefei Sun[1] · Jiawei Gu[1] · Haodong Liu[3] · Jinbao Zhao[1] · Qiaobao Zhang[1,2,4] · Li Zhang[1]

Received: 27 May 2024 / Revised: 24 July 2024 / Accepted: 22 September 2024

Abstract

Hard carbon, a prominent member of carbonaceous materials, shows immense potential as a high-performance anode for energy storage in batteries, attracting significant attention. Its structural diversity offers superior performance and high tunability, making it ideal for use as an anode in lithium-ion batteries, sodium-ion batteries, and potassium-ion batteries. To develop higher-performance hard carbon anode materials, extensive research has been conducted to understand the storage mechanisms of alkali metal ions in hard carbon. Building on this foundation, this paper provides an in-depth review of the relationship between the structure of hard carbon and its electrochemical properties with alkali metal ions. It emphasizes the structural design and characterization of hard carbon, the storage mechanisms of alkali metal ions, and key strategies for structural modulation. Additionally, it offers a forward-looking perspective on the future potential of hard carbon. This review aims to provide a comprehensive overview of the current state of hard carbon anodes in battery research and highlights the promising future of this rapidly evolving field in advancing the development of next-generation alkali metal-ion batteries.

Keywords Hard carbon · Alkali metal ion batteries · Structure design strategy · Electrochemical energy storage · Storage mechanism

1 Introduction

Over the years, the structural investigation of carbon materials has become a highly scrutinized field of study. It is widely recognized that carbon materials synthesized through pyrolysis primarily fall into two major categories: graphitizable carbon, also known as soft carbon, and non-graphitizable carbon [1, 2], commonly referred to as hard carbon. This fundamental classification is rooted in the pioneering research conducted by Rosalind Franklin on carbon materials. She undertook extensive studies of coal's structure, focusing on crucial aspects, such as density and porosity [3]. Using X-ray diffraction (XRD) techniques [4], Franklin meticulously analyzed the structural changes in carbon during the graphitization process at temperatures reaching up to 3000 °C. Her exceptional contributions have greatly advanced our understanding of the structural properties of carbon materials. Hard carbon is characterized by features, such as short-range order, non-graphitizability, porosity, and amorphousness [5]. Depending on its application, hard carbon may be referred to as amorphous carbon, non-graphitizable carbon, or disordered carbon [6]. While these terms may not precisely define the structure of hard carbon, they collectively capture the structural diversity inherent in this type of carbon material.

✉ Qiaobao Zhang
zhangqiaobao@xmu.edu.cn

✉ Li Zhang
zhangli81@xmu.edu.cn

[1] State Key Laboratory of Physical Chemistry of Solid Surfaces, College of Chemistry and Chemical Engineering, College of Materials, Tan Kah Kee Innovation Laboratory, Collaborative Innovation Center of Chemistry for Energy Materials (iChEM), Xiamen University, Xiamen 361005, Fujian, China

[2] Longmen Laboratory, Luoyang 471023, Henan, China

[3] Center for Memory and Recording Research Building, UC San Diego, La Jolla, CA 92093, USA

[4] Shenzhen Research Institute of Xiamen University, Shenzhen 518000, Guangdong, China

Hard carbon, with its diverse microstructures, is crucial in various applications, especially in alkali metal ion storage, where its structural benefits are becoming increasingly recognized (Fig. 1). Research into hard carbon for energy storage in lithium-ion batteries (LIBs) began in the 1970s [7–9], driven by the quest for optimal anode materials. Although graphite has since become the predominant anode material in LIBs [10, 11], hard carbon has retained its relevance due to its versatile microstructural properties, which enable significant structural tunability. As LIBs technology has evolved and research into hard carbon has advanced, this material has demonstrated remarkable cycle performance, improved low-temperature functionality, and rapid charging capability [5, 12]. These exceptional attributes have fueled extensive global research, underscoring hard carbon's growing prominence in energy storage solutions.

The unique microstructure of hard carbon significantly enhances its electrochemical performance in Na^+ storage [2, 13]. Early research into the interaction between hard carbon and Na^+ emerged from studies on carbon anodes used in aluminum smelting [14]. Subsequent investigations revealed that the complex structure of hard carbon enables it to achieve a sodium storage capacity notably higher than that of graphite [15]. As a result, hard carbon has gained attention for potential applications in sodium-ion batteries (SIBs) [16]. Notably, in 1996, Dubois and colleagues were pioneers in reporting the intercalation behavior of hard carbon derived from poly(para-phenylene) for both Li^+ and Na^+ storage [17]. Subsequently, Dahn and his team made a pivotal discovery, demonstrating that hard carbon derived from glucose could achieve a reversible Na^+ storage capacity of up to 300 mAh g^{-1}. This breakthrough significantly advanced the development of SIBs [18]. In recent years, hard carbon has emerged as one of the most promising anode materials for potential commercial applications in SIBs [19]. As SIB technology has progressed, there has been a notable increase in both research and review articles focused on the sodium storage capabilities of hard carbon [20–24].

Additionally, due to the physical and chemical similarities between K^+ and Li^+ or Na^+, hard carbon also shows promise for K^+ storage. Initial studies into the performance of carbon anodes for K^+ were limited by the larger ionic size of K^+, leading to concerns that carbon materials might struggle to effectively accommodate K^+ ions [25]. However, a landmark study in 2016 by Jian and colleagues demonstrated the electrochemical intercalation behavior of hard carbon for K^+, revealing a reversible capacity of 262 mAh g^{-1} and notable rate performance [25]. This significant finding garnered substantial interest and spurred further research into the structural design of hard carbon and the mechanisms of K^+ storage [26–28]. The complex microstructure of hard carbon provides new opportunities for K^+ storage, and ongoing research aims to develop advanced hard carbon materials for potassium-ion batteries (PIBs).

Given the above, hard carbon demonstrates exceptional electrochemical performance across LIBs, SIBs, and PIBs. Compared to other electrode materials, hard carbon offers distinct advantages, including lower voltage, higher capacity, lower cost, and excellent fast-charging performance, which have attracted considerable interest. However, due to its diverse structure-performance relationships with different alkali metal ions, precise structural control of hard carbon is essential. In contrast to the relatively simple and ordered structure of graphite, the internal structure of hard

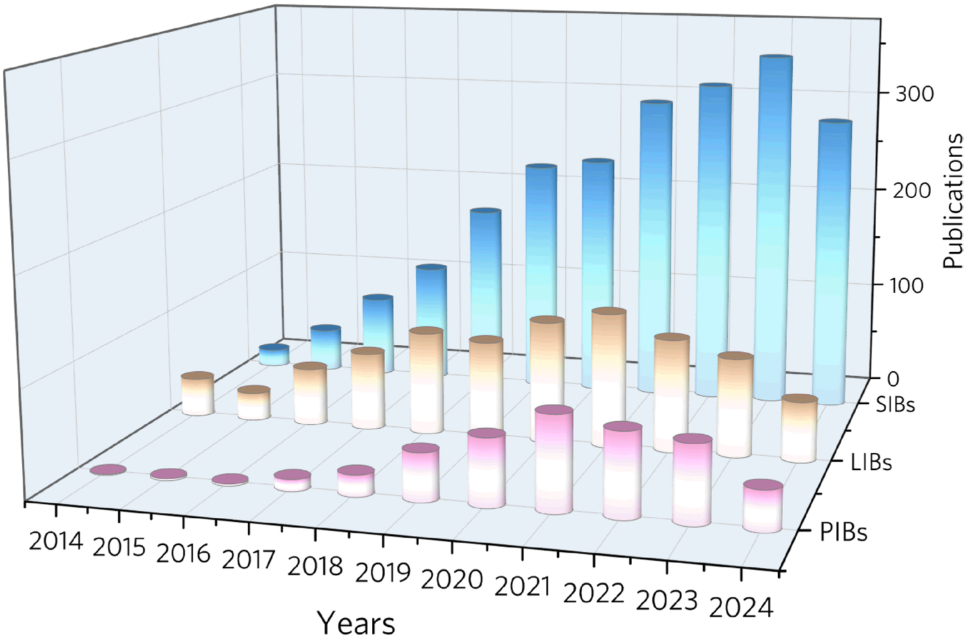

Fig. 1 Number of publications related to hard carbon used in SIBs, LIBs, and PIBs from 2014 to 2024 (data summarized from Web of Science)

carbon is markedly complex and varied. This multifaceted structure significantly enhances hard carbon's exceptional electrochemical performance, with various factors contributing to its high degree of diversity. To elucidate the complex relationship between hard carbon's structure and its performance, extensive research and experiments have been conducted. Despite these efforts, a comprehensive understanding of hard carbon's structure remains a significant challenge [10], constrained by our current knowledge base. Additionally, while numerous studies focus on specific hard carbon materials, there is a notable lack of comprehensive reviews exploring the correlation between hard carbon's structure and its performance.

This review aims to investigate the fundamental principles governing the relationship between hard carbon's structure and its electrochemical performance in alkali metal-ion batteries. We begin with a comprehensive examination of the structural characteristics of hard carbon, detailing the diversity and evolution of its structure under different precursors and synthesis conditions. This review will cover key structural aspects of hard carbon and the methodologies used for its characterization. More importantly, we will evaluate how the structure of hard carbon impacts the storage mechanisms of Li^+, Na^+, K^+, and its influence on overall electrochemical performance. The paper will also examine strategies for controlling key structural parameters of hard carbon and discuss the associated challenges and future prospects for its use as an anode material in alkali metal-ion batteries. By systematically reviewing the correlation between the hard carbon's structure and its electrochemical performance, this overview aims to aid both newcomers and researchers in understanding the complex relationship between hard carbon's structure and its electrochemical behavior. It seeks to offer insights into methods and technologies for modulating hard carbon's structure and identifying effective synthesis strategies, ultimately advancing the practical application of hard carbon research in alkali metal-ion batteries.

2 Structures and Characterization Techniques of Hard Carbon

2.1 The Origin of Hard Carbon Formation and Its Structural Diversity

Understanding the formation process of hard carbon is essential for gaining insights into its diverse structures. Hard carbon is typically produced through the thermal treatment of organic macromolecules or biomass materials [29–31], referred to as "precursors." During this "carbonization" process, the carbon content of the material increases [6]. This process is inherently complex and can be divided into stages, such as pyrolysis, carbonization, and graphitization [32]. Each of these interconnected stages contribute to the structural diversity observed in hard carbon.

The diversity in precursor structures plays a fundamental role in determining the various structures of hard carbon. These precursors, ranging from biomass and resins to fossil-based materials, exhibit significant differences in their post-carbonization structures [33–35]. This variation is primarily influenced by two factors: the spatial structure of the precursor and its chemical composition. First, the spatial structure of the precursor is crucial. Precursor materials are organic macromolecular substances with intricate spatial arrangements. During carbonization, the macromolecular structure of the precursor does not fully collapse. Instead, a portion of the original molecular framework is preserved, leading to similar microscopic structures and morphologies between the precursor and the resulting hard carbon. For instance, the pyrolysis products of walnut shells and natural leaves retain microscopic structures similar to their precursors [36, 37]. Additionally, variations in the chemical composition and content of different precursors lead to diverse structures in the final pyrolysis products [38]. Precursors are typically mixtures of organic macromolecules, and even a single precursor often contains molecules with varying molecular weights and chemical formulas [39]. Moreover, the differences in chemical composition and content among precursors significantly contribute to the structural diversity observed in hard carbon.

The intricate nature of precursors, combined with the complex thermal processing conditions and methodologies, significantly enhances the structural complexity of hard carbons. The transition through the phases of precursor pyrolysis and carbonization exhibits considerable variability. Pyrolysis generally occurs at temperatures below 1000 °C [6]. As previously noted, the structures formed post-pyrolysis are influenced by various chemical constituents, leading to diverse reaction pathways. The pyrolysis stage involves multiple concurrent reactions, resulting in distinct pyrolysis pathways for various precursors [40]. Moreover, even identical chemical components do not undergo a singular pyrolysis reaction. In the pyrolysis of organic compounds, numerous reactions often occur simultaneously, and variations in reaction conditions can alter the predominant reaction. For instance, starch undergoes different principal reactions at various temperatures during this pyrolysis [41]. This process is also characterized by the emission of small molecular gases, such as H_2O, CO_2 and N_2 [42, 43]. The generation rate and dispersion pathways of these gases further impact the spatial architecture of hard carbon materials [6]. Consequently, the pyrolysis of precursors is a complex, multifactorial process. Research by Jeff Dahn and colleagues supports this notion, demonstrating that variations in pyrolysis conditions, such as the heating rate and gas flow rate, significantly influence the final structure of hard carbon [44]. The carbonization process, which typically occurs at temperatures above 1000 °C, involves a range of simultaneous reactions, including dehydrogenation, condensation, hydrogen transfer, and isomerization [6, 42]. Through these reactions, carbon atoms rearrange, leading to the formation of expanded carbon layers and the development of rigid, cross-linked structures within the hard carbon. However, this recombination does not result in a perfect graphene structure, instead producing numerous defects, micropores, and residual oxygen functional groups [45, 46] These imperfections contribute to the hard carbon structure. Additionally, under certain conditions, the process of precursor pyrolysis and carbonization can occur concurrently, with each process influencing the other, thereby further complicating the structure of the carbon material.

Hard carbon's structural complexity is attributed to its characterization as a "carbon alloy" [47], which includes pseudo-graphitic microdomains and amorphous carbon. The presence of C–O–C bonds and cross-linked structures inhibits the transition to a fluid phase at high temperatures [5, 48], resulting in a disordered, swirled structure. During graphitization, defects within the carbon layers decrease, and local layers rearrange to form graphite microdomains. These microdomains, which vary in size and distribution, persist in a randomly stacked, turbostratic arrangement [1]. In summary, the diversity in hard carbon structures arises from the variety of precursors and the intricate thermal processes involved in its formation. This rich structure variety contributes to hard carbon's unique properties and makes it a valuable material for various applications (Fig. 2).

2.2 Hard Carbon Microstructures Trigger Complex Alkali Metal Ion Storage Mechanisms

The structural diversity of hard carbon is most apparent in its complex carbon layer arrangement. During the carbonization process, as heteroatoms are expelled and carbon atoms rearrange, a broad network of carbon predominantly comprises sp^2-hybridized carbon atoms. Macroscopically, this work appears as discrete, profiled carbon sheets, commonly referred to as graphene sheets [6]. On these sheets, carbon atoms are interconnected through sp^2 bridging bonds and sp^3 diamond bonds, leading to various structural formations, including pentagons, heptagons, hexagons, triangles, edge sites, and methyl sites (Fig. 3a) [49]. The six-membered ring network, predominantly composed of sp^2-hybridized carbon, represents the ideal structure of graphene sheets and is the most prevalent. Deviations from this ideal structure are classified as defects [50]. These defects can be categorized into intrinsic and extrinsic types. Intrinsic defects include vacancies, voids, and edges on nanosheets, which are mainly characterized by dangling bonds and sp^3-hybridized carbon [20] This category also encompasses formations, such as pentagons, hexagons, heptagons, and other non-hexagonal structures. In contrast, extrinsic defects primarily involve heteroatoms and oxygen functional groups, often found at vacancies and edges. Notably, some defects play a distinctive role in the structure of hard carbon. For example, Stone–Wales defects prevent graphene sheets from achieving a fully flat configuration, leading to a profiled state and subsequent rearrangement of carbon layers. Additionally, these graphene sheets are not isolated; they exhibit complex properties related to their scale and orientation. The size of graphene sheets in hard carbon ranges from 5 to 500 nm, displaying diverse orientations and appearing isotropic on a larger scale [5]. These sheets are interconnected by sp^3-hybridized carbon bonds or "bridges," which are crucial for anchoring the sheets, including wrinkles and folds, and impeding the graphitization process [48]. The abundant free graphene sheets in hard carbon provide an exceptionally high specific surface area, which enhances the pseudocapacitive adsorption of alkali metal ions [51]. Additionally, the numerous defects on the graphene sheets, such as heteroatoms, vacancies, and varied oxygen functional groups, further augment the adsorption capacity for alkali metal ions (Fig. 3 b–e) [52]. Consequently, hard carbon with a significant proportion of free graphene sheets often exhibits excellent rate performance and high-capacity. However, the strong binding energies and diffusion barriers associated with these defects present challenges in releasing the bound ions, leading to a considerable amount of irreversible

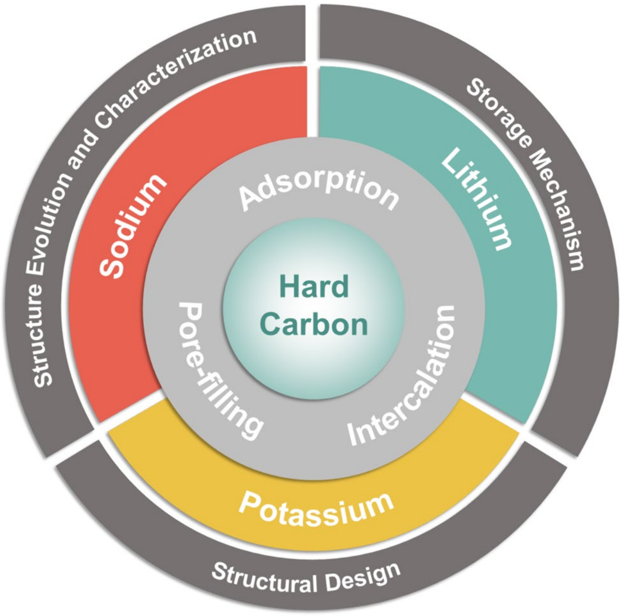

Fig. 2 The overview of what this review covers

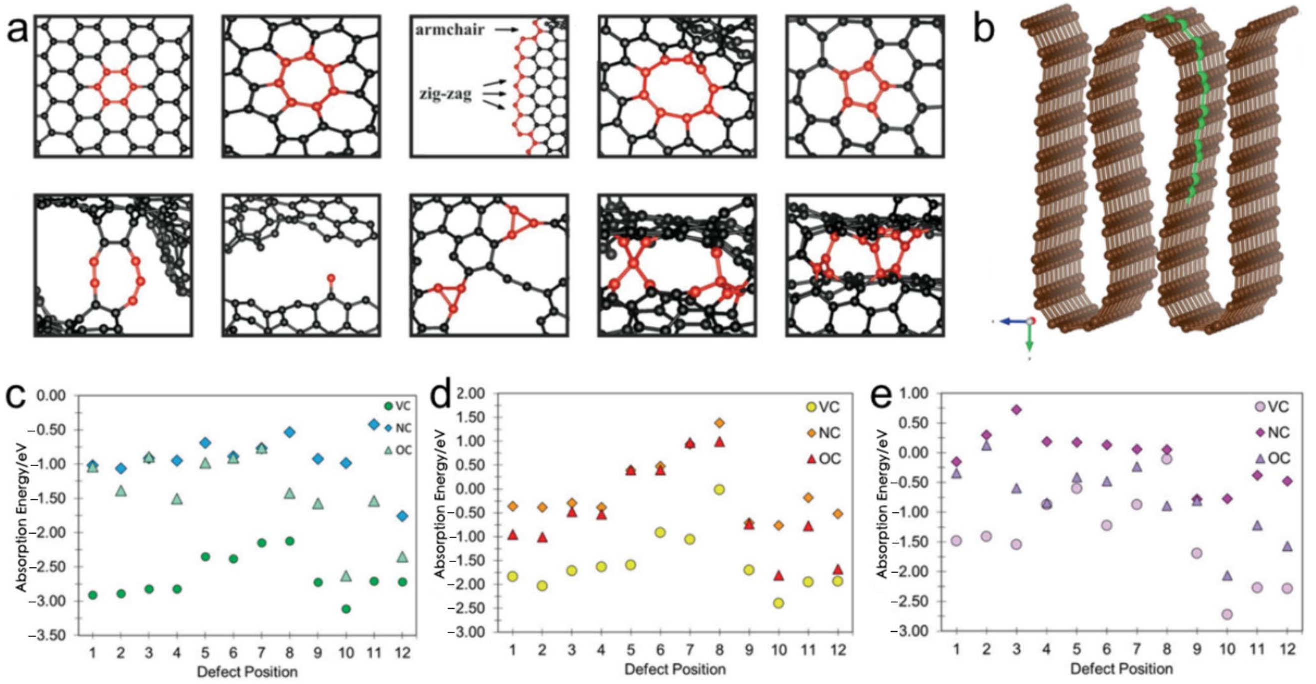

Fig. 3 **a** Schematics representation of key structural motifs in HC: hexagonal rings, 7-membered rings, edge sites, pores (≈3.8 Å diameter shown), 5-membered ring, methylene sites, methyl sites, 3-membered rings, sp^3 diamond bonds, and sp^2 bridging bonds. Reprinted with permission from Ref. [49]. Copyright © 2022, Wiley-VCH GmbH. **b** Simulation cell showing the spatial arrangement, with brown spheres representing carbon atoms and green spheres indicating carbon atoms at the general defect positions. The red arrow denotes the *x*-direction, green the *y*-direction, and blue the *z*-direction. Metal adsorption energies for **c** Li, **d** Na, and **e** K in the VC, NC, and OC defect systems. Reprinted with permission from Ref. [52]. Copyright © 2021, Wiley-VCH GmbH

capacity during the initial cycle. This phenomenon contributes to lower initial coulombic efficiency (ICE) and a higher average potential in hard carbon [50, 53–55].

Due to van der Waals forces, some graphene layers within hard carbon tend to stack at high temperatures, forming, forming localized nanodomains known as quasi-graphite microcrystals or pseudo-graphitic microdomains [6, 56]. This concept originates from the "house of cards" model proposed by Dahn and colleagues, which describes hard carbon as consisting of pseudo-graphitic microdomains (stacked graphene layers in a pseudo-graphitic arrangement with sp^2 hybridization) and amorphous regions (including edges and defects in graphene layers with sp^3 hybridization) [57]. These pseudo-graphitic microdomains display crystalline characteristics and a certain degree of anisotropy, making them resemble crystalline domains. During the formation of these pseudo-graphitic microdomains, free graphene layers within hard carbon are consumed, altering the balance between crystalline and amorphous regions. Unlike graphite crystals, pseudo-graphitic microdomains are generally smaller, exhibiting short-range order but with random orientation on a larger scale [18]. Additionally, their stacking order is less regular than in graphite due to the profiled nature of graphene layers, leading to what is known as imperfect stacking. This imperfect stacking creates larger interlayer spacing (d(002)), which is crucial for alkali metal ions storage. Larger interlayer spacing facilitates superior ion transport kinetics, especially improving the electrochemical performance under low temperatures and under high-rate conditions. The interlayer spacing also significantly impacts the storage efficiency for specific alkali metal ions [58]. For sodium ions, smaller interlayer spacing is generally less favorable for insertion, with optimal spacing for sodium storage typically between 3.7 and 4.2 Å [59, 60]. Lithium and potassium ions, which face fewer energy barriers, can be stored effectively in spacings above 3.5 Å [61]. Furthermore, as the temperature increases, the size of pseudo-graphitic microdomains grows. Relevant metrics used to describe these microdomains include the coherent length along the basal plane (L_a) and the coherent length along the stacking direction (L_c) [20, 50]. Research indicates that below a carbonization temperature of 1500 °C, growth along the *a*-axis is more energetically favorable than along the *c*-axis [20]. The presence of pseudo-graphitic microdomains facilitates intercalation reactions of alkali metal ions, providing numerous active sites for such processes. Typically, hard carbon contains both free graphene layers and stacked pseudo-graphitic microdomains, offering both adsorption and intercalation sites. This dual mechanism in hard carbon opens up broader possibilities and more nuanced control for alkali metal ion storage.

Despite local stacking, the orientation of pseudo-graphitic microdomains within hard carbon remains largely random on a broader spatial scale [7]. These microcrystals merge to form a complex porous structure, with the porous regions predominantly composed of pseudo-graphitic microdomains often referred to as having a turbostratic structure [48]. This extensive porous structure is advantageous for hard carbon, as it typically exhibits minimal volume expansion during alkali metal ion storage, a critical factor contributing to the material's commendable cycling stability. The porous structure of carbon materials has been extensively investigated, generally characterized by micropores and mesopores with diameters of less than 2.0 nm and up to 50.0 nm, respectively. In the context of alkali metal-ion batteries, ultra-micropores, averaging less than 1.0 nm in diameter, are essential for enhancing hard carbon's electrochemical capacity [6]. These ultra-micropores, featuring a distinctive closed pore architecture, are integral to hard carbon's structure (Fig. 4a) [62]. Hard carbon pore structures are differentiated into closed and open pores. Open pores, frequently highlighted in carbon material research, have larger openings that allow gases such as N_2 and CO_2 to enter [20, 42]. These pores increase the interface area

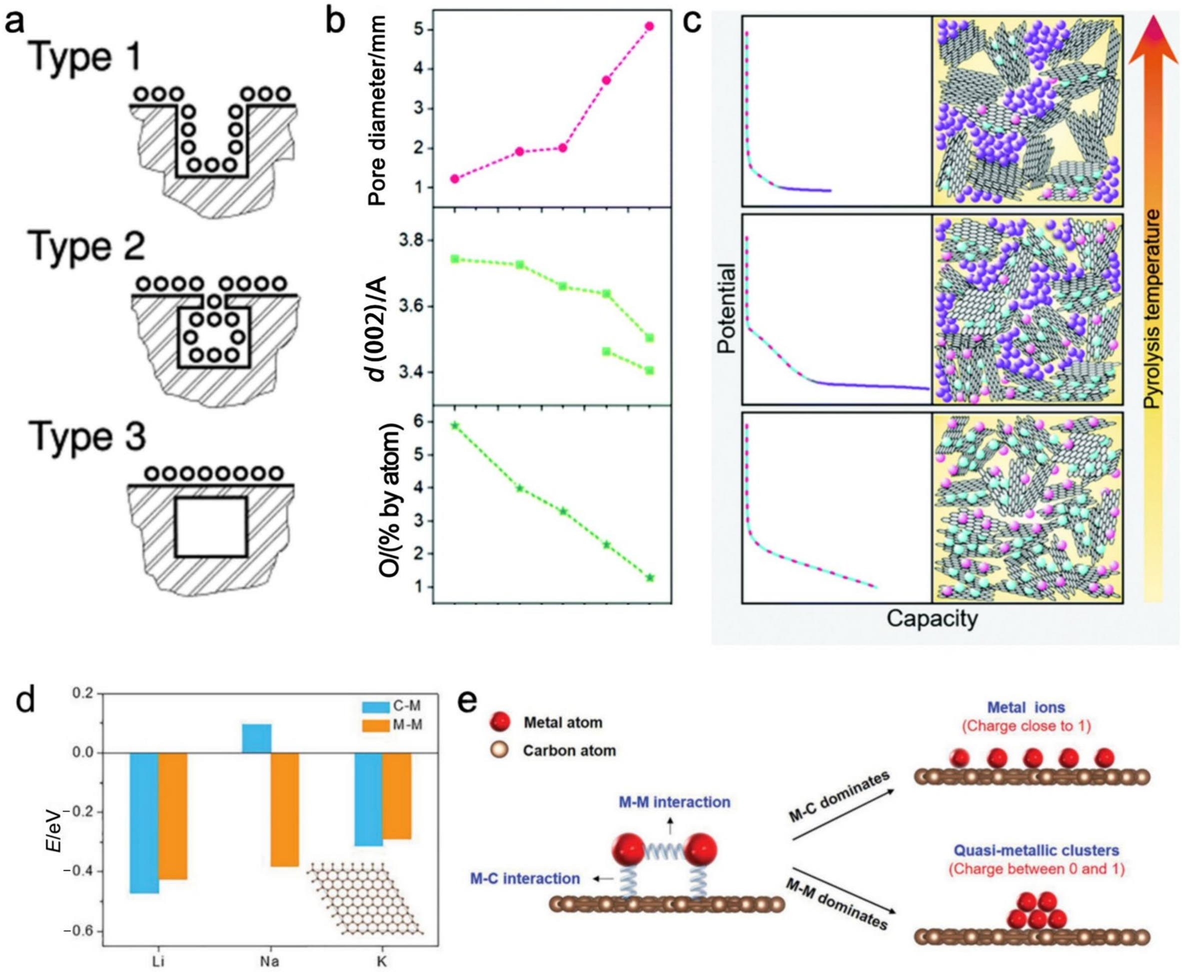

Fig. 4 **a** Model of micropore closure depicting open micropores (Type 1), partially closed micropores (Type 2) and fully closed micropores (Type 3). Reprinted with permission from Ref. [62]. Copyright © 1999, Elsevier. **b** Summary of the structural evolution of hard carbons with increasing pyrolysis temperature (lines are a guide for the eye only). **c** Schematic illustration of the proposed sodium storage mechanism. Note that stack thickness and plane size are not to scale, and defects and curvature are not explicitly shown. Reprinted with permission from Ref. [63]. Copyright © 2020, Royal Society of Chemistry. **d** M-C and M-M interaction of alkali metal atoms on the graphene nanosheet (C and M correspond to carbon and the alkali metal atom, respectively). **e** Schematic illustration of how the M-M and M-C interactions determine alkali metal storage states on the carbon layer. Metal and carbon atoms are drawn as red and brown spheres, respectively. The springs between the alkali metal and carbon atoms represent M-C interaction, while the springs between the metal and metal atoms represent M-M interaction. Reprinted with permission from Ref. [64]. Copyright © 2023, Wiley-VCH GmbH

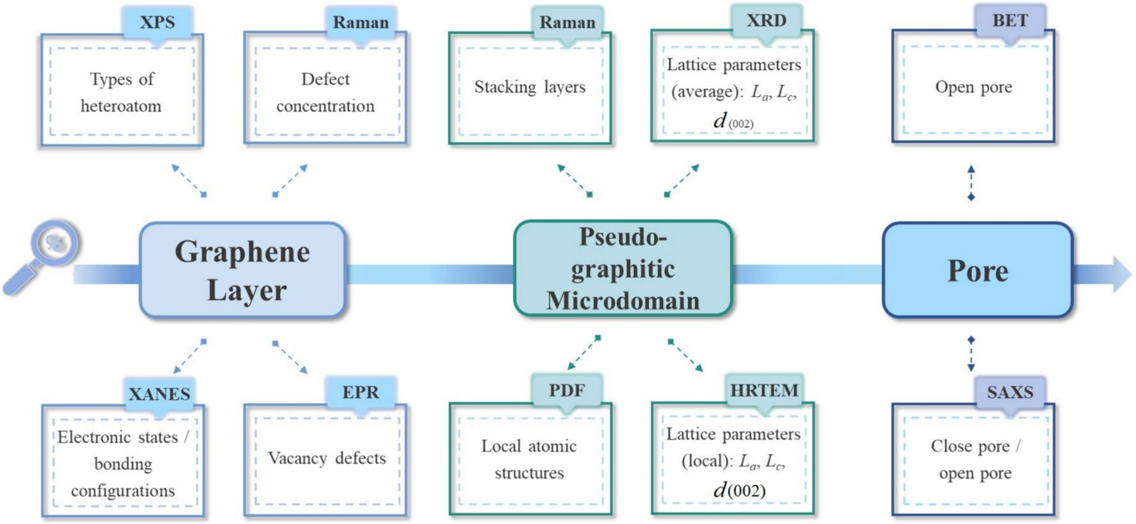

Fig. 5 Characterization techniques to analyze structural information of hard carbon

between hard carbon and the electrolyte, thereby playing a crucial role in the material's functionality. However, electrolyte decomposition on the hard carbon surface can lead to the formation of a solid electrolyte interface film, which results in irreversible capacity loss. Thus, the specific surface area of open pores is a vital determinant of the initial ICE of hard carbon [50]. Contrastingly, closed pores, characterized by their diminutive openings, impede the entry of gas molecules and require metal ions to penetrate the interior through solid-state diffusion.

Additionally, the pores in hard carbon can transition from open to closed states under certain conditions. During the precursor carbonization process, the decomposition of organic polymers and the gas evolution result in numerous open pores [5, 65]. These pores gradually close at elevated temperatures, transitioning into closed pores. The presence of defects within the carbon material plays a crucial role in this process, as it affects the closure of open pores at high temperatures. If defect content is insufficient, open pores may fail to self-heal [66–69]. As temperatures continue to increase, the evolution of graphene layers and pseudo-graphitic microdomain structures leads to the formation, growth, and merging of new closed pores (Fig. 4b). These closed pores in hard carbon are acknowledged as potential sites for alkali metal ion storage (Fig. 4c [63]. The walls of these pores serve as adsorption sites, and recent studies indicate the possibility of storing alkali metal ions in the form of quasi-metallic clusters within these pores (Fig. 4d, e) [64]. This utilization of pore size significantly enhances the theoretical capacity for alkali metal ion storage in hard carbon. Notably, different alkali metal ions exhibit varying interactions with these pores, requiring specific pore diameters for optimal storage [70]. Therefore, optimizing the pore diameter and quantity in hard carbon is essential for maximizing its contribution to overall efficiency and capacity in alkali metal-ion batteries.

In conclusion, the intricate microstructures of hard carbon lead to multiple alkali metal ion storage mechanisms coexisting within the material. This complexity allows for extensive modulation and optimization of the performance of hard carbon, underscoring its potential as a versatile and efficient material for energy storage applications.

2.3 Characterization Technologies of Hard Carbon

The microstructure of hard carbon is pivotal to its electrochemical performance, and utilizing advanced characterization techniques facilitates a deeper and more intuitive understanding of this structure. Within the complex architecture of hard carbon, key structural structures, such as graphene layers, quasi-graphite microcrystals, and pores, play a significant role in determining its electrochemical efficiency [20]. This section focuses on introducing and elucidating the characterization techniques specifically designed to analyze these three critical structural elements (Fig. 5).

2.3.1 Graphene Layers

The analysis of graphene layers within hard carbon focuses on the characterization of defects and crystallinity. Raman spectroscopy, a widely used technique in this field, effectively distinguishes the hybridization states of carbon atoms in hard carbon by analyzing the sp^2 and sp^3 hybridizations, thereby determining the concentration of defects within graphene layers. Figure 6a and b shows different Raman spectra of carbon-based and graphene-based materials [71]. In the

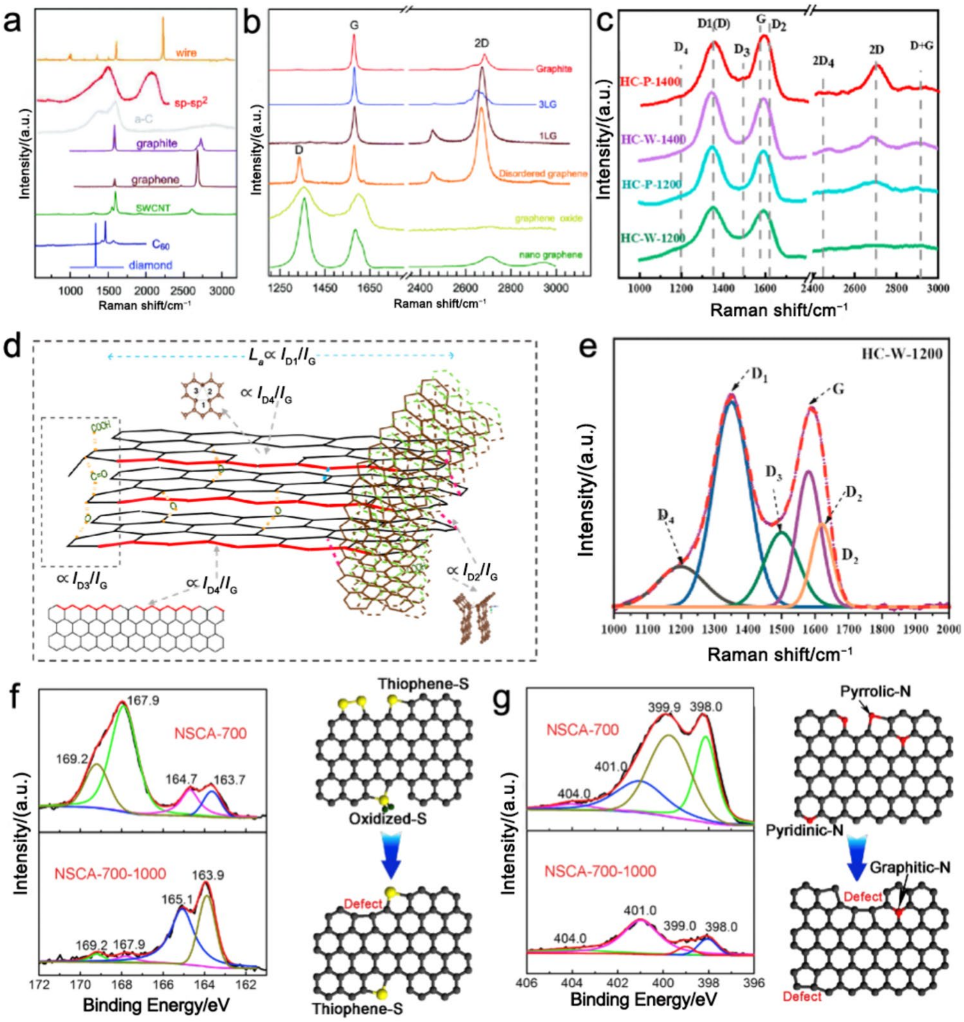

Fig. 6 **a** Typical Raman spectra of carbon-based materials and nanostructures. **b** Raman spectra of graphene-based materials. Reprinted with permission from Ref. [71]. Copyright © 2018, Royal Society of Chemistry. **c** Raman spectra of hard carbon at different temperatures. **d** Schematic diagram illustrating the relationship between the intensity ratios of the D-band and the G-band. **e** Proposed spectral deconvolution. Reprinted with permission from Ref. [72]. Copyright © 2021, American Chemical Society. **f** XPS images of S-doped defective sites in different forms. **g** XPS images of N-doped defective sites in different forms. Reprinted with permission from Ref. [73]. Copyright © 2018, Elsevier

Raman spectrum of hard carbon, the D-band appears around 1350 cm^{-1} and the G-band around 1580 cm^{-1} (Fig. 6c) [72]. The D-band is indicative of the stretching vibrations of sp^3 carbon atoms, while the G-band corresponds to the vibrations of sp^2 carbon atoms and π electrons. The ratio of the intensities of these bands, denoted as I_D/I_G, is a commonly used metric to assess the concentration of defects in hard carbon, with a lower I_D/I_G ratio suggesting a reduced concentration of defects. Further deconvolution and fitting of the D-band can yield more precise insights into sp^3 hybridization. This band can be subdivided into D$_1$, D$_2$, D$_3$, and D$_4$ components, allowing for the separation and identification of specific sp^3 hybridization information (Fig. 6d, e) [72]. The D$_1$ and D$_2$ bands correspond to the vibrational modes of microcrystalline graphite and disordered graphite lattices, respectively. The D$_3$ band is associated with significant amounts of amorphous carbon, while the D$_4$ band is linked to terminal groups of C–C bonds or, more broadly, to adsorbed molecules or molecular fragments. Analyzing the D$_3$ and D$_4$ bands provides independent insights into sp^3 hybridized carbon.

Additionally, X-ray photoelectron spectroscopy (XPS) serves as a crucial surface analysis technique for determining the chemical composition, oxidation states, and molecular structures on a material's surface. Widely applied in characterizing defects in hard carbon, XPS enables both qualitative and quantitative analyses of heteroatoms like N, O, and S, revealing the types and concentrations of defects present (Fig. 6f, g) [73]. Further, the analysis of the C spectrum via XPS can reveal pertinent details about C–C and C = C bonds. Comparing the peak areas of these bonds offers insights into the proportions of sp^2 and sp^3 carbon, allowing for an assessment of defect concentrations in hard carbon. Emerging technologies, such as X-ray absorption spectroscopy (XAS) and electron paramagnetic resonance (EPR), are also becoming crucial for detecting and analyzing edges and vacancies in graphene layers. These technologies offer detailed insights into deviations from the ideal hexagonal carbon network and the complexities of π electron structures. X-ray Absorption Near-Edge Spectroscopy (XANES), a subset of XAS, utilizes absorption peak positions and intensities to explore the electronic states and bonding configurations of carbon atoms, uncovering subtle variations in the electronic structure of carbon atoms and providing a deeper understanding of the nature of defects and their impact on the material's properties [73, 74]. Conversely, EPR, known for its sensitivity to unpaired electron states, excels at detecting vacancy defects in carbon materials [75]. The technique measures the magnetic fields at which electrons in unpaired states resonate, providing information about the nature and density of these defects. Changes in EPR peak intensity, particularly when tested across equivalent sample volumes, offer a reliable metric for assessing variations in vacancy concentrations within carbon materials[76]. Recent studies have also explored the relationship between EPR signals and the capacity of hard carbon, demonstrating that EPR can predict the capacity of hard carbon and the extent of charge stored in both sloping and plateau regions during constant current testing [77, 78]. The integration of these advanced spectroscopic methods into the analysis of hard carbon structures significantly enhances our understanding of its microstructure, particularly in terms of defect concentrations and electron configurations, thus facilitating the tailoring of hard carbon materials for specific applications, especially in fields that require precise control over material properties.

2.3.2 Pseudo-Graphitic Microdomains

XRD is a primary tool for acquiring information about pseudo-graphitic microdomains in hard carbon. Typical XRD patterns of hard carbon feature prominent peaks, such as (002) and (100) (Fig. 7a) [79]. Further analysis of these interlayer (002) and in-plane (100) diffraction peaks sheds light on the layered structures and microdomain architecture. Commonly, by examining the angle of the (002) peak and applying Bragg's equation, the interlayer distance $d(002)$ can be calculated. Due to peak broadening in hard carbon, the average thickness L_c and width L_a of the internal vortex layered nanodomains can be determined by using the Scherrer equation, based on the full width at half maximum of the peak. By employing the formula $L = k\lambda/B\cos\theta$, the number of graphene layers within the domains can be estimated by dividing the domain thickness by the calculated average interlayer spacing [80]. Another method to assess the degree of graphite stacking in hard carbon involves comparing the intensity of the (002) peak to the background intensity (Fig. 7b) [79]. A lower ratio suggests a more disordered

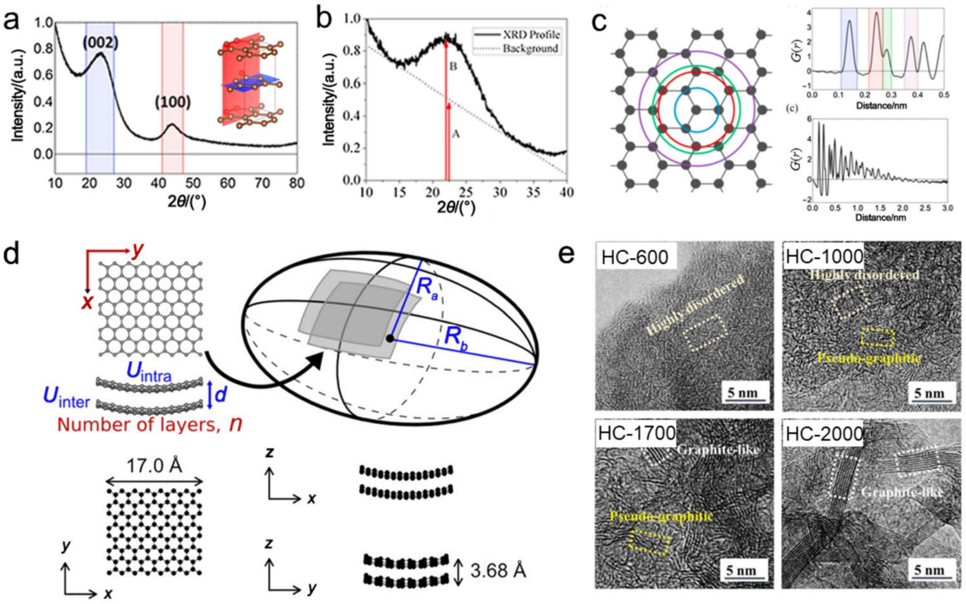

Fig. 7 **a** Typical XRD pattern of a hard carbon sample. The inset shows a schematic of a graphitic structure, with the (002) plane marked in blue and the (100) plane in red. **b** Empirical measure of amorphicity. **c** Schematic illustration of expected coordination lengths on a graphene sheet, accompanied by the simulated PDF measurement of a single graphene sheet, demonstrating both short- and long-range order. Reprinted with permission from Ref. [79]. Copyright © 2018, Elsevier. **d** Schematic diagram of structural parameters extracted from PDF analysis and the actual model obtained after practical analysis. Reprinted with permission from Ref. [82]. Copyright © 2021, American Chemical Society. **e** HRTEM images of biomass-derived hard carbons pyrolyzed at different temperatures. Reprinted with permission from Ref. [83]. Copyright © 2019, Wiley–VCH GmbH

structure, though this method is not widely used currently and is referenced in only a few publications [81].

Pair distribution function (PDF) analysis allows for the investigation of short-to-medium range order in carbon, revealing pertinent local atomic structures (Fig. 7c) [79]. Compared to traditional XRD, PDF offers more detailed information on nearest-neighbor bonding. Employing PDF to analyze the size of crystalline domains and microdomains provides an additional approach to understanding the structural characteristics of hard carbon (Fig. 7d) [82].

Raman spectroscopy also provides valuable insights into pseudo-graphitic microdomains. According to the empirical equation L_a (nm) = $(2.4\times10^{-10})\lambda(I_G/I_D)$, the I_G/I_D ratio offers relevant information about L_a [20, 84]. Additionally, the less frequently mentioned 2D-band, located around 2700 cm^{-1}, reflects graphitization information and is typically associated with the stacking number of graphene layers, making it useful in studying short-to-medium range ordered structures [85]. High-resolution transmission electron microscopy (HRTEM) is a commonly used tool for visualizing the projection morphology of microcrystals (Fig. 7e) [83]. TEM enables direct imaging of lattice parameters, defects, and other structures within the pseudo-graphitic microdomains of hard carbon. Given the heterogeneous internal structure of hard carbon, TEM allows for quantitative, site-specific analysis of its local structure [86]. Recent developments have leveraged HRTEM to analyze lattice fringe lengths, tortuosity, and average curvature [6]. However, due to the relatively small characterization area in TEM, the results obtained may lack representativeness.

In summary, a comprehensive understanding of pseudo-graphitic microdomains in hard carbon comprehensively requires integrating the insights provided by XRD, Raman spectroscopy, and TEM, allowing for a holistic view of these complex structures.

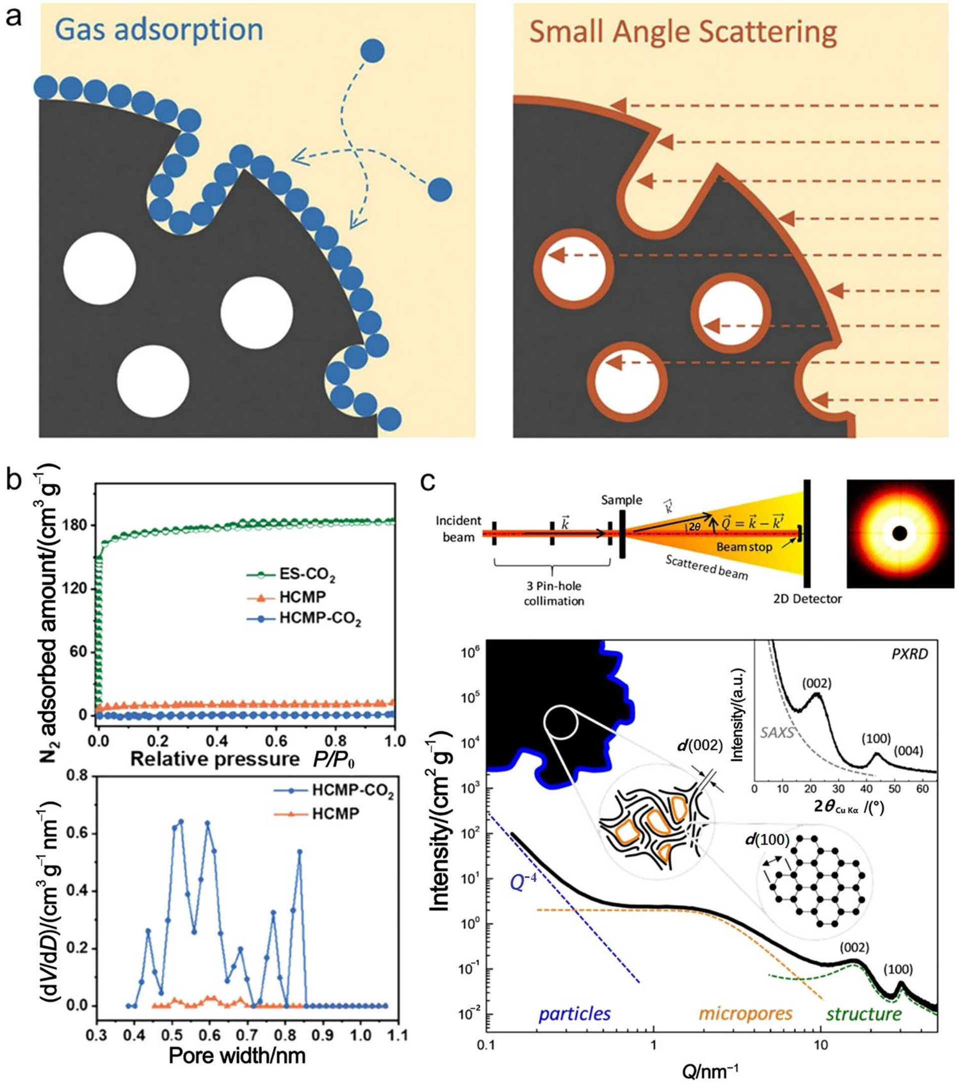

Fig. 8 **a** Schematic representation of gas adsorption and small-angle scattering applied to analyze porosity in carbon materials (dark gray area). Reprinted with permission from Ref. [42]. Copyright © 2018, Wiley-VCH GmbH. **b** N_2 adsorption–desorption isotherms and pore size distribution of ES-CO_2, HCMP and HCMP-CO_2. Reprinted with permission from Ref. [65]. Copyright © 2023, Wiley-VCH GmbH. **c** Top panel: schematic representation of the geometry of the SAXS instrument used for the present study. Bottom panel: typical intensity versus the scattering vector profile on a log–log scale of microporous non-graphitic carbon, along with a schematic drawing of the structural, microstructural and morphological features related to the observed intensity in large, intermediate and low Q ranges. Inset: linear scale representation of the same pattern vs. the scattering angle 2θ as it is usually done for PXRD patterns. Reprinted with permission from Ref. [87]. Copyright © 2018, Elsevier

2.3.3 Open/Closed Pores

Characterizing the porous structure of hard carbon is crucial for understanding its electrochemical properties, particularly in distinguishing between open and closed pores (Fig. 8a) [42]. Open pores, which allow gas molecules to enter, are typically assessed using the Brunauer–Emmett–Teller (BET) gas adsorption–desorption method. This technique involves generating adsorption and desorption profiles of gas molecules on the material's surface, which aids in identifying pore types and determining the specific surface area of the material (Fig. 8b) [65]. Additional modeling provides insights into parameters, such as pore size and volume for open pores. However, the results of this method can vary depending on the gas used for adsorption tests, making BET a tool for relative comparison. Notably, BET is less effective for analyzing closed pores, as gases cannot penetrate the interior of hard carbon.

In contrast, small-angle X-ray scattering (SAXS) offers several advantages for porosity determination in hard carbon. SAXS involves passing a beam of X-rays or neutrons through a sample, where it interacts with atoms or molecules, causing scattering at very small angles (typically less than 10°). X-rays, capable of penetrating materials without causing damage, allow for non-destructive characterization. SAXS is effective in providing topological information from the molecular to the mesoscale, irrespective of the sample's crystallinity. Typical SAXS patterns reveal the relationship between absolute scattering intensity and the scattering vector Q [$Q = (4\pi \sin\theta)/\lambda$] (Fig. 8c) [87]. By combining true density testing with model fitting of scattering profiles, SAXS can accurately depict the complex structure of disordered carbon, extracting quantitative data on pore size, volume, and more. It is important to note that SAXS-derived pore data encompass both closed and open pores, necessitating the subtraction of the closed pore volume from the total to obtain an accurate representation.

While BET is instrumental in assessing open pores in hard carbon, SAXS excels in providing a comprehensive view of both open and closed pores, offering a more thorough understanding of the material's porous architecture. This level of detailed characterization is essential for tailoring hard carbon for specific applications, especially in fields where pore structure is critical to performance. To achieve a complete quantitative evaluation of hard carbon's pore structures, combining SAXS with BET analyses is indispensable.

However, despite these advanced techniques, accurately characterizing the intricate structure of hard carbon remains a formidable challenge. The complexity and disordered nature of hard carbon means that current characterization methods often provide only averaged structural data, and the resolution limitations make it difficult to precisely determine specific aspects, such as the proportions of amorphous versus crystalline regions, local orientations, and precise pore shapes. Moreover, the reliance on model fitting in SAXS and BET analyses introduces potential discrepancies between observed and actual values, highlighting the limitations of existing methods. These challenges underscore the need for ongoing development and refinement of characterization techniques. Enhancing methods will enable a more nuanced and detailed understanding of hard carbon's structure, crucial for tailoring its properties for targeted applications. As such, advancing more sophisticated and accurate characterization technologies remains a priority in the study of hard carbon materials, driving progress on material science and enhancing our ability to harness hard carbon's full potential.

3 Storage Mechanism of Various Alkali Metal Ions in Hard Carbons

The complex structure of hard carbon makes it an exceptionally effective anode material for alkali metal-ion batteries, with extensive applications in this field. Lithium, sodium, and potassium ions, all belonging to the alkali metal ion group, share similar physical and chemical properties, leading to broadly analogous storage behaviors in carbon materials. Nonetheless, differences in ion radius and energy significantly affect the structure-performance relationships, resulting in distinctive electrochemical behaviors.

This section explores the storage behaviors of Li, Na, and K ions in hard carbon anode materials, aiming to unravel the intrinsic connections between these behaviors and the structural characteristics of hard carbon. By conducting thorough investigations into the storage of alkali metal ions in hard carbon, a more comprehensive understanding of their characteristics can be obtained. This knowledge is instrumental in advancing the development of innovative energy storage systems, particularly in sodium-ion and potassium-ion batteries, where optimizing these interactions between ions and hard carbon is essential for optimizing performance and efficiency.

3.1 The Correlation Between Hard Carbon Structure and Li^+ Storage Electrochemistry

The diverse structural features of hard carbon materials result in varying electrochemical performances during the lithium-ion storage. Although significant insights have emerged from ongoing research, a definitive consensus on the lithium storage mechanism within hard carbon has not yet been established. It is broadly accepted that both "intercalation" and "adsorption" mechanisms play major roles in lithium storage; however, the existence of a "filling" mechanism remains a topic of debate. The specific behaviors associated with these mechanisms in hard carbon are still under discussion within the scientific community [57, 88–91]. Despite the challenges in pinpointing the exact mechanisms, understanding the relationship between the structure of hard carbon and Li^+ storage is crucial for elucidating the lithium-ion storage processes in these materials. Such explorations are anticipated to inform the future design and optimization of hard carbon materials, thereby advancing lithium-ion battery technology toward higher performance and reliability.

For synthesizing high-capacity lithium-ion hard carbon, the preparation temperature is a key factor. Typically ranging from 800 to 1300°C, the optimal temperature for synthesizing lithium-ion hard carbon is generally between 1000 and 1100 °C. At these temperatures, hard carbon experiences pyrolysis and partial carbonization, resulting in a low degree of graphitization. This process leads to a hard carbon with numerous free graphene layers, increased hydrogen atoms and defects, smaller particle sizes, higher disorder, and fewer stacking interactions between layers. Additionally, due to the relatively low sintering temperature, many open pores remain unclosed, and closed pores are still forming internally. As a result, this form of hard carbon maintains a high specific surface area, fewer closed pores, and smaller pore sizes, attributes that are key for its performance in lithium-ion storage applications (Table 1).

The intricate and varied surface of hard carbon materials, characterized by numerous free graphene layers, offers a plethora of active sites for adsorption, including both physical and chemical modalities. It is widely recognized that the surfaces and internal graphene layers of hard carbon serve as physical adsorption sites for lithium ions [106], enabling adsorption similar to double-layer capacitors (Fig. 9a) [104]. Moreover, the abundant free graphene fragments within hard carbon provide substantial chemical adsorption sites, facilitating the storage of lithium ions through pseudocapacitive adsorption mechanisms (Fig. 9b) [105]. The capacity achieved through chemical adsorption significantly surpasses that of physical adsorption, making chemical adsorption the predominant process (Fig. 9c) [91]. The presence of oxygen functional groups, albeit limited, at the edges of graphene fragments, enhances adsorption capacity through redox reactions [107]. During lithium ion adsorption, physical adsorption processes are characterized by rapid reaction kinetics (Fig. 9d) [91], which is reflected in the higher diffusion coefficients of hard carbon at elevated voltages. Reactions involving oxygen functional groups demonstrate similar rapid kinetics. Conversely, chemical adsorption shows a marked decrease in diffusion coefficients and occurs just below the potential of physical adsorption. This difference is evident in the characteristic inclined profiles observed in charge–discharge cycles during Li^+ storage. Given the abundance of chemical adsorption

Table 1 Reported high-capacity hard carbon materials for LIBs, including precursors, structures, and relevant electrochemical performances

Precursors	*T*/°C	*d*(002)/nm	*V*/(V vs. Li^+/Li)	*CD*/((mA g^{-1})/(mA cm^{-2}))	*C*/(mAh g^{-1})	References
Potato starch	1000	0.407	0–2.0	CC 0.1 C to 0 V CV 0 V to 3 mA	531	[92]
Sucrose	1100	0.402	0.002–2.0	25 mA g^{-1}	551	[75]
Pitch/$NH_4S_2O_8$	1100	–	0.001–1.3	CC 1 mA cm^{-2} to 0 V CV 0V to 12 h	470	[93]
Mangrove wood	1000	–	0.003–1.5	30 mA g^{-1}	424	[94]
Lignin	800	0.381	0–2.0	0.1 C	550	[95]
Sugar	1050	–	−0.02–3.0	4.65 mA g^{-1}	627	[96]
Pistachio nut shell/ Propionaldehyde	1000	0.381	0.01–1.5	40 mA g^{-1}	404	[97]
Phenolic resin	1100	–	0–2.0	100 mA g^{-1}	420	[98]
Cellulose	1100	0.451	0–2.0	40 mA g^{-1}	397	[99]
Cellulose	1000	0.383	0.005–1.5	18.6 mA g^{-1}	385	[33]
Glucose	1100	–	0–1.5	20 mA g^{-1}	350	[100]
Phenolic-formaldehyde resin	900	–	0.001–1.5	50 mA g^{-1}	550	[101]
Sweet Gum	1000	0.389	0.005–2.5	50 mA g^{-1}	375	[102]
Anthracites	1100	–	0–3.0	CC 30 mA g^{-1} to 0 V CV 0 V to 6 h	370	[103]

T pyrolysis temperature (°C), *d*(002) interlayer spacing (nm), *V* voltage window (V vs. Li^+/Li), *CD* current density ((mA g^{-1})/(mA cm^{-2})), *C* specific capacity (mAh g^{-1}), *CV* constant voltage *CC* constant current. Data are extracted from multiple data sources, and thus are with different significant digits

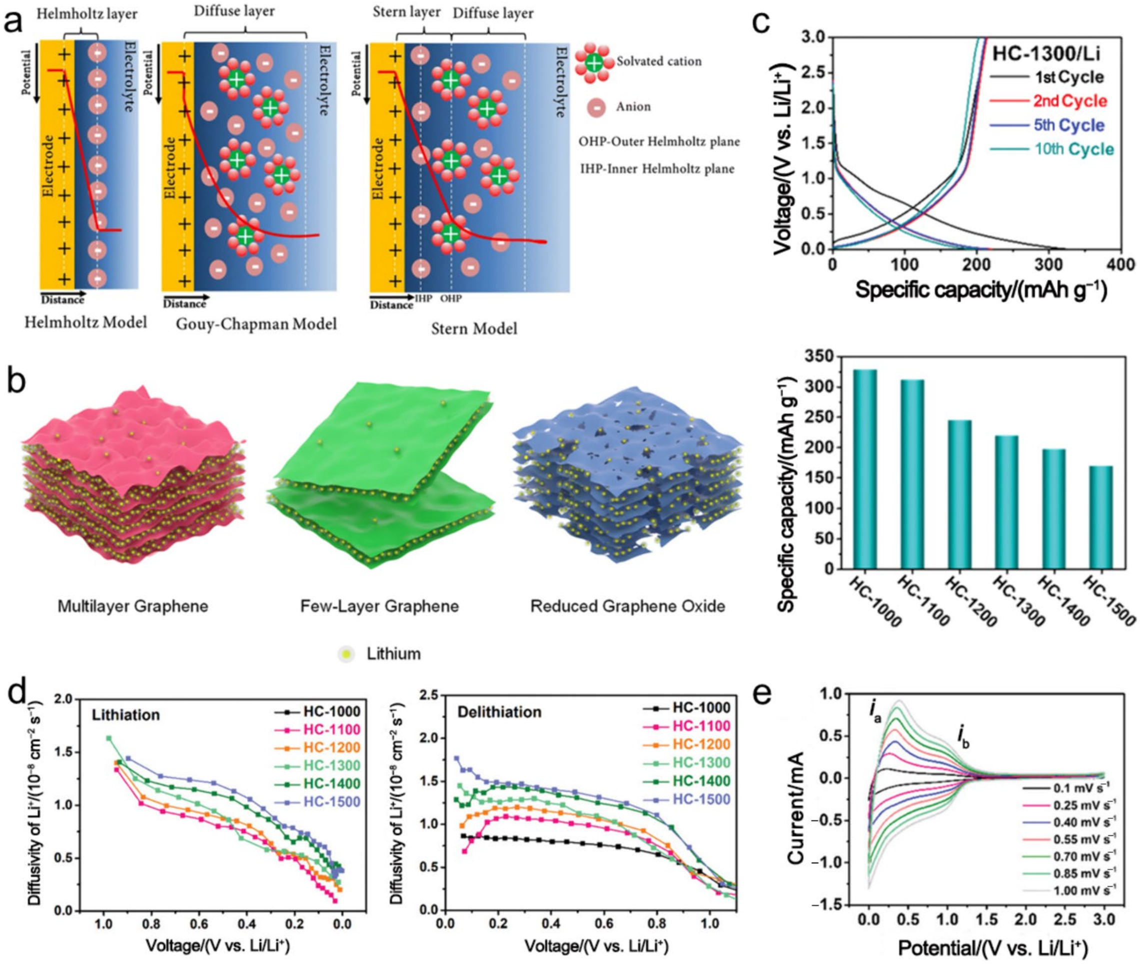

Fig. 9 **a** Diagrams of EDLC structures: Helmholtz model, Gouy–Chapman model and Gouy–Chapman–Stern model. Schematic representation of the charge storage mechanisms in pseudocapacitors. Reprinted with permission from Ref. [104]. Copyright © 2020, Springer Nature. **b** Schematic illustrations of lithiated graphene with different microstructures. Reprinted with permission from Ref. [105]. Copyright © 2022, Elsevier. **c** Discharge–charge profiles of the initial 10 cycles of HC-1300/Li and the capacities of different carbonization temperatures in LIBs. **d** Apparent lithium-ion diffusion coefficients calculated from GITT profiles during the lithiation and delithiation. **e** CV profiles of HC-1300 at scan rates ranging from 0.1 to 1.00 mV s^{-1} in LIBs. Reprinted with permission from Ref. [91]. Copyright © 2018, Wiley-VCH GmbH

sites in hard carbon, this form of adsorption significantly contributes to the overall capacity for lithium-ion storage. Moreover, the excellent kinetic behavior of lithium ions under the adsorption mechanism enhances the magnification and low-temperature performance of hard carbon materials. Therefore, an increase in the contribution of the adsorption mechanism will help improve these properties. However, while the extensive specific surface area and rich internal structure of hard carbon offer numerous adsorption sites, they also lead to increased electrolyte consumption [108]. Research indicates that defects and higher hydrogen content in the graphene layers can cause voltage hysteresis, impacting the ICE of hard carbon [109]. Therefore, it is crucial to carefully manage the defect content and concentration of free graphene layers in hard carbon to maintain an optimal balance. This balance is crucial to maximizing the material's efficacy and efficiency in lithium-ion storage applications.

Further investigations have revealed that the stacking of graphene layers in hard carbon leads to the formation of pseudo-graphitic microdomains, which provides potential sites for Li^+ intercalation [18, 110]. Early studies on intercalation in carbon materials primarily focused on graphite, and due to structural similarities between graphite and hard carbon, insights from graphite intercalation have greatly enhanced our understanding of Li^+ storage in hard carbon. In graphite, Li^+ forms intercalation compounds, such as LiC_6 (Fig. 10a) [111]. The long-range ordered structure and distinct stacking pattern of graphite enable Li^+ to insert in a stepwise manner [112], resulting in a characteristic three-stage pattern in its electrochemical profile. In contrast, hard

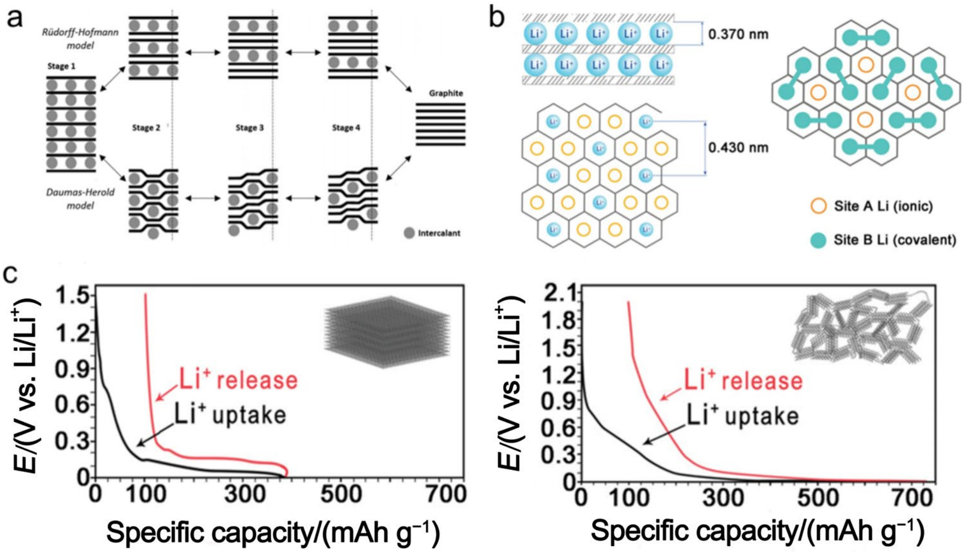

Fig. 10 **a** Illustration of the intercalation of secondary species into the layered graphite structure via the staging mechanism according to Rüdorff-Hofmann (RH) theory (top pathway) and Daumas-Herold theory (bottom pathway). Reprinted with permission from Ref. [111]. Copyright © 2014, Royal Society of Chemistry. **b** Schematic illustration for the coexistence of two types of Li sites in poly(p-phenylene)-based carbons, with Li ions and atoms denoted by empty and solid circles at sites A and B, respectively. Covalent bonds between two Li atoms on site B are shown by bold lines. Reprinted with permission from Ref. [113]. Copyright © 1994, AAAS. **c** Constant current discharge/charge profiles of graphite and hard carbons. Profiles were reprinted with permission from Ref. [114]. Copyright © 1998, Wiley-VCH GmbH

carbon's pseudo-graphitic microdomains exhibit short-range order and less regular stacking, which leads to different electrochemical charge characteristics compared to graphite [5]. Researches have indicated that the strong Li–C interactions in hard carbon results in lithium predominantly existing in an ionic state [64]. It has been also suggested that lithium ions in hard carbon can occupy both ionic and covalent sites on the carbon layers, forming structures such as Li_2^+ and combining with carbon layers as LiC_2 (Fig. 10b) [113], which has a high energy density. The imperfect stacking and larger interlayer spacing in hard carbon facilitate a more continuous intercalation process, typically resulting in a single, inclined profile in the electrochemical data, which contrasts with the characteristic profiles observed in graphite (Fig. 10c) [114].

Compared to adsorption, the intercalation of lithium ions into hard carbon exhibits lower reaction kinetics and a reduced diffusion coefficient due to the narrower interlayer spacing. This results in poor rate performance and lower performance at low temperatures. During lithium intercalation, hard carbon experiences changes in the layered structure of pseudo-graphitic microdomains. Unlike the phase transitions in pseudo-graphitic microdomains, which result in significant peak shifts and new peaks in XRD patterns, the structural changes in hard carbon are relatively subtle. This was demonstrated by Dahn, who used in situ XRD to observe a decrease and subsequent recovery in the intensity of the (002) peak in the XRD spectrum upon lithium ions insertion and removal [14, 18, 57]. Similar findings have been reported in subsequent studies. Additionally, during Li^+ insertion, enhancements in the G-band of the Raman spectrum suggest changes in the electron cloud density and a weakening of C–C bonds in the carbon layers [90]. These research findings provide a comprehensive understanding of the intercalation behavior and mechanisms of hard carbon in Li^+ storage, providing critical insights for optimizing hard carbon materials for LIBs. The intricate nanoscale pore structure within hard carbon plays a crucial role in the storage of Li^+, often in the form of clusters. The pioneering research by Jeff Dahn and colleagues, using BET testing, identified Type I isotherms and hysteresis between adsorption and desorption branches [14], indicating the presence of restricted nanoscale pores within hard carbon. Their work suggested that electron cloud density changes during low-voltage discharge correspond to the insertion of Li^+ into these nanoscale pores. Subsequent research proposed that defects within these pores prompt lithium ions to absorb onto pore walls and fill the pores. Ishida and colleagues further advanced the understanding of this nanoscale pore lithium storage mechanism, utilizing nuclear magnetic resonance (NMR) technology [115], revealing that lithium can exist as clusters within these nanoscale pores, typically during constant voltage discharge (CV) mode [116]. Unlike underpotential deposition, these quasi-metallic lithium clusters comprise both ionic and covalent lithium, forming a cationic network structure, a concept initially introduced in studies on Li_6C [117]. This quasi-metallic lithium storage mechanism enhances the theoretical capacity of hard carbon. Research into lithium clusters suggests that these clusters do not result in lithium dendrite formation [115]. Further investigation indicates that ionic Li gradually transitions to metallic Li upon interaction with the carbon plane, forming Li_2 dimers and planar Li_4 clusters [75]. Due to the small radius of Li^+ and weak Li–Li interactions, the formation of large lithium clusters is constrained [64]. Additionally, the non-uniformity of internal pores in hard carbon can lead to uneven removal of lithium clusters, potentially causing voltage hysteresis and contributing to partial irreversible capacity.

Although a unified consensus on the mechanism of lithium storage in hard carbon remains elusive, exploring the interaction between the structure of hard carbon and Li^+ can illuminate the relationship between Li^+ adsorption, intercalation, and filling behaviors, and the internal structure of hard carbon. By tailoring specific structures within hard carbon, it is possible to enhance the capacity of these processes and regulate their contributions to Li^+ storage. For instance, optimizing the defect structure within hard carbon is crucial for applications requiring fast-charging or low-temperature performance. Furthermore, in order to achieve high energy density in hard carbon, it is crucial to generate more pseudo-graphitic microdomains and minimize pore closure. It is important to note that due to limited understanding of the filling mechanism, a significant portion of pores in hard carbon remains unexplored. As we advance toward the next generation of hard carbon anode materials, focusing on refining the filling behavior while maintaining effective adsorption and intercalation mechanisms will be crucial for improving Li^+ storage performance.

3.2 The Correlation Between Hard Carbon Structure and Na^+ Storage Electrochemistry

The chemical similarities between Na^+ and Li^+ lead to analogous storage mechanisms for SIBs and LIBs when hard carbon is used as the anode material. While findings from LIB research offer valuable insights, significant differences arise due to the larger ionic radius and higher potential of Na^+. These differences mean that not all principles applicable to Li^+ storage are directly transferable to Na^+ systems, leading to distinct storage mechanisms for Na^+ in hard carbon [61]. Typically, the capacity-voltage profile for Na^+ storage in hard carbon shows a sloping region at higher voltages and a plateau at lower voltages. The specific storage mechanism for Na^+ remains a topic of debate, with two major viewpoints: "adsorption-filling" and "adsorption-intercalation/filling" [30, 70, 118, 119]. There is ongoing discussion about whether intercalation occurs in the sloping region or the plateau region [18, 70].

Structurally, the optimal temperature range for synthesizing high-capacity Na^+ hard carbon is higher than that that for Li^+ hard carbon, typically between 1200 and1500 °C. This higher temperature range ensures complete pyrolysis and carbonization while avoiding excessive graphitization. This results in numerous free-standing graphene layers, with a certain degree of defects. These layers are typically larger, more densely stacked, exhibit short-range order, and have reduced interlayer spacing. Consequently, many open pores in hard carbon close up, leading to a reduction in specific surface area and an increase in the number and size of closed pores compared to lithium-ion based hard carbon. In this section, we will focus on the structural aspects of hard carbon to explore potential sodium-ion storage mechanisms and their characterization methods, which are crucial for optimizing hard carbon for sodium-ion storage and advancing SIB technology (Table 2).

The adsorption mechanisms for Na^+ on graphene layers in hard carbon, encompassing both physical and chemical adsorption, are similar to those observed for Li^+. The presence of hydrogen and other heteroatoms (like N, O, S) on the graphene layers enhances the electron density at defect sites, creating favorable bonding sites for Na^+ [50]. The surface of hard carbon also serves as a site for physical adsorption, which augments the storage capacity of Na^+ in the material. Analogous to Li^+, hard carbon materials with a higher ratio of adsorption mechanisms exhibit improved rate and low-temperature performance. Additionally, surface reactions during initial charge–discharge cycles in SIBs can lead to electrolyte decomposition, contributing to the low ICE often observed in hard carbon [139, 140]. Furthermore, the free-standing graphene layers offer abundant active sites for the chemical adsorption of Na^+ [141]. Techniques such as the galvanostatic intermittent titration technique (GITT) and cyclic voltammetry are useful for distinguishing and characterizing the physical and chemical adsorption behaviors of sodium ions [91]. These methods facilitate the calculation of the pseudo-capacitance ratio, offering a more detailed understanding of these processes. During adsorption, defect sites in the carbon material are gradually filled, leading to observable changes in the electron cloud density of the carbon layer. This is reflected as a decrease in the I_D/I_G ratio and a redshift of the G-bond in Raman spectra during discharge [70, 142, 143]. Although Na^+ has a larger radius compared to Li^+ and thus a lower storage capacity, it still contributes significantly to the overall capacity.

The intercalation behavior of Na^+ differs markedly from that of Li^+ and remains a subject of ongoing debate. Some researchers categorize sodium ion intercalation as insertion into pseudo-graphitic domains, while others view it as regular insertion at defects or increased *d*-spacing [63, 70, 144]. Despite these differing perspectives, the fundamental relationship between the pseudo-graphitic microdomain

Table 2 Reported high-capacity hard carbon materials for SIBs, including precursors, structures, and relevant electrochemical performances

Precursors	*T*/°C	*d*(002)/nm	*V*/(V vs. Na^+/Na)	*CD*/(mA g^{-1})	*C*/(mAh g^{-1})	References
Pinecones	1400	0.381	0.001–2.0	30	370	[80]
Borassus flabellifer	1400	0.385	0.001–2.5	20	367	[120]
Maple leaves	1000	–	0.001–2.5	10	358	[37]
Banana peels	1100	0.391	0.001–2.8	50	355	[85]
Lotus stems	1400	0.368	0–3.0	100	350	[121]
Cotton	1300	0.410	0–2.0	30	315	[30]
Corn stalks	1200	0.384	0.01–3.0	50	321	[122]
Mangosteen	1500	0.367	0–2.0	20	330	[123]
Dandelion	1200	0.374	0.001–3.0	50	361	[124]
Corn straw piths	1400	–	0.01–3.0	50	310	[125]
Kelp	1300	0.390	0.01–2.0	25	334	[126]
Coconut endocarp	1100	0.4012	0.01–3.0	50	313	[127]
Wheat starch/Glycerol	1100	0.374	0.001–2.7	30	320	[128]
Walnut	1300	0.370	0.–3.0	25	315	[129]
Camphor wood residues	1300	0.379	0–3.0	20	324	[130]
Reed straw	1300	0.391	0–3.0	25	372	[131]
Rice husk	1300	0.395	0.01–2.0	25	372	[132]
Maple tree	1400	–	0–2.5	30	337	[133]
Wool	1100	0.376	0–2.0	10	303	[134]
Starch	1300	0.398	0.01–3.0	25	487	[65]
Magnesium gluconate/Glucose	1500	0.379	0.002–2.0	25	478	[135]
Zinc gluconate/Glucose	1400	0.377	0.002–2.0	25	418	[136]
DAFR/Zinc acetate	1300	0.408	0.01–2.0	10	546	[24]
MPF	1400	–	0.01–2.5	30	399	[137]
Pitch/Zinc gluconate	1200	3.706	0.01–3.0	30	320	[21]
Pitch	1400	–	0–2.5	30	300	[138]

T pyrolysis temperature (^{o}C), *d*(002) interlayer spacing (nm), *V* voltage window (V vs. Na^+/Na), *CD* current density (mA g^{-1}), *C* specific capacity (mAh g^{-1}). Data are extracted from multiple data sources, and thus are with different significant digits

structure and sodium ion storage remains consistent. Although initial studies considered sodium ion intercalation in graphite as negligible due to the mismatched ion radius and interlayer spacing, further research has shown potential for Na^+ intercalation in hard carbon due to its larger interlayer spacing [15, 145]. Hard carbon is thought to form intercalation compounds like NaC_8, with a theoretical capacity of 279 mAh g^{-1}, primarily reflected in the plateau region of the electrochemical profile [60, 70]. Theoretical calculations suggest that sodium ions require larger interlayer spacings for effective intercalation compared to Li^+, indicating that expanding the interlayer spacing could enhance Na^+ storage [70]. The intercalation of Na^+ distorts the carbon layer structure, resulting in a sloping plateau on the electrochemical profile. In situ XRD observations have shown increases and recoveries in interlayer spacing in hard carbon during charge and discharge processes [146]. However, some studies have not observed changes in interlayer spacing, possibly due to the structural complexity of hard carbon and challenges of detecting its amorphous nature [60].

In the context of SIBs, the role of hard carbon as an anode electrode material has been extensively studied, particularly focusing on how its pore structure influences sodium-ion storage mechanisms. Early research suggested that nano-pores within hard carbon serve as active sites for sodium-ion storage via a "pore filling" process [61]. During discharge, these nano-pores facilitate the chemical adsorption of sodium ions onto their walls through a pseudo-capacitance mechanism [64]. Recent studies have indicated that within these pores, sodium ions adopt a unique "quasi-metallic state" (Fig. 11a) [147], forming quasi-metallic sodium clusters that differ in charge, size, and morphology from traditional metallic coatings [64]. Defect sites within the pores are crucial in this process, as they influence the interactions between sodium atoms and between sodium atoms and carbon, leading to the formation of these unique quasi-metallic clusters. The concentration of defects in hard carbon significantly impacts the formation and characteristics of sodium clusters. Higher defect concentrations generally result in smaller clusters filling smaller pores, while lower

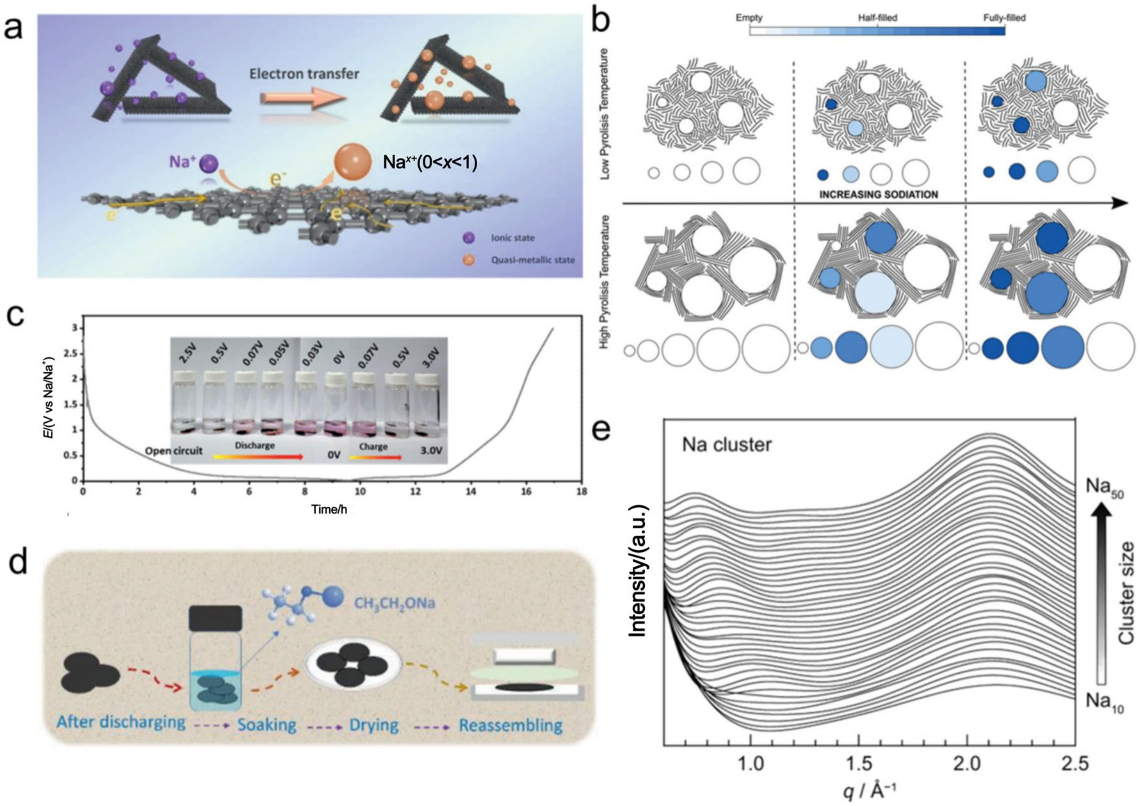

Fig. 11 **a** Schematic illustration of the steady states of sodium in hard carbon. The insertion of Na ions into the HC electrode is accompanied by partial electron transfer, resulting in the formation of quasi-metallic sodium. Reprinted with permission from Ref. [147]. Copyright © 2021, Wiley-VCH GmbH. **b** Schematic representation of the microstructure and the storage of sodium ions in closed pores for HCs synthesized at different pyrolysis temperatures. Circles represent closed pores whereas black lines represent graphene layers. The blue scale represents the extent of sodium ion filling: white indicates empty pores, and while dark blue indicates fully filled pores. Reprinted with permission from Ref. [148]. Copyright © 2023, Wiley-VCH GmbH. **c** Chemical reactions of protic solvents of the HC electrode after discharged/charged to different voltages. The typical charge–discharge profile of the HC electrode and the color changes in ethanol containing 1% phenolphthalein after reaction with HC at different potentials are shown. The structure and electrochemical properties of HC before and after being soaked in ethanol are also depicted. **d** Schematic illustration of reassembly of the battery after the fully sodiated HC soaked in ethanol. Reprinted with permission from Ref. [147]. Copyright © 2021, Wiley-VCH GmbH. **e** Scattering patterns of sodium cluster obtained from DFT-molecular dynamics (MD) simulation. Reprinted with permission from Ref. [149]. Copyright © 2019, Wiley-VCH GmbH

defect concentrations lead to the formation of quasi-metallic sodium clusters in average-sized pores (Fig. 11b) [148]. The amount of defects is a critical factor, as excessive defects can create barriers to metal migration, thereby hindering ion diffusion. Quasi-metallic sodium clusters typically exhibit a triangular shape [75], with a limit on their maximum size. Not all pores in hard carbon are suitable for sodium-ion storage; pores in the range of 1 to 2 nm are particularly favorable for the formation of quasi-metallic sodium clusters [82]. Various techniques can be employed to characterize these sodium clusters within hard carbon, including observing changes in pore structure and signals indicative of quasi-metallic sodium (Fig. 11c and d) [147]. Sodium NMR, SAXS, and XRD are key methods used to analyze the relationship between the pore structure of hard carbon and the formation of sodium clusters (Fig. 11e) [149].

The storage mechanisms for Na^+ in hard carbon differ from those for Li^+, involving both sodium ion intercalation and pore filling. This distinction underscores the need for a quantitative analysis of processes and highlights the importance of controlling structural characteristics of hard carbon, including defects, interlayer spacing, and pore size distribution. Future optimization of hard carbon anode materials will likely involve reducing surface defects, increasing interlayer spacings, and enhancing pore utilization. By precisely adjusting these structural characteristics, it is anticipated that hard carbon anodes can be enhanced to deliver superior performance in SIBs, resulting in more reliable and efficient energy storage solutions.

3.3 Correlation Between Hard Carbon Structure and K^+ Storage Electrochemistry

PIBs are gaining attention as a viable alternative for energy storage due to their larger capacity and mechanisms similar to those of LIBs. With a larger ionic radius compared to Li^+ and a lower reduction potential of approximately − 2.93V vs. the standard hydrogen electrode [SHE], PIBs have the potential for higher energy density [28]. Although research on hard carbon as a storage material for potassium ions is still in its early stages, it is believed that the storage mechanism for potassium ions in hard carbon resembles those for lithium and sodium ions, involving "adsorption," "intercalation," and "pore filling" [23, 26, 91]. Current research is focused on understanding these specific storage mechanisms and optimizing the structure of hard carbon to enhance potassium storage performance. In hard carbon, factors such as pore size, interlayer spacing, and surface defects are crucial in determining the efficiency of K^+ storage through these mechanisms [136, 150]. Ongoing research aims to understand how modifications to hard carbon structure influence potassium ion storage, which is essential for developing efficient and stable PIBs systems. Future research directions are likely to explore the relationship between hard carbon structure and K^+ storage in greater detail, aiming to design optimized structures that meet the specific requirements of K^+ storage. This approach is expected to advance the field of PIBs technology significantly.

In terms of preparation, high-capacity K^+ hard carbon materials are typically synthesized over a broad temperature range, resulting in diverse and complex structures. At lower temperatures (900–1800 °C), hard carbon features fragmented graphene layers and pseudo-graphitic microdomains, offering a rich surface structure and varied pore characteristics that support chemical adsorption and contribute to capacity in the sloping region. At higher temperatures (1500–2900 °C), hard carbon shows a higher degree of graphitization, with fewer free graphene layers and larger pseudo-graphitic microdomains [151]. This leads to a lower surface area but potentially more extensive storage spaces for K^+. This increased graphitization results in a transformation from imperfect to more perfect stacking in pseudo-graphitic microdomains, affecting K^+ storage and diffusion behaviors. This structure provides numerous filling and intercalation sites for K^+ storage, making the plateau region the primary contributor to the capacity of hard carbon in PIBs (Table 3).

The storage behavior of K^+ on graphene layers bears significant similarities to that observed for Li^+ and Na^+ systems. Recent studies have demonstrated that both graphene and hard carbon surfaces offer active sites for K^+ adsorption, indicating their potential as effective energy storage materials in PIBs [28]. The incorporation of heteroatoms like hydrogen, oxygen, nitrogen, and sulfur into these layers and surfaces is pivotal for enhancing K^+ storage [167, 169]. Figure 12a shows the K^+ storage mechanism [167], where K^+ is accommodated on graphene surfaces via capacitive mechanisms, including both double-layer and pseudocapacitance processes [170]. This enhances the potential of graphene layers for efficient potassium-ion adsorption.

Table 3 Reported high-capacity hard carbon materials for LIBs, including precursors, structures, and relevant electrochemical performances

Precursors	*T*/°C	*d*(002)/nm	*V*/(V vs. K^+/K)	*CD*/(mA g^{-1})	*C*/(mAh g^{-1})	References
Rice husk	1300	0.384	0.01–3.0	30	245	[152]
Cellulose	1500	0.382	0.002–2.0	25	290	[153]
Macroporous phenolic resin	1500	0.3832	0.002–2.0	10	336	[154]
Black tea	1300	0.368	0.01–2.0	20	230	[155]
Coconut shell	1000	0.386	0.001–3.0	30	254	[156]
Skimmed cotton	1200	0.388	0.01–2.0	40	253	[157]
Lignin	1300	0.42	0.01–3.0	50	283	[27]
Ganoderma lucidum spore	850	–	0.02–3.0	200	283.54	[158]
Hard-wood	1100	0.398	0.01–2.5	20	233.2	[159]
Potato	1000	–	0.01–2.7	100	269.9	[160]
Bagasse	1200	0.42	0.01–3.0	100	235	[161]
Walnum spetum	800	0.376	0.005–3.0	100	263.6	[162]
D-glucose	1200	–	0.1–2.5	30	248	[163]
Melamine–formaldehyde (MF) resin	1300	0.356	0.01–2.0	28	340	[164]
Peppers	1200	0.3859	0.01–2.0	27.9	284	[165]
Starch	1100	0.443	0.02–2.0	27.9	200	[166]

T pyrolysis temperature (°C), *d*(002) interlayer spacing (nm), *V* voltage window (V vs. K^+/K), *CD* current density (mA g^{-1}), *C* specific capacity, (mAh g^{-1}). Data are extracted from multiple data sources, and thus are with different significant digits

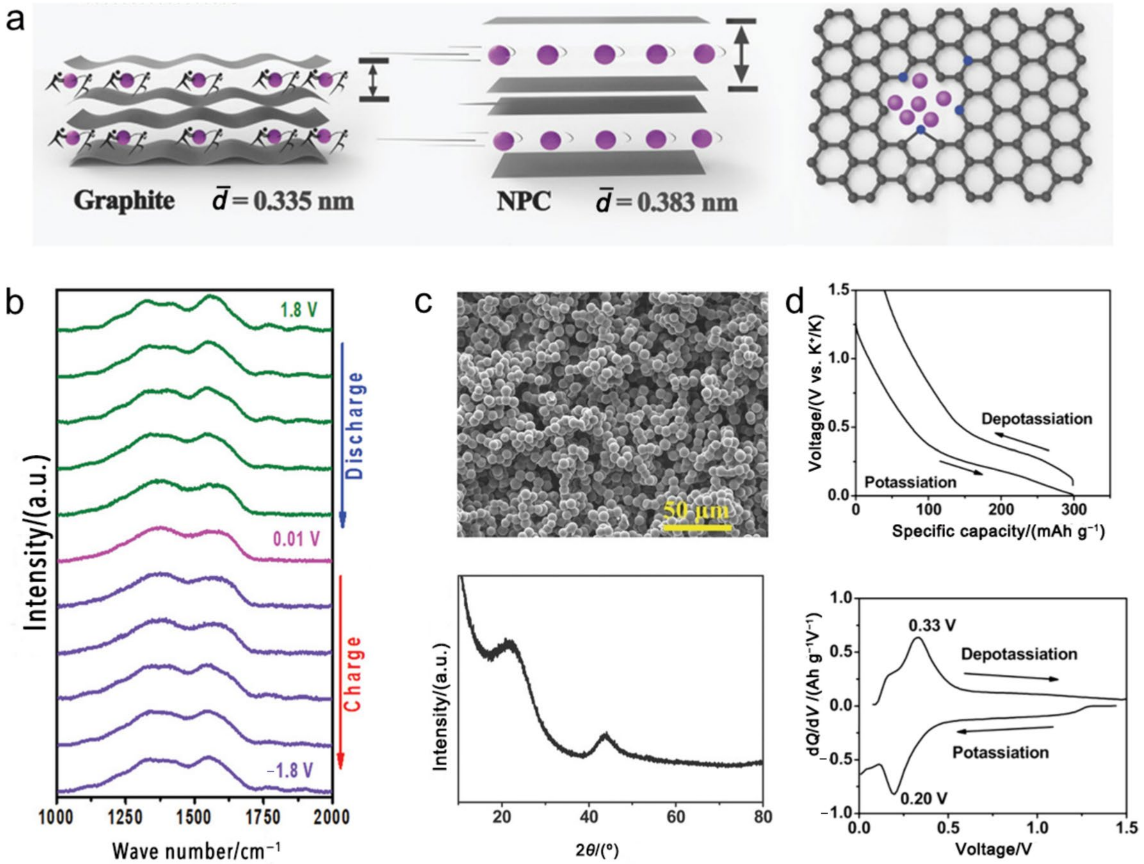

Fig. 12 **a** Schematic of the potassium storage mechanism. Reprinted with permission from Ref. [167]. Copyright © 2018, Wiley-VCH GmbH. **b** K-ion intercalation/de-intercalation analysis. In situ Raman spectra in a charging/discharging cycle from bottom to top. Reprinted with permission from Ref. [168]. Copyright © 2019, Wiley-VCH GmbH. **c** SEM image of HCS and the XRD pattern of HCS. **d** Discharge/charge profiles at C/10 in the second cycle of the HCS/K cell and d*Q*/d*V* profiles corresponding to HCS/K. Reprinted with permission from Ref. [25]. Copyright © 2015, Wiley-VCH GmbH

The introduction of heteroatoms modifies the intrinsic sp^2 structure and electronic characteristics of graphene layers, affecting factors, such as the Fermi level, charge transport, bandgap, and local electronic states [171, 172]. These alterations notably boost the potassium ion adsorption capability of graphene layers. Furthermore, potassium ion adsorption is characterized by rapid kinetics, facilitating fast-charging and discharging in PIBs. Advanced techniques, such as GITT and CV, are employed to probe the nuances of K$^+$ adsorption, storage, and release. During adsorption, defects in graphene layers become filled, leading to a reduction in the I_D/I_G ratio observed in Raman spectra upon discharge (Fig. 12b) [168], which serves as an indirect measure of the K$^+$ storage process. However, it is important to recognize that an increase in defects and a larger specific surface area can adversely affect the ICE of hard carbon in K$^+$ storage, similar to the degradation processes observed in Li$^+$ and Na$^+$ systems [173, 174]. These findings underscore the need for further investigation into the role of graphene layers and hard carbon in PIBs, emphasizing the importance of in-depth research into their kinetics, electronic structures, and storage mechanisms.

The pseudo-graphitic microdomains within hard carbon play a significant role in the storage of K$^+$. Despite the larger radius of K$^+$ compared to Na$^+$, which is typically thought to impede its intercalation into carbon materials, K$^+$ can still form stable intercalation compounds with carbon from an energetic perspective, thereby allowing for some degree of intercalation into graphite [145]. Understanding K$^+$ intercalation in graphite is crucial for elucidating its insertion mechanism in hard carbon. In 2015, graphite was first utilized as an anode material for PIBs, achieving a practical capacity of 273 mAh g^{-1}, close to its theoretical capacity of 279 mAh g^{-1} for KC$_8$ [175]. XRD studies revealed three distinct phase transitions, similar to those observed with Li$^+$ in graphite, suggesting that the intercalation behavior of K$^+$ might be more akin to that of Li$^+$. In the same year, hard carbon was also reported as a K$^+$ anode material, exhibiting a reversible capacity of up to 263 mAh g^{-1} (Fig. 12c and d) [25]. The intercalation of K^+ occurs between the microdomains with graphitic characteristics, exhibiting a sloping profile characteristic at low potentials due to the short-range order and imperfect stacking of the hard carbon structure. Notably, the microdomains within hard carbon comprise both perfectly and imperfectly stacked structures, each exhibiting different kinetic behaviors and voltage characteristics during K^+ intercalation reaction [151]. Generally, intercalation kinetics in graphitic microdomains is slow, with perfectly stacked structures showing lower kinetics due to their smaller interlayer distances compared to imperfectly stacked ones. During potassium ion insertion, hard carbon demonstrates superior kinetics and better cycle stability than graphite, with a smaller expansion rate. Furthermore, increasing the interlayer spacing of hard carbon could enhance its rate performance. The intercalation process causes observable expansion in the interlayer distance through XRD. During potassiation, the interlayer distance increases, and diffraction peaks shift to lower angles. During the charging process, the shift of the (002) peak to higher angles indicates that the insertion of K^+ is highly reversible [150]. These insights into the impact of graphitic microdomains in hard carbon on potassium ion storage are vital for advancing the development of high-performance PIBs.

The internal pore structure of hard carbon plays a role in K^+ storage, exhibiting similarities to Na^+ storage. Researchers have found that, due to pore defects, the interaction forces between potassium ions (K–K forces) become dominant, similar to Na–Na forces observed in Na^+. This results in both K^+ and Na^+ being stored in a quasi-metallic cluster state [64]. Due to these similarities, the electrochemical behavior of K^+ filling in pores mirrors that of Na^+, characterized by plateau discharge behavior and relatively lower kinetic responses [23]. Recent studies have made progress on understanding K^+ storage behavior in pores [176, 177]. Techniques like SAXS have detected changes in the porosity of hard carbon before and after discharge, suggesting that the pores serve as active sites for K^+ storage [136]. TEM observations confirm the presence of quasi-metallic potassium clusters, experimentally demonstrating the feasibility of storing potassium in pores in a quasi-metallic state [75].

K^+ exhibits intercalation behavior in hard carbon similar to that of Li^+, while its filling behavior resembles that of Na^+. This dual characteristic is dictated by the binding capability of K^+ with carbon and its ionic radius. Therefore, tailored strategies are needed for optimizing K^+ storage in hard carbon, distinct from those used for Li^+ or Na^+. Increasing the number of internal graphite microdomains and constructing larger interlayer spacings could enhance K^+ storage capacity and performance.

3.4 Matching Li-/Na-/K-Ion Batteries Through Regulating the Same Type of Hard Carbon

Studying the performance of hard carbon in storing different alkali metal ions (Li^+, Na^+, and K^+) offers valuable insights into the relationship between the structure of hard carbon and its electrochemical properties. By analyzing the behavior of the same hard carbon material with different ions, we can explore variations in storage mechanisms, such as adsorption, intercalation, and pore filling. This comparative analysis enhances our understanding of ion insertion and release behaviors, and evaluates the applicability of hard carbon for various ion batteries. The structure and characteristics of hard carbon significantly influence the storage capacity for each ion, making it essential to assess its performance across different systems to determine its advantages and limitations [64, 75, 91]. This understanding is pivotal for designing and synthesizing hard carbon anode materials that are both targeted and universally applicable.

Research into how the structure of hard carbon evolves and impacts the storage performance of Li^+, Na^+, and K^+ offers new perspectives on alkali metal storage mechanisms (Fig. 13a). As the degree of graphitization in hard carbon increases, the capacity in the slope region for these ions typically decreases, aligning with the gradual reduction of free graphene layer structures. The structure and quantity of graphene layers are key factors affecting slope capacity, highlighting the need for precise control over these layers. In terms of plateau capacity, different behaviors are observed for lithium, sodium, and potassium ions (Fig. 13b and c). K^+ shows a continuous increase, whereas Li^+ and Na^+ demonstrate a turning point in the plateau region. The changing interlayer distance and pore size during the heating process of hard carbon, along with varying pore utilization rates, suggest an optimal value for storage, particularly for Li^+ and Na^+. This emphasizes the role of pores as active sites and the need to optimize pore structures for improved plateau capacity. For PIBs, the transition from imperfect to perfect stacking in pseudo-graphitic microdomains during heating significantly impacts the dynamics in the plateau region. Small interlayer distances can affect potassium ion transport, leading to larger voltage hysteresis [75]. Research by Jin has shown that the active sites for Li^+ and Na^+ in the slope region differ and do not interfere with each other, while in the plateau region, their active sites overlap (Fig. 13d) [178]. Quantitative analysis of these storage sites for Li^+ and Na^+ revealed detailed similarities and differences in alkali metal ion storage mechanisms in hard carbon. Further investigation into the storage behavior of Li^+ and K^+ ions in hard carbon revealed that while the intercalation sites for K^+ and Li^+ in hard carbon overlap, their performance varies with the degree of graphitization. K^+ intercalation primarily occurs in poorly developed graphite structures

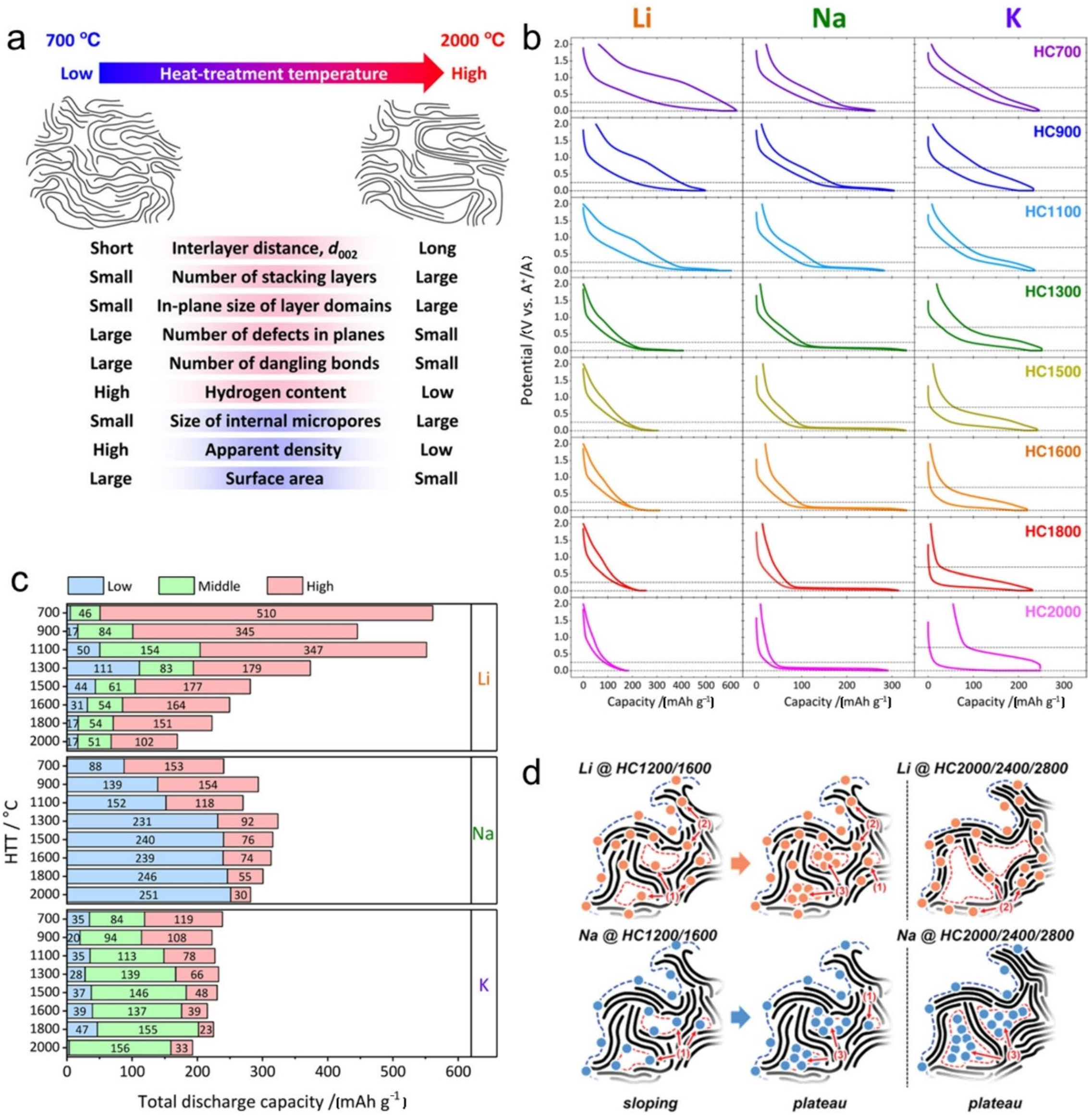

Fig. 13 **a** Schematic illustrations of hard carbon structures prepared at 700 and 2000°C, highlighting their structural parameters. **b** Charge/discharge profiles for hard carbon samples prepared at different HTTs in Li cells (left), Na cells (middle), and K cells (right) at the second cycle. Dashed lines represent the potential of 0.0 and 0.25 V for Li and Na cells and 0.0 and 0.7 V for K cells to guide the eye. **c** HTT dependence of discharge (alkali metal extraction) capacities for hard carbon electrodes in Li, Na, and K cells at the second cycle. "Low" represents capacities in the low-potential regions of 0.002–0.05 V vs. Li^+/Li for Li cells, 0.002–0.25 V vs. Na^+/Na for Na cells, and 0.002–0.20 V vs. K^+/K for K cells. "Middle" represents the capacities in the middle-potential regions of 0.05–0.25 V vs. Li^+/Li for Li cells and 0.20–0.70 V vs. K^+/K for K cells. "High" represents the capacities in the high–potential regions of 0.25–2.0 V vs. A^+/A (A = Li and Na) for Li and Na cells and 0.70–2.0 V vs. K^+/K for K cells. Reprinted with permission from Ref. [75]. Copyright © 2021, American Chemical Society. **d** Schematics of lithium and sodium storage mechanisms based on microstructural changes in hard carbons due to thermal annealing: bulk chemisorption, intercalation, and nanoclustering. Reprinted with permission from Ref. [178]. Copyright © 2019, Wiley-VCH GmbH

with expanded *d*-spacing (more than 3.5 Å), whereas Li^+ intercalation is more effective in well-developed graphite structures with *d*-spacing of less than 3.46 Å. Consequently, the storage capacity of K^+ in hard carbon decreases with increased graphitization, whereas the storage capacity of Li^+ significantly increases. This is because Li^+ intercalation is highly sensitive to the microstructure of graphite. In disordered graphite structures, most of the charge for lithium ions is stored through chemical adsorption. However, due to the substantial increase in charge transfer resistance, the larger K^+ intercalation reaction is physically constrained by the ordered development of the graphite in hard carbon, resulting in poorer intercalation capacity [26]. These findings offer valuable insights for the future design and optimization of anode materials like hard carbon, promoting the development of alkali metal-ion battery technology.

Understanding the distinct storage mechanisms for Li^+, Na^+, and K^+ in hard carbon, along with the variations in slope and plateau regions, is crucial for optimizing hard carbon structures and developing high-performance anode materials. Insights into K^+ insertion and the impact of interlayer spacings on ionic dynamics offer important clues for future battery design and development. Such knowledge lays a solid foundation for advancing energy storage technologies, fostering innovation in sustainable energy applications, and contributing to the development of next-generation energy storage systems.

4 General Regulation Strategies for Key Structures of Hard Carbon

The microstructure of hard carbon is closely related to its electrochemical performance, making precise regulation of its microstructure a viable route to achieving high performance. Given the inherent complexity of hard carbon structures, comprehensive design and control of the entire structure pose challenges. However, focusing on optimizing the local structure of hard carbon has proven to be a simple and effective strategy [42, 61]. Tailoring specific structural features within hard carbon to meet application-specific requirements is a common approach for enhancing its performance. Various strategies have been developed for the precise control of the microstructure of hard carbon's microstructure, aiming to achieve higher performance as an anode material.

4.1 Defect Regulation

Defects within carbon layers significantly influence the structure and charge distribution, especially in the context of alkali metal storage. Different types of defects exhibit diverse mechanisms of action [50, 172]. Research indicates that defects can significantly enhance hard carbon's ability to store alkali metal ions by boosting the adsorption mechanism, thus improving kinetic behavior, rate performance, and low-temperature performance. However, defects also introduce substantial irreversible capacity, hindering the effective extraction of alkali metal ions. It is noteworthy that the favorable and unfavorable impacts of defects on hard carbon performance depend directly on the type of defects. Therefore, optimizing defect types and concentrations is crucial for enhancing the performance of carbon layers in alkali metal storage. This study provides crucial guidance for fine-tuning carbon layer structures to enhance their applicability in energy storage applications.

4.1.1 Doping of Defects

Research on introducing a large number of active defects into carbon materials has been extensively explored. By selecting specific precursors, researchers can synthesize hard carbon materials with high defect concentrations [179]. Mitlin and colleagues used banana peels as a carbon source and carbonized them at 1400°C, resulting in hard carbon materials with an I_D/I_G ratio of 0.93, indicating a high defect concentration [180]. Additionally, reducing the carbonization temperature is another effective method to increase the defect concentration in hard carbon. Tan and colleagues employed cellulose-coated PVDF as a carbon source and subjected it to pyrolysis at different temperatures [99]. Raman analysis showed that lower temperatures were more conducive to retaining a higher number of defects. While controlling precursors and carbonization temperatures has proven effective for producing high-defect materials, achieving further improvements in the electrochemical performance of hard carbon requires precise defect engineering.

Highly defective hard carbon materials are frequently produced by carbonizing precursors rich in heteroatoms, as introducing these heteroatoms enhances the defect concentration in hard carbon. Heteroatom doping is a commonly used method for precisely introducing defects, which improves electrical conductivity and increases the reversible capacity of hard carbon [182]. Additionally, heteroatom doping often leads to increased interlayer spacing in hard carbon due to changes in the electron cloud density of the carbon layers. The effects of doping vary with different elements, as each dopant can impart unique synergistic effects or electronic properties to the electrochemical reactions [50]. Targeted doping with specific heteroatoms enables precise control over defect introduction. Common doping methods involve doping in the precursor or during the carbonization process to obtain the final doped carbon product. It is noteworthy that doping during the precursor stage can create additional defect sites. For example, Zhou and colleagues designed a synthesis method involving the amination reaction of benzidine and formaldehyde to form benzidine-formaldehyde (MPF) resin microspheres. These microspheres were further carbonized to produce nitrogen-rich carbon precursors. During high-temperature carbonization, nitrogen atoms were gradually removed, leading to numerous defect sites. Even after high-temperature carbonization, nitrogen signals were still detected in NHCMs, and optimized NHCM-1400 retained up to 4.64% nitrogen content, enriching the graphene layers with defects (Fig. 14a) [137]. This material achieved a reversible capacity of up to 399 mAh g^{-1}

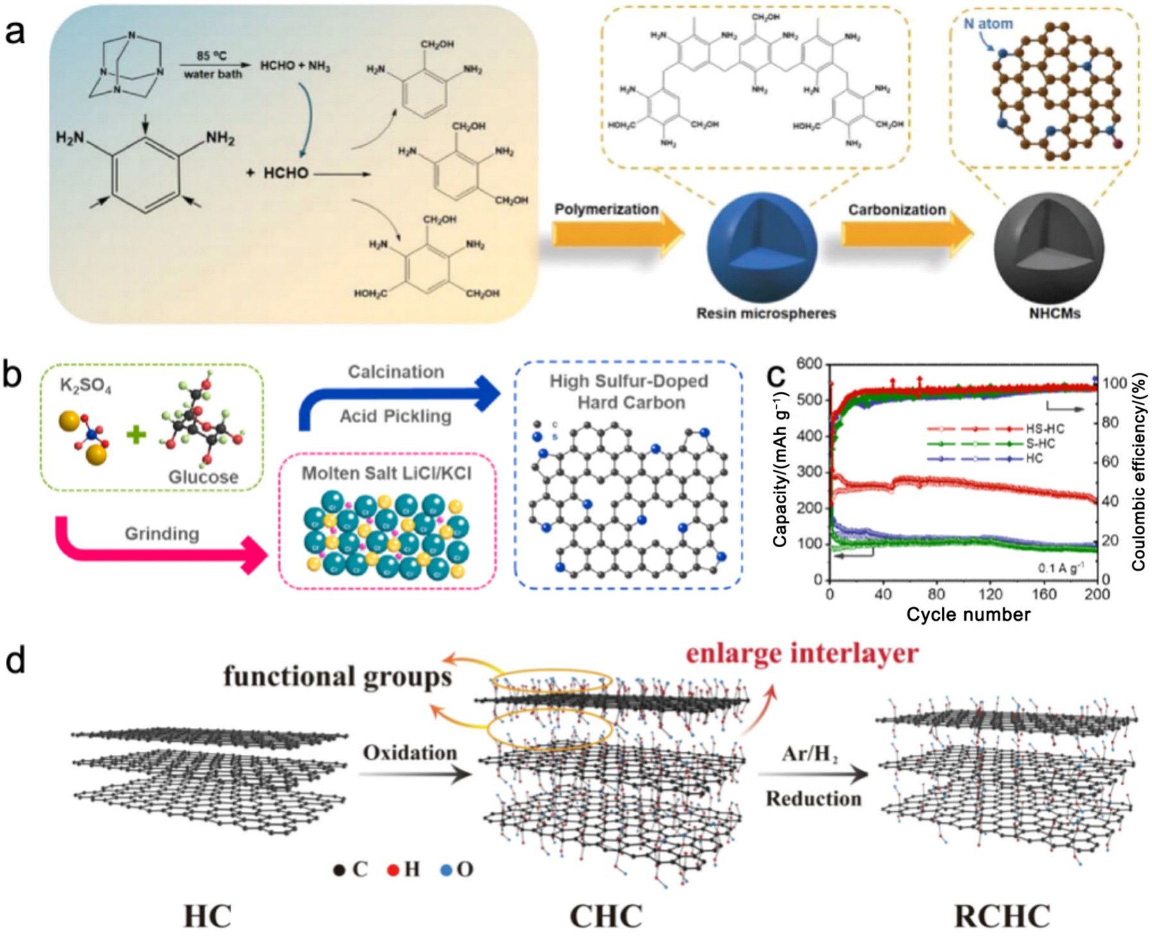

Fig. 14 **a** Schematic synthesis procedure of the NHCMs via amine–aldehyde condensation and carbonization. Reprinted with permission from Ref. [137]. Copyright © 2023, Wiley-VCH GmbH. **b** Schematic Diagram for Preparation of HS-HC. **c** Cycle performances at a current density of 0.1 A g^{-1}. Reprinted with permission from Ref. [170]. Copyright © 2020, American Chemical Society. **d** Schematic diagram of the oxidation and reduction processes. Reprinted with permission from Ref. [181]. Copyright © 2022, Elsevier

at 30 mA g^{-1} for SIBs. Furthermore, adjusting the ratio and type of heteroatoms in the precursor allows for the synthesis of hard carbon materials with varying levels of and types of doping. Shi and colleagues utilized lignin as an oxygen source, mixing it with PFNS in different ratios using spray drying to obtain oxygen-doped microsphere powders [183]. After carbonization at 1100°C in an Ar atmosphere, different oxygen content-doped ONCMs were synthesized. The oxygen doping was reflected in different proportions of C = O and C–OH functional groups on the graphene sheets. Raman analysis indicated that the disorder in the synthesized carbon materials was proportional to the oxygen doping content, demonstrating precise control over carbon layer disorder through defect adjustment. Ji and colleagues used sucrose as a carbon source, uniformly incorporating phosphorus into the precursor by mixing H_3PO_4 with a sucrose solution [184]. After 1100°C pyrolysis, P-uniformly doped P–HC was successfully synthesized. XPS and XANES results revealed that most of the doped phosphorus was in the form of PO_x rather than elemental phosphorus. XRD and Raman analysis indicated that phosphorus doping significantly widened the interlayer spacing *d*(002) of hard carbon, and increased the defect concentration in the turbostratic nanodomains. The introduction of heteroatoms during the carbonization process is often achieved by mixing the precursor with the dopant. Ji and colleagues reported a method for synthesizing high-sulfur-content hard carbon using a molten salt approach, combining glucose with sulfate and annealing in a KCl/LiCl mixed salt (Fig. 14b) [170]. Since carbon reduces sulfate, the sulfur content in HS–HC was as high as 25.8% by weight, exhibiting higher disorder. What is more, due to the sulfur doping, HS–HC shows higher capacity (Fig. 14c). Another approach involved mixing sublimated sulfur with powdered camphor tree branches to synthesize sulfur-doped carbon materials. XPS analysis revealed various thiol-type sulfur species on the graphene sheets, and sulfur doping led to a significant increase in interlayer spacing compared to untreated hard carbon. Post-treatment of the carbonized product is a method of introducing heteroatoms by introducing functional groups. Tang and colleagues applied an oxidizing agent to commercial hard carbon (Fig. 14d) [181]. XPS testing showed that the oxidized carbon layer contained a large number of C = O groups. Importantly, the introduction of these functional groups occurred not only on the surface carbon layer but also inside the hard carbon microdomains. This strategy of introducing a large number of oxygen-containing functional groups on the carbon layer enhanced the defect abundance in the carbon layer, making hard carbon exhibit higher disorder. Additionally, due to the oxidation of the internal carbon layers in microdomains, the treated hard carbon also showed increased interlayer spacing and better electrochemical performance, which can be up to 341 mAh g^{-1} at 20 mA g^{-1}.

In addition to introducing heteroatoms, defect self-doping, where sp^2 carbon is directly transformed into sp^3 carbon without adding heteroatoms, is another effective strategy for defect engineering. Dong and colleagues achieved self-doping in carbon materials through high-energy ball milling (Fig. 15a) [185]. This process caused EG to evolve from a structure with clearly identifiable layered, highly crystalline flat platelets to a basin-shaped morphology. In this new morphology, amorphous sp^3 "islands" were randomly distributed among crystalline sp^2 "rivers." This coexistence of sp^2/sp^3 hybrid structures did not disrupt the conductive network of the carbon layers, allowing electrons to rapidly transfer in the rivers formed by sp^2 hybridization (Fig. 15b) [185]. However, ball milling has drawbacks in terms of uniformity and defect depth, and considerations regarding its generality and cost are important. Li and colleagues further reported a method for inducing self-doping defects in carbon materials using γ-ray irradiation (Fig. 15c) [186]. The high-energy, penetrating nature of ^{60}Co γ-rays facilitated the transformation of sp^2 carbon into sp^3 carbon within HC layers. Raman testing further showed that γ-ray irradiation increased the formation of smaller graphite-induced domains, reducing the average size of sp^2 carbon particles. This method generated numerous conjugated ring defects, offering more active sites for alkali metal ion absorption. This irradiation-induced "self-doping" defect strategy has unique advantages of high efficiency, simplicity, and large-scale modification. Plasma etching is another effective method for self-doping carbon materials. High-energy plasma particles can disrupt and reconstruct the surface structure of carbon materials. Mu and colleagues used hydrogen plasma to etch carbon surface, and XRD and Raman analyses revealed an increased proportion of amorphous carbon and higher disorder on the treated surface [187]. Wang and colleagues utilized Ar plasma to create numerous nanoscale holes on graphene layers [188]. The I_D/I_G ratio increased from 1.16 to 1.51 after treatment, effectively enhancing the defect concentration of

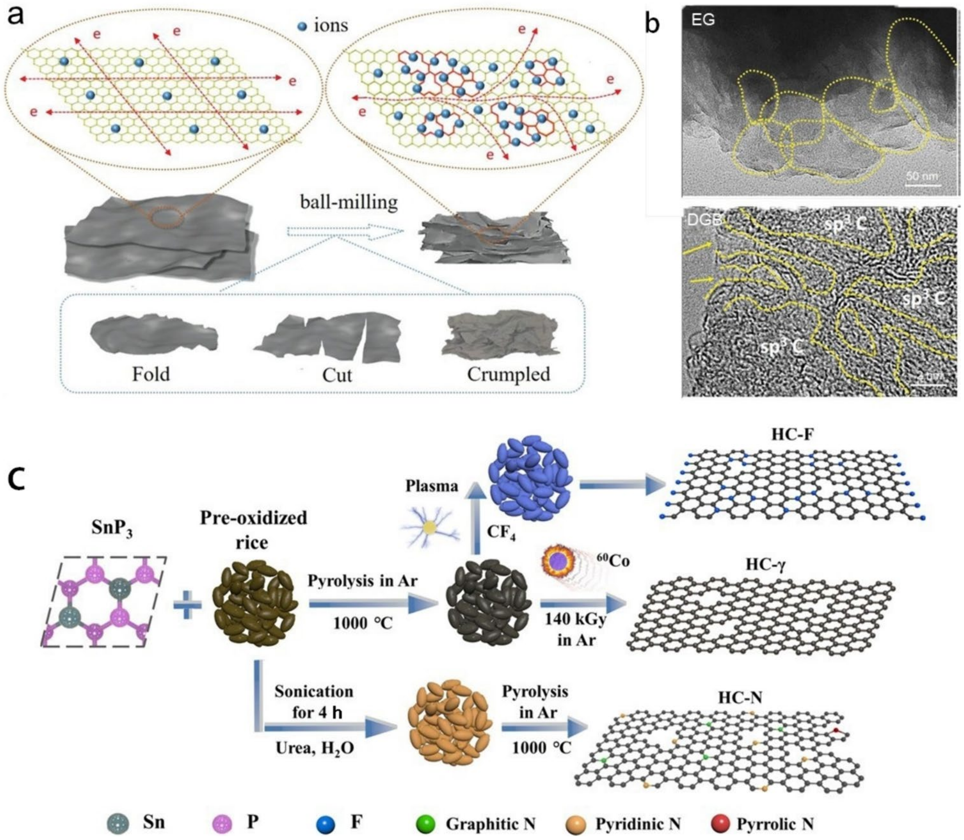

Fig. 15 **a** Structural evolution of EG during ball milling. The flat and highly crystallized EG platelets are folded, cut, and reassembled during ball milling, introducing abundant "self-doping" defects. This results in the formation of a dense DGB with a novel "river basin" like defect distribution. The "self-doping" defects act as active sites for ion storage with an electrical double-layer behavior, and the highly crystallized regions allow fast electron transport in the entire block. **b** HRTEM images of EG and DGB. Reprinted with permission from Ref. [185]. Copyright © 2019, Wiley-VCH GmbH. **c** Schematic illustration of the preparation process of HC–F, HC–γ and HC–N defects engineering. Reprinted with permission from Ref. [186]. Copyright © 2021, Elsevier

the graphene layers. Additionally, Ji and collaborators used microwaves to heat hard carbon annealed at 650 °C for a few seconds, resulting in highly defective hard carbon [189]. Neutron total scattering and related PDF studies indicated that microwaving for just 6 s generated a substantial number of defects within the hard carbon.

4.1.2 Suppression of Defects

Recent research has advanced several techniques to mitigate defects in carbon materials. Early studies demonstrated that elevating the graphitization degree at high temperatures can effectively reduce defect content in carbon layers. Elevated carbonization temperatures lead to a more ordered carbon structure, as sp^3 carbon gradually transitions into sp^2 carbon, resulting in hard carbon materials with reduced defect densities [75, 151]. Liu and colleagues further found that slower heating rates are beneficial for synthesizing hard carbon with fewer defects [190, 191]. A gradual heating process allows for better gas escape and rearrangement of carbon atoms within the carbon matrix, minimizing defect formation during carbonization.

Liu and colleagues reported a “template method” to promote ordered structures in carbon layers. They used eggshell membranes and sucrose as precursors, positioning them between graphite blocks or mixing them with graphite powder. This approach enabled the synthesis of hard carbon materials enriched with graphite crystals at a relatively low temperature of 1300 °C. The graphite template induced a highly ordered carbon layer structure, leading to rapid loss of oxygen functional groups from the precursor and facilitating the diffusion of decomposed carbon atoms into graphite crystals and pseudo-graphitic microdomains. This process promoted the growth of highly ordered hard carbon materials. Furthermore, the group proposed optimizing the template method by adjusting parameters such as template preheating temperature and time, achieving fully crystalline carbon at 1300 °C with exceptional graphitization (Fig. 16a and b) [192]. The resulting carbon exhibited a highly ordered carbon layer structure with almost no observable D bond in Raman spectra, and an ICE of up to 99.5%. Similarly, highly ordered graphene can also serve as a template for graphitization. Huang and colleagues developed a novel graphene-assisted method for graphitization [193]. By leveraging hydrogen bonding interactions, they induced the arrangement of aromatic rings in phenolic resin along the graphene layers, leading to a higher proportion of sp^2-hybridized carbon and a reduction in defect density. This method significantly enhanced the structural quality of the hard carbon, resulting in a superior ICE of 90.4%.

In addition to the template method, metals can also catalyze the graphitization of carbon, facilitating the transformation from sp^3 to sp^2. Early studies involved the pyrolysis of mixtures of metal powder and amorphous carbon, leading to varying types of carbon, such as graphite or turbostratic/graphite, due to distinct graphitization mechanisms [196]. One mechanism involves the formation and subsequent decomposition of metal carbides, while the other involves the dissolution of carbon into the catalyst followed by its precipitation. Studies indicate that even "non-graphitizable" carbon can undergo graphitization at relatively low temperatures (<1400 °C) when catalyzed by metals, enabling the production of hard carbon materials with low defect densities at these temperatures. Li and coworkers utilized Ni^{2+} as a catalyst with coal as the precursor, achieving coal-based porous carbon materials with a high degree of graphitization and low defect density through pyrolysis at 800 °C [197]. Various transition metals have been employed to promote catalytic graphitization, with iron being particularly attractive due to its abundance and low toxicity. Graphitization catalyzed by iron can be applied in processes such as chemical vapor for the production of graphite or carbon nanotubes, as well as within blast furnaces. Ramirez-Rico and colleagues conducted in-depth research on this process’s mechanism [196, 198]. The study revealed that Fe facilitates graphitization at low temperatures (<750 °C) by the formation and decomposition of Fe_3C compounds. The efficiency of iron in catalyzing graphitization is influenced by the local structure of amorphous carbon, the size, and the initial oxidation state of the catalyst. The catalytic effect of Fe in the graphitization process of carbon materials diminishes at higher temperatures. In addition to promoting graphitization and reducing defects, metal ions can also repair defects in hard carbon. Chou and colleagues recently investigated the metal ion-catalyzed pyrolysis of flexible tissue paper for HC anode preparation [194]. By coordinating catalytic ions with oxygen defects, they used Mn^{2+} to successfully regulate defects and ion channels in hard carbons. Their study explored the effects of temperature, concentration, and element type on this process (Fig. 16c). The concentration of 0.04 mol L^{-1} Mn^{2+} is considered optimal, as at this concentration, the material exhibits the highest capacity, with an ICE as high as 92.1% (Fig. 16d). At this concentration, Mn^{2+} can catalyze the growth of graphite layers into long-stepped graphene layers. At high temperatures, Mn^{2+} disrupted carbon bridges between sp^3 graphene layers, allowing the layers to arrange freely and form nano-graphite domains and carbon micropores. This facilitated the removal of irreversible oxygen-containing defects caused by the interaction between metal ions and oxygen. Suitable heating atmospheres can achieve similar defect repair effects in carbon layers. Wang and colleagues reported a method to precisely control oxygen atoms/defects by adjusting the atmosphere during heating [195]. They employed cyclohexane to create an argon/cyclohexane mixed

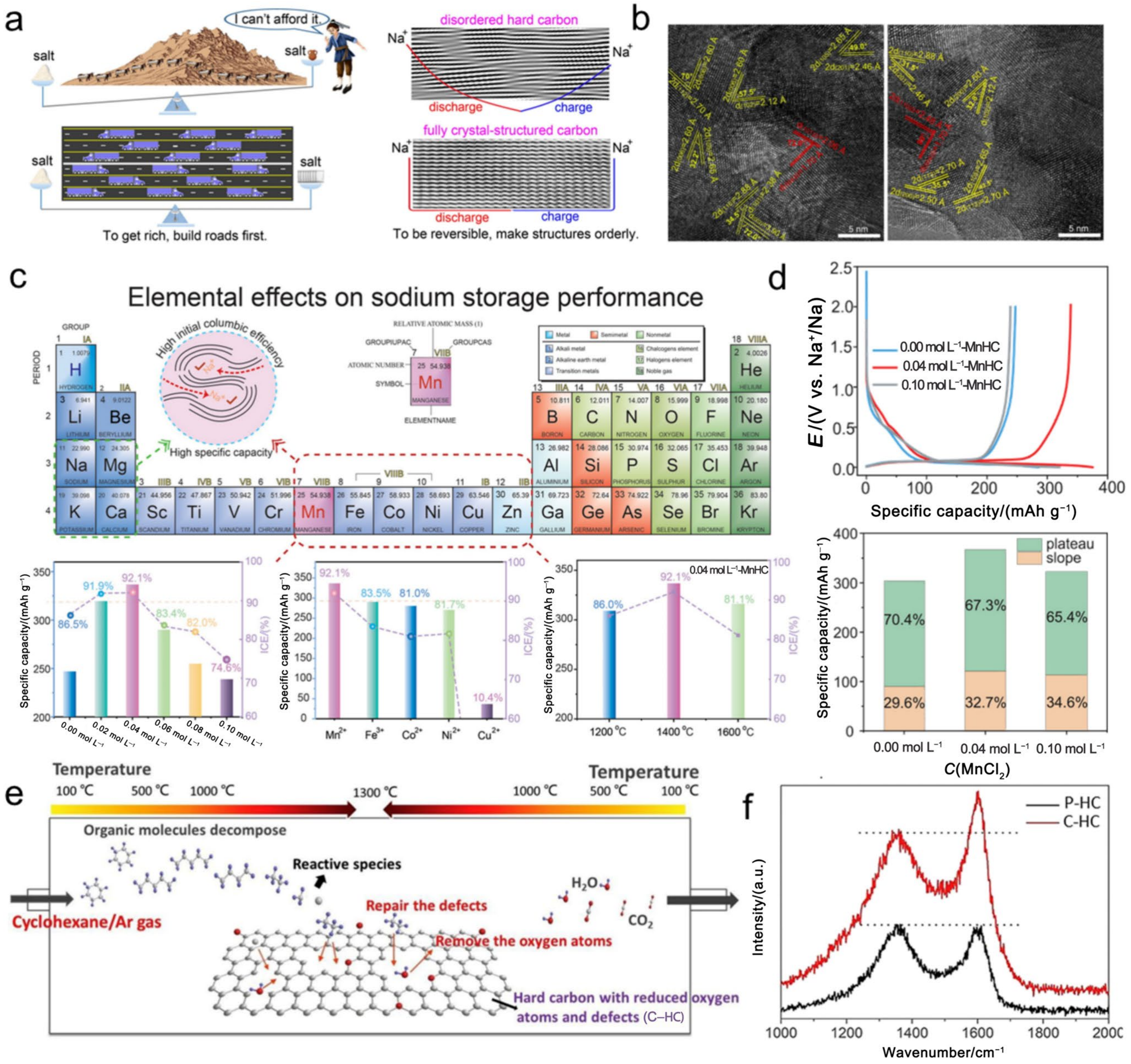

Fig. 16 **a** Schematic illustration of fully crystallized carbon. **b** HRTEM images of EM-380 °C-36 h-1300 °C. Reprinted with permission from Ref. [192]. Copyright © 2022, Elsevier. **c** Pathway to produce high-performance HC using various metal chloride salts found in the periodic table. Structural illustrations of HC regulated by different manganese salt concentrations. Investigating the impact of modifications with different concentrations of manganese chloride, various metal chloride salts and manganese chlorides at varying carbonization temperatures on the reversible capacity and ICE of HC. **d** Comparison of the first discharge/charge curves for different concentrations of manganese chloride in half cells and contribution ratios of the slope capacity and plateau capacity in the second cycle discharge curves. Reprinted with permission from Ref. [194]. Copyright © 2023, Wiley-VCH GmbH. **e** Schematic illustration of the in situ engineering process of hard carbon. **f** Raman spectra of as-prepared samples C–HC and P–HC. Reprinted with permission from Ref. [195]. Copyright © 2019, Elsevier

atmosphere, which repaired defect sites in the carbon layer (Fig. 16e and f). This technique involved generating highly reactive small carbons from the reaction of cyclohexane with oxygen functional groups at high temperatures, producing gaseous H_2O and CO_2. This technique effectively reduced the oxygen atom/defect content in the carbon layer. Similarly, removing foreign atoms from the surface of the carbon layer can significantly reduce defect density. Huang and colleagues reported an effective approach by employing a straightforward annealing method to minimize defects in carbon layers. High-temperature annealing treatment of commercial hard carbon materials removed N, O, and other foreign atoms from the carbon layer surface. This treatment not only decreased the presence of these foreign atoms but also reduced the irreversible capacity of hard carbon during alkali metal storage, leading to improved performance in storage applications [199].

4.2 Precise Control of the Growth of Pseudo-Graphitic Microdomains

The typical short-range order and random orientation of pseudo-graphitic microdomains in non-graphitizable hard carbon are crucial contributors to its distinctive electrochemical behavior. Studies indicate that larger, long-range ordered structures are disadvantageous for the electrochemical performance of hard carbon. Therefore, it is necessary to develop methods to control the proportion of pseudo-graphitic microdomains while ensuring that they maintain a randomly oriented structure on a larger scale.

Research has demonstrated that the extensive cross-linking and the presence of C–O–C bonds in hard carbon are critical factors in hindering its further graphitization. Enhancing the degree of cross-linking and increasing the C–O–C content within the carbon layers can effectively suppress the growth of pseudo-graphitic microdomains and long-range order in hard carbon. One of the simplest ways to obtain a highly cross-linked hard carbon is through careful selection of the precursor materials. Precursors such as thermosetting phenolic resin and highly crystalline cellulose have inherently high cross-linking degrees and abundant oxygen-containing bonds [153, 200]. When these precursors undergo pyrolysis, they yield products with high concentrations of C–O–C bonds and highly cross-linked structures. The subsequent carbonization process results in hard carbon structures with small, stable pseudo-graphitic microdomains, resulting in excellent alkali metal ion storage performance. However, not all precursors inherently possess the same level of cross-linking and oxygen content, making it necessary to modify them through special treatments to enhance their cross-linking degree. As precursors are essentially polymers carrying various functional groups such as carboxyl, amino, and hydroxyl, these functional groups with high reactivity can serve as sites for cross-linking. By optimizing the precursor treatment conditions to encourage reactions among these functional groups, the cross-linking degree of the precursor can be effectively increased. Li and colleagues proposed a starch pretreatment method to successfully prepare highly cross-linked starch [92]. This method involved heating potato starch in an Ar atmosphere at 200–230 °C for 60 h, producing a loose black starch powder. After further pyrolysis, the starch remains in a loose powder state without any apparent melting between particles, leading to a hard carbon material for LIBs with a capacity of up to 531 mAh g^{-1}. The authors further suggested that using an air atmosphere during pyrolysis could reduce the heat treatment time, achieving more efficient pretreatment. In addition to utilizing the precursor's self-condensable functional groups as cross-linking sites, another effective approach is introducing new cross-linking sites through the use of cross-linking agents. Chen and colleagues used maleic anhydride as an esterifying agent to react with starch, successfully suppressing the swelling of starch particles during pyrolysis and maintaining their integrity after pyrolysis [201]. Fourier transform infrared spectroscopy (FT-IR) showed a significant decrease in –OH group content in the cross-linked starch, alongside the emergence of stronger ester and ether bond peaks, indicative of extensive cross-linking reactions within the starch particles. However, due to the relatively large size of starch particles, the esterifying agent struggles to penetrate and diffuse into the interior via solid-state diffusion, making it challenging for the cross-linking agent to function inside the starch. For other precursors, such as petroleum-based precursors like asphalt, which is composed mainly of aromatic hydrocarbon complexes with low molecular weights, the challenge lies in preventing the carbon layers from rearranging into long-range ordered structures during pyrolysis. Therefore, for these precursors, it is necessary to suppress the growth of pseudo-graphitic microdomains through cross-linking. However, these precursors contain fewer inherently cross-linkable functional groups, making direct cross-linking difficult. Therefore, it is necessary to introduce sufficient functional groups inside them before proceeding to enhance their cross-linking.

Pre-oxidation treatment of asphalt is a widely used strategy to enhance its oxygen content, with the resulting oxygen-containing functional groups endowing the asphalt with self-cross-linking capabilities [202]. Studies have shown that the degree of disorder in asphalt-based hard carbon is related to its oxygen content [93, 203]. The diffusion of oxygen molecules within the asphalt can cause cross-linking and polymerization of its basic structural units. With increasing temperature, the cross-linked structures formed by aldehyde, carboxyl, ester, and anhydrides undergo solid-state pyrolysis, during which CO_2 and CO are released, liberating oxygen functional groups. This process prevents the rearrangement of carbon layers during carbonization. Yang and colleagues successfully synthesized sodium-ion hard carbon with a high-capacity of up to 315 mAh g^{-1} by employing a low-temperature pyrolysis oxidation method, effectively suppressing the graphitization of asphalt by adjusting its state before oxidation [204]. Fujimoto and colleagues used phosphorus pentoxide and ammonium persulfate as oxidants to co-heat treat asphalt at 270–310 °C, resulting in a loose, black asphalt powder [93]. The pre-treated asphalt showed a higher oxygen content, which further suppressed the growth of graphite microcrystals during carbonization, allowing pseudo-graphitic microdomains to remain smaller. Similarly, Hu and colleagues employed air pre-oxidation to treat asphalt and anthracite, effectively inhibiting the growth of graphite microdomains during pyrolysis, preventing the formation of long-range ordered structures in the carbon materials, and maintaining a larger degree of disorder. Compared to untreated samples, the pre-oxidized samples exhibited superior alkali metal ion storage performance [93].

Hard carbon, a versatile carbon alloy, possesses tunable properties through its compositional flexibility. Based on this characteristic, researchers have developed methods to control the formation of pseudo-graphitic microdomains in hard carbon by compounding different precursors. By regulating the components and their ratios within the precursor, the size and quantity of these microdomains can be finely controlled. Taking wood as an example, a common biomass precursor mainly composed of cellulose, hemicellulose, and lignin, the structures formed after the pyrolysis of cellulose, hemicellulose, and lignin are different [39]. These components play different roles in the pyrolysis process. By adjusting the proportion of each component in the precursor, specific

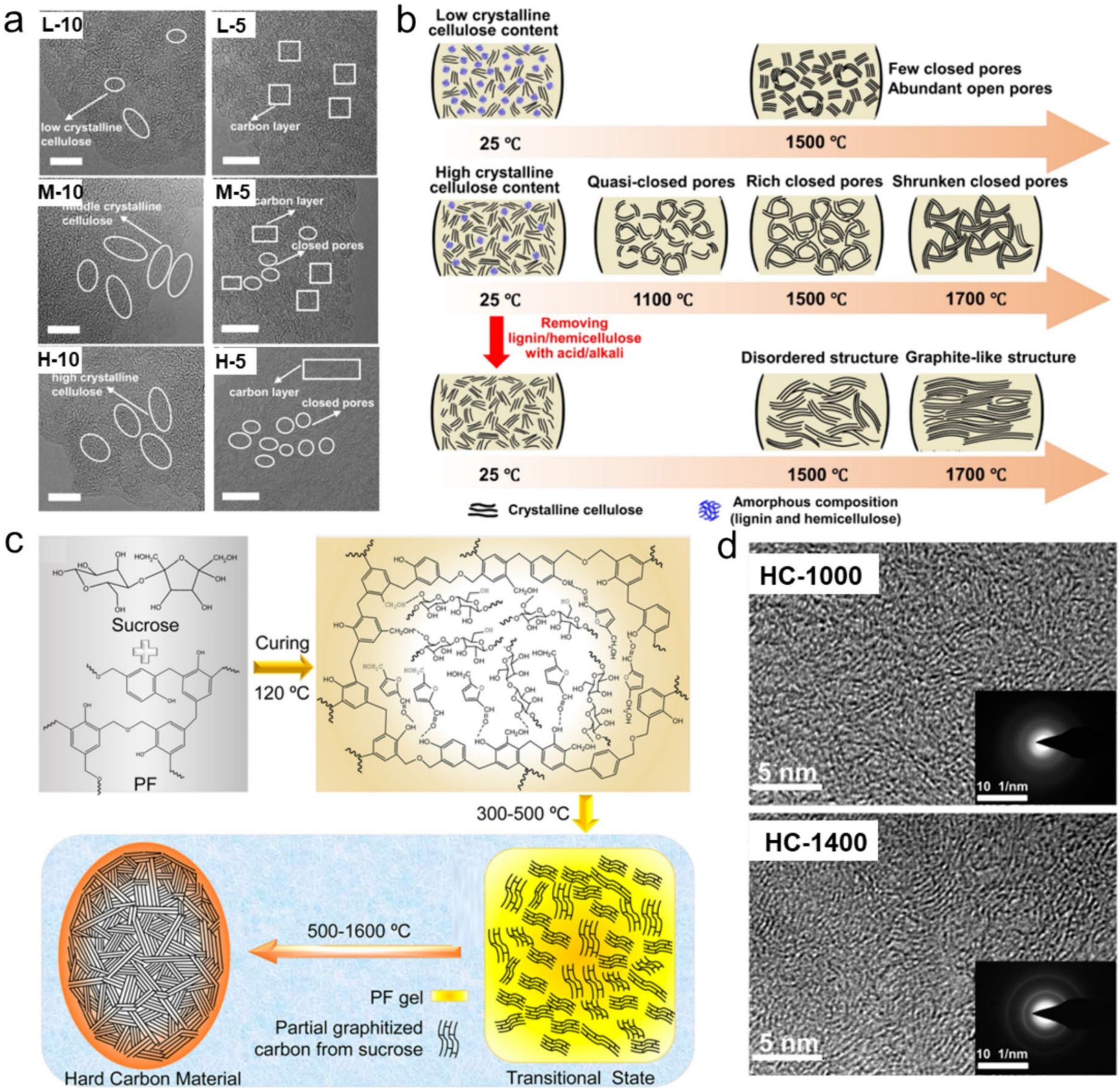

Fig. 17 **a** HRTEM images of cellulose with different degrees of crystallinity: low, medium, and high resolution. **b** Both the composition of wood precursor (crystallinity cellulose and amorphous hemicellulose/lignin) and the carbonization temperature play important roles in affecting the microstructure (such as number, size and wall thickness) of closed pores. Reprinted with permission from Ref. [38]. Copyright © 2022, Springer Nature. **c** Schematic illustration of the process flow diagram for PF/sucrose-based hard carbon synthesis. **d** Typical TEM and SAED images of HCM-1000, and HCM-1400. Reprinted with permission from Ref. [205]. Copyright © 2017, American Chemical Society

structures within the carbonized product can be selectively enhanced. Shao and colleague explored this by using precursors with varying ratios of crystalline cellulose, investigating the roles of crystalline and amorphous components in the microdomain formation process (Fig. 17a) [38]. Their findings showed that an increase in crystalline cellulose content enriched the quantity of pseudo-graphitic microdomains in the final pyrolysis product, while amorphous components, such as hemicellulose suppressed their growth, hindering the formation of long-range ordered structures (Fig. 17b) [38]. Beyond utilizing natural differences in component composition, researchers have also successfully employed artificial adjustments to precursor components. Yang and colleagues dehydrated a phenolic resin and sucrose precursor at 200 °C for 24 h, utilizing the functional groups between sucrose and phenolic resin to cross-link them (Fig. 17c and d) [205]. This approach effectively inhibited carbon atom rearrangement during sucrose pyrolysis, successfully addressing the foaming issue associated with sucrose. Similarly, Zhang and colleagues synthesized hard carbon materials from a composite precursor of asphalt and phenolic resin [40]. Experimental results showed that during high-temperature pyrolysis, asphalt first formed a viscous intermediate product, which then transformed into soft carbon with a high degree of graphitization through liquid-phase carbonization. Meanwhile, the resin remained in the solid phase, eventually forming hard carbon that resisted graphitization. By adjusting the mass ratio of asphalt to resin, the proportion of graphite microdomains in the carbonized product could be effectively adjusted. Additionally, the cross-linking between asphalt and resin, along with the gases released during resin pyrolysis, inhibited the liquefaction and graphitization of asphalt. In another approach, Titiric and colleagues combined a hard carbon precursor FP with a soft carbon precursor MP in varying ratios for carbonization [206]. By integrating the disordered structures formed from FP with the ordered structures generated by the pyrolysis of MP, they were able to control the quantity of internal microdomains within the hard carbon. TEM observations reflected these results, indicating that with an increase in the proportion of MP, the quantity of long-range ordered pseudo-graphitic microdomains in hard carbon also increased. By tuning the MP content in hard carbon, it was possible to control the internal disorder of hard carbon, thereby enhancing its ability to store alkali metal ions.

4.3 Rational Regulation of Closed Pores

The closed-cell structure of hard carbon originates from the stacking of pseudo-graphitic microdomains. Studies have indicated that the pore structure can be controlled by adjusting the size and quantity of these pseudo-graphitic microdomains within hard carbon. However, many methods for controlling microdomain size are inherently complex, making it even more challenging to further control the pore structure. To address this, several strategies for directly controlling pore structures have been proposed. One effective method is to control the porosity of the precursor material. Using porous materials such as wood and porous carbon as precursors can result in hard carbon materials with rich pore structures [46, 207]. Kono and colleagues synthesized a new carbon material with a substantial closed-cell volume by using porous carbon as a precursor at 2100 °C [208]. Xia and others employed bamboo as a precursor to synthesize hard carbon material with a significant amount of closed-cell structures at 1300 °C [46].

For materials with inherently poor pore structures, modification strategies can be employed to optimize the precursor for achieving porous structures. Komaba et al. successfully synthesized a phenolic resin material with large pores by adjusting the resin synthesis strategy [154]. The resulting hard carbon exhibited high porosity and larger pore size after heat treatment, demonstrating excellent alkali metal ion storage performance. Additionally, the group proposed a “template method” using metal particles as templates, which has become a classic strategy for pore formation. In the production of porous carbon, templates such as zeolites and magnesium oxide are often used. Based on this, Komaba and others successfully synthesized magnesium-templated hard carbon as a high-capacity anode material for sodium-ion batteries by heating a mixture of magnesium gluconate and glucose. The thermal decomposition of magnesium organic compounds resulted in the formation of appropriately sized nanostructured MgO within the carbon matrix, which could be removed by acid washing to create nano-sized pores [135]. Further adjustments to Mg source and content allowed for fine-tuning the MgO template pore size and quantity. Moreover, the group extended this approach by using MgO, ZnO, and $CaCO_3$ as nano-pore templates to explore the effectiveness of different templates in pore formation (Fig. 18a–c) [136].

Experimental results showed differences in pore size depending on the template used, with HC-Ca having fewer closed pores than HC-Mg and HC-Zn. The optimal parameters for ZnO templates differed from those for MgO, likely due to variations in crystal size, crystallinity, and particle size distribution of the oxide embedded in the carbon precursor. Hu and colleagues proposed a chemical control method using ethanol as a pore-forming agent and phenolic resin as a carbon precursor [209]. By mixing ethanol and resin through solvent heating, they obtained solidified PF. Their study showed that ethanol could serve both as a reactant to accelerate the solidification process and as a vapor generator to induce pores in the cross-linked matrix. The resulting optimal anodes exhibited a high Na storage capacity of ca. 410 mAh g^{-1}. It was found

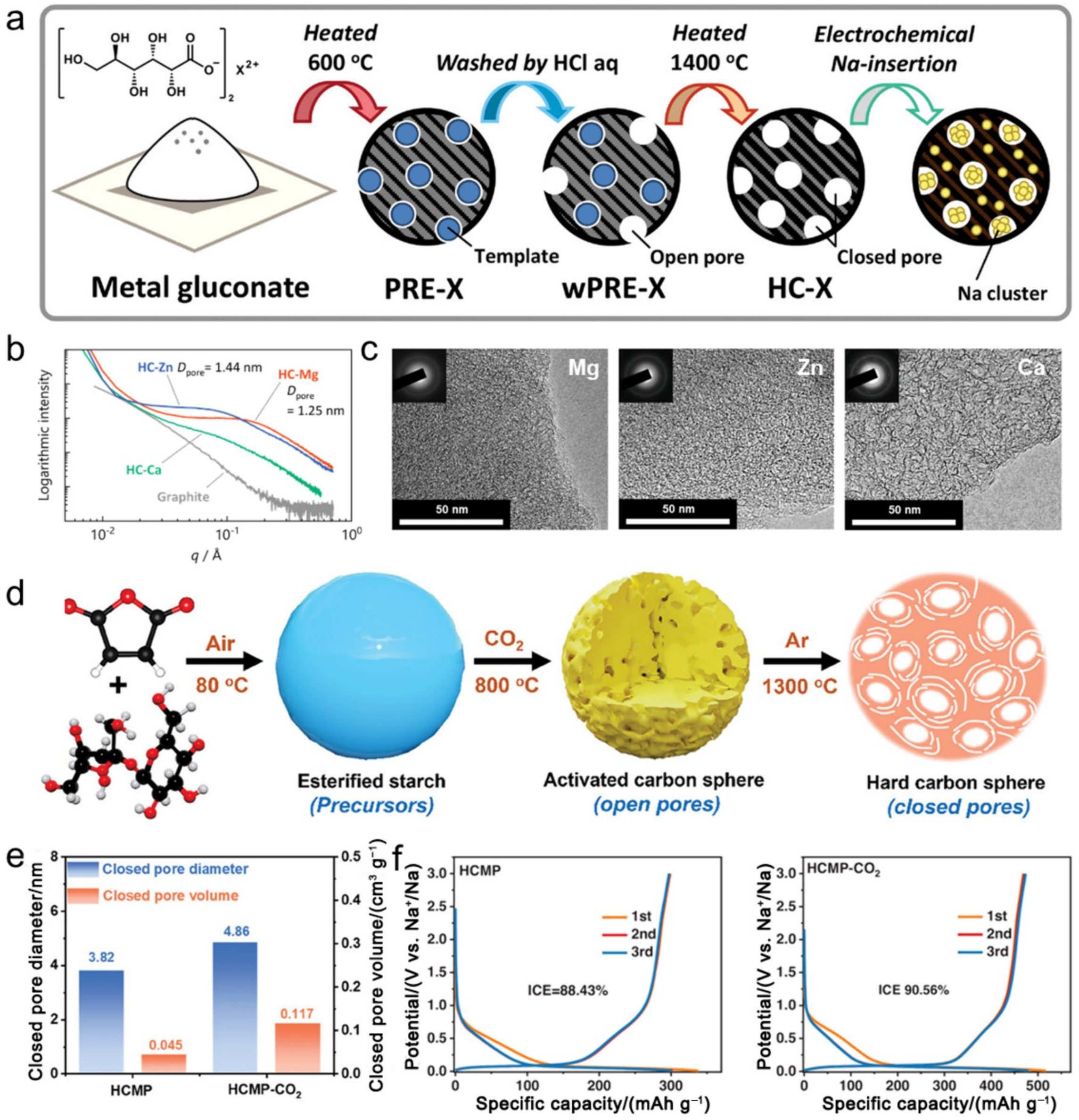

Fig. 18 **a** Schematic illustration of template synthesis methods of PRE-X and wPRE-X, where X = Mg, Zn, or Ca. **b** SAXS patterns of HCs and graphite. **c** HRTEM images of HC-Mg (left), HC-Zn (middle), and HC-Ca (right). Reprinted with permission from Ref. [136]. Copyright © 2023, Wiley-VCH GmbH. **d** Fabrication and structure of hard carbon with closed pores microspheres. Schematic of the synthesis of HCMP-CO_2. **e** Closed pore diameter and closed pore volume. **f** HCMP and HCMP-CO_2 in the potential range of 0.01–3 V at 25 mA g^{-1}. Reprinted with permission from Ref. [65]. Copyright © 2023, Wiley-VCH GmbH

that during further carbonization, larger steam gas might crack to open pores, while a small amount of ethanol might solidify together with PF without generating enough steam to promote a porous structure. Therefore, adjusting the ethanol content is crucial for achieving the desired microstructure. Similarly, using molten salt to etch carbon materials and create internal porous structures is a common method. KOH is a commonly used etchant for synthesizing porous carbon. Molten KOH reacts with carbon sources and impurities at high temperatures, etching the carbon material and producing a large amount of gas to form numerous pores inside the carbon structure. Zhao and others employed KOH as an activation agent, pre-carbonizing a mixture of KOH and anthracite at 800 °C [210]. The activation effect of KOH introduced a large number of open nano-sized pores and disordered carbon structures into the resulting carbon material. After further carbonization, the open pores introduced during etching were almost completely closed, resulting in a pore volume far greater than that of the untreated sample, with up to 54 times the surface area and larger pore diameters. Similarly, Hong and colleagues achieved similar effects by changing the pyrolysis atmosphere. Zheng used CO_2 as an etchant to treat esterified starch carbonization at 200 °C (Fig. 18–f) [65]. Based on the principle of CO_2 reacting with carbon to generate CO at high temperatures, numerous pores were formed in the carbon substrate. Subsequent high-temperature treatment was used to close the pore structure. Further characterization revealed that the introduced open pores during etching were almost completely closed, and the sample after etching exhibited a pore volume much higher than that of the directly carbonized sample. Overall, whether using the template method or the etching method, the essence is to introduce new pore sources into the carbon structure. This is achieved by increasing the porosity within the carbon material to enhance the number of closed pores in hard carbon. This pore-forming strategy is mainly applied to precursor materials with low inherent porosity, but it also benefits carbon materials with relatively high porosity by increasing the number of closed pores.

It is worth mentioning that, unlike traditional high-temperature closed-cell formation and templating methods, Yang and colleagues proposed an innovative strategy to close the pores at the openings of porous carbon using methane chemical vapor deposition (CVD). This method creates a sieve carbon material enriched with closed-cell structures (Fig. 19a and b) [211]. By carefully controlling reaction conditions, methane can diffuse into pores larger than methane molecules within the porous carbon structure. Methane adsorbs onto the pore walls around the entrance and undergoes continuous pyrolysis and polymerization, ultimately depositing on the walls and gradually reducing the pore entrance diameter. The treated sieve carbon (SC) exhibited an almost zero specific surface area in BET tests, while SAXS tests showed that the pore abundance remained similar to that before treatment. This indicates that CVD successfully tightened the pore openings while retaining the pore structure, effectively transitioning from open-cell to closed-cell structures. This treatment resulted in a sieving carbon anode with a record-high plateau capacity of 400 mAh g^{-1}. Unlike previous strategies, this approach focuses on converting open pores into closed ones to enhance the utilization of the internal porosity of the carbon structure, creating numerous closed pore structures within hard carbon. This pore filling strategy is primarily applied to porous carbon materials and also allows for some degree of control over the size of the existing pore structures.

Cao and colleagues further proposed a strategy utilizing SC-CVD technology to fill pseudo-graphitic microdomains into narrow micropores within activated carbon (AC), constructing a filled carbon (FC) material with restricted growth of pseudo-graphitic microdomains and microporous structures [213]. The pseudo-graphitic microdomains are relatively large laterally and consist of multiple layers in thickness, matching well with the fissure-like micropores in AC. With the fissure-like framework of AC, areas inaccessible to vapor simultaneously generate microporous structures. By controlling the SC-CVD process, the content of pseudo-graphitic carbon domains and microstructures in the fissure sand pores of AC can be precisely adjusted. The as-prepared FC demonstrates an excellent sodium storage capacity of 435.5 mAh g^{-1} at 20 mA g^{-1}. Tests indicate that during this process, some pores in AC are filled with pseudo-graphitic microdomains while others become open-cell structures. Subsequent heat treatment further improves the open-cell volume and total pore volume as the filled pseudo-graphitic domains rearrange and contract during graphitization. Similarly, Xv and colleagues developed a strategy utilizing polypropylene (PP) waste masks to convert open pores in AC to closed ones (Fig. 19c, d). This strategy involves carbonizing PP at high temperatures to form a carbon layer at the pore entrance of AC, thereby controlling the porosity of AC and transforming its open pores into closed ones. This method effectively expands the capacity of alkali metal ions at low voltages [212].

5 Summary and Perspectives

Over the past few decades, researchers have persistently investigated the structure of hard carbons. Numerous structural models for hard carbons have been proposed to describe their features. Unfortunately, despite these valuable insights, these models have yet to accurately represent the actual structure of hard carbons. The precise structure of hard carbons remains a contentious area. Fortunately, the efforts of many researchers in the field of hard carbons over the decades have deepened our understanding of the local structure of hard carbons. Building upon this knowledge, a plethora of hard carbon materials with excellent electrochemical performance in alkali metal-ion batteries have been developed (Fig. 20).

Over the past years, hard carbons have been extensively studied as anode electrodes in alkali metal-ion batteries, particularly in emerging battery systems such as SIBs and PIBs, where they demonstrate significant potential. However, new requirements often bring new challenges for hard carbons. Depending on the application scenario, designing appropriate hard carbon structures becomes crucial. To aid researchers in finding suitable structural modulation strategies, it is necessary to summarize the interaction mechanisms between hard carbon structures and different alkali metal ions.

This review provides a thorough analysis of the diverse hard carbon structures, their origins, and the evolution of key structural features. It addresses the challenges associated with studying hard carbon structures and,

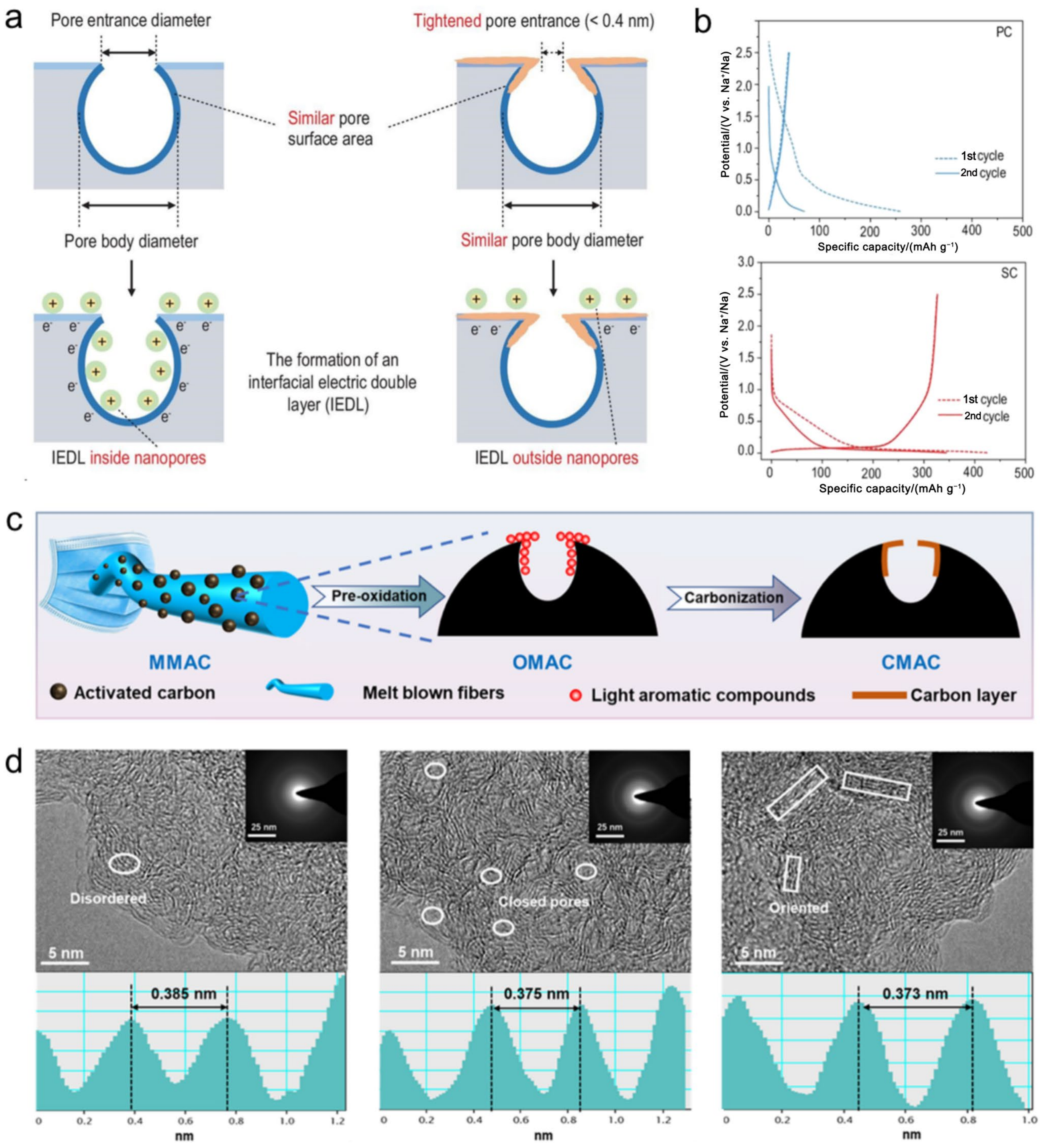

Fig. 19 **a** Schematic showing the control of the nano-pores of a typical porous carbon (left) to produce the target sieving carbon (right), and the comparison between their different IEDLs. PyC, the solvated shell, and Na are drawn as brown irregular strips, green circles and yellow solid circles with a positive sign, respectively. **b** Charge/discharge curves for the first two cycles, at a current density of 50 mA g^{-1}. Reprinted with permission from Ref. [211]. Copyright © 2022, Oxford University Press. **c** Schematic illustration for the synthesis procedures of CMAC-*x*. **d** HRTEM images of CAC, CMAC-2, CMAC-3 and corresponding fast Fourier transform patterns. Reprinted with permission from Ref. [212]. Copyright © 2024, Elsevier

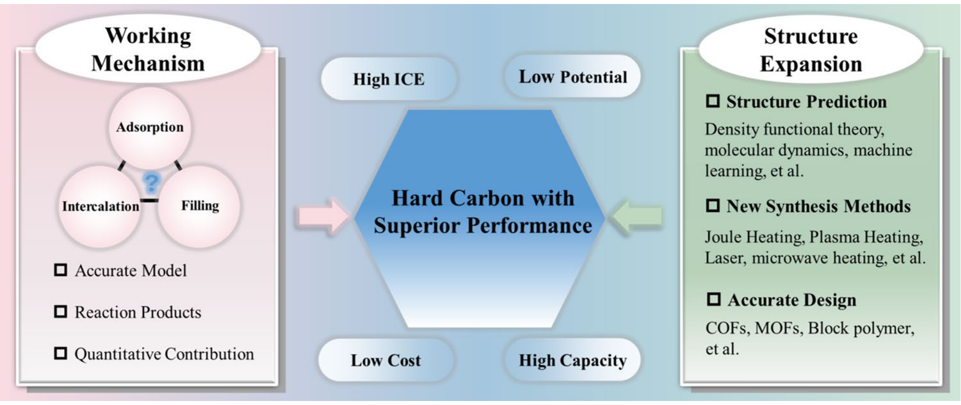

Fig. 20 The schematic diagram of future work prospects

through a comparative analysis in the fields of LIBs, SIBs, and PIBs, highlights the key structural differences in various application scenarios. The review elucidates the relationships between different alkali metal ions and key hard carbon structures and compares the electrochemical behaviors of these ions in hard carbons. Based on the structure-performance relationship of hard carbons with alkali metal ions, it offers a comprehensive summary of strategies for regulating three key structures: carbon layer surfaces, pseudo-graphitic microdomains, and pores.

In order to realize the commercial potential of hard carbon, it is imperative to meet criteria such as low cost, high initial efficiency, high-capacity, and excellent overall performance. Achieving these goals necessitates a deeper understanding and design of the structure of hard carbons. To develop hard carbon materials with superior performance, further research should delve into a deeper exploration of the relationship between hard carbon structures and alkali metal ion storage behaviors, enabling more precise control over these structures, and build on this foundation to further develop hard carbon structures and construct hard carbon materials with different structures.

5.1 Exploration and Determination of the "Structure-Electrochemistry" Relationship of Hard Carbon

5.1.1 Building Accurate Model of Hard Carbon Structure

The internal structure of hard carbons is complex and unevenly distributed, making it challenging to achieve an accurate description of the overall structure using a single characterization method. Therefore, there is a strong need to develop precise models for hard carbons. Although many structural models for hard carbons have been proposed, the inherent diversity of hard carbon structures makes it difficult for any single model to encompass all variations. Future research should focus on integrating characterization techniques with theoretical models based on current structural understanding to achieve a more accurate description of hard carbon structures.

Creating precise models for hard carbons requires advanced characterization techniques. TEM, which provides direct observation of hard carbon structures, holds significant importance in the construction of precise hard carbon models. Currently, TEM is commonly used for determining the single-layer carbon structure of hard carbons by producing 2D images of the hard carbon structure. However, these 2D images fall short of revealing the stacking arrangement of internal microcrystals and the shapes of pores within hard carbons. Accurate 3D models necessitate technologies capable of capturing the 3D morphology of hard carbons. Emerging TEM-based 3D reconstruction techniques have the potential to fulfill this goal [214]. These techniques involve acquiring 2D images from different sample orientations and using specialized algorithms to synthesize these images into a 3D model. Techniques such as cryo-electron microscopy and phase reconstruction can achieve 3D reconstruction within an ultra-high resolution range. Similarly, the use of synchrotron radiation can achieve similar results. Synchrotron radiation-based 3D reconstruction is widely applied across various fields, providing high spatial and temporal resolution for in situ characterization of processes. Current synchrotron radiation X-ray imaging technology offers micrometer-level spatial resolution, and advancements in synchrotron technology could potentially achieve nanometer-level resolution for 3D reconstruction of hard carbon structures.

Furthermore, combining multiple characterization techniques will further enhance the accuracy of model construction. Various testing methods for hard carbons can provide rich structural information. Combining techniques such as XRD, SAXS and TEM, and utilizing computational fitting methods will offer more precise structural information.

5.1.2 Characterization and Determination of Hard Carbon Products

Understanding the mechanism by which hard carbons store alkali metal ions is essential, and analyzing the reaction products will contribute to this. Due to the differing physicochemical properties of lithium ions, sodium ions, and potassium ions, their storage behaviors in hard carbons vary. The debate over their storage mechanisms generally centers around three processes: adsorption, intercalation, and filling. Under these three mechanisms, the binding of alkali metal ions to carbon materials differs, and characterizing the products obtained under these mechanisms will clarify the alkali metal ion storage mechanism in hard carbons.

Among these mechanisms, the characterization of quasi-metallic alkali metals is relatively straightforward. Their presence can be intuitively observed through phenolphthalein coloration and the characterization of related reaction products. Additionally, quasi-metallic alkali metals can be directly observed by using TEM. Techniques such as NMR and XPS also provide relevant signals. Nevertheless, directly observing adsorbed and intercalated species becomes challenging. Unlike graphite, which undergoes noticeable color changes upon forming intercalation compounds, hard carbons do not exhibit significant color changes during alkali metal ion storage. Identification of adsorption and intercalation behaviors is typically achieved by monitoring changes in the structure of hard carbons during charge and discharge processes. Techniques such as Raman spectroscopy and XRD are employed to characterize changes in defects and interlayer distances, helping to determine reaction sites and infer the mechanism. Whereas, structures like pores allow both adsorption and the formation of metal clusters. Moreover, the adsorption of alkali metal ions in hard carbons actually occurs between layers of free-standing graphene, complicating the determination of the mechanism based on the structure of hard carbons. Therefore, characterizing reaction products becomes particularly important. In future research, developing new methods for the direct characterization of reaction products in hard carbons, especially intercalation products, is imperative.

5.1.3 Quantitative Analysis of Ion Storage Contributions from Different Mechanisms in Hard Carbons

Alkali metal ion storage behavior in hard carbons includes adsorption, intercalation, and filling. The complex mechanisms pose challenges in understanding the electrochemical processes involved. Current analyses of alkali metal ion electrochemical behavior mostly focus on qualitative aspects, with quantitative analyses being less common. However, quantifying the contributions of different mechanisms is beneficial for determining the alkali metal ion mechanism and enables the evaluation of rates and cycling performance under different conditions. Precise control and optimization of these contributions can lead to the synthesis of hard carbon materials with superior properties [53].

Some literature has already quantitatively analyzed the contributions of different parts of hard carbon. Common approaches include analyzing the proportions of diffusion and pseudo-capacitance contributions based on dynamic differences among various components. Additionally, quantifying the filling contributions using pore size parameters combined with density functional theory (DFT) calculations has been used. These approaches can assist in a deeper analysis of the structure-performance relationship between hard carbons and alkali metal ions. It is worth noting that, despite these strategies being proposed, the use of different quantification standards in different studies makes cross-comparisons challenging.

In future research, a more quantitative analysis of electrochemical behaviors of hard carbons, separately discussing the rate performance in the plateau and slope regions, will deepen our understanding of alkali metal ion behavior in hard carbons. To achieve a more systematic analysis, it is necessary to develop new quantification methods and establish uniform quantification standards.

5.2 Design and Synthesis of New Hard Carbon Structures

5.2.1 Theoretical Calculations Provide Guidance for Design of Hard Carbon Structures

While there is general agreement on the broad approach to structural regulation strategies for hard carbon, the specifics of the ideal structure for optimal alkali metal ion storage remain unclear. Theoretical calculations can provide valuable guidance on the direction of structural regulation for fine-tuning hard carbon [218].

Utilizing computational methods such as MD simulations, DFT, and machine learning, along with extensive experimental data, enables us to construct relatively accurate models of hard carbon. These models provide crucial information about the energy characteristics of hard carbon structures and their interactions with alkali metal ions, facilitating the establishment of structure–property relationships. Computational analysis of different structural models allows for performance predictions and the identification of theoretically optimal structures, such as optimal interlayer spacing and pore size. Subsequently, by further employing predictive models to guide the design of new materials, efficient screening and precise design of hard carbons can be achieved.

5.2.2 Development and Application of Novel Synthesis Technologies

Despite the continuous development of structural design strategies for hard carbons over the past few decades, exploration and development in this area remain insufficient in the face of the abundant structural possibilities. Considerable untapped potential exists within the structural space of hard carbons. To further develop the structures of hard carbons, it is essential to seek new control strategies developing novel synthesis techniques.

Traditional tube furnace heating is widely used in the synthesis of hard carbon materials. However, this method involves long treatment time and results in structures primarily determined by temperature, thus limiting structural control. While adjustments to precursor materials and heating conditions offer some degree of fine-tuning, these approaches are limited by their spatial and temporal resolution. Achieving breakthroughs in this aspect would be beneficial for expanding the structural possibilities of carbon materials.

Several methods with high spatial or temporal resolution have been proposed. Hong and colleagues developed a plasma heating technique that enables hard carbon synthesis in a matter of minutes[215]. Similarly, Hu and his colleagues introduced Joule heating, achieving synthesis on a second timescale [216]. It is noteworthy that this technique allows for synthesis in an extremely short time. This high temporal resolution technique is expected to enable the synthesis of metastable structures under dynamic control, potentially unlocking new structural possibilities and enhancing performance. Jean-Marie and others proposed a method for laser synthesis of hard carbon, achieving localized graphitization through laser irradiation [217]. Compared to traditional tube furnace heating, this technique offers higher spatial resolution, enabling more precise design and optimization of hard carbon structures.

5.2.3 Accurate Design and Regulation of Hard Carbon Structures

Further characterization of precursor structures has revealed the challenges in achieving precise control over the structure of hard carbons. The incomplete understanding of the specific structures in the precursors introduces numerous uncontrollable factors into the evolution of hard carbon, ultimately preventing accurate control. Adopting a bottom-up synthesis approach holds the potential to address this issue [219–222].

Phenolic resins, as artificially synthesized precursors, exhibit excellent alkali metal ion storage capabilities. Conventional control often focuses on the broad management of resin components. Integrating organic polymer structure design into precursor synthesis can achieve precision in controlling precursor structures. Research on covalent organic frameworks, metal–organic frameworks, and polymer chain segments has been widely reported. Leveraging this knowledge, designing molecular types, polymerization degrees, and spatial structures can help further refine the spatial arrangement of hard carbons after carbonization. By adjusting the structure of polymer chain segments, artificially designing graphitizable components, and introducing components that restrict graphitization, we can gain clearer insights into the precursor's structure.

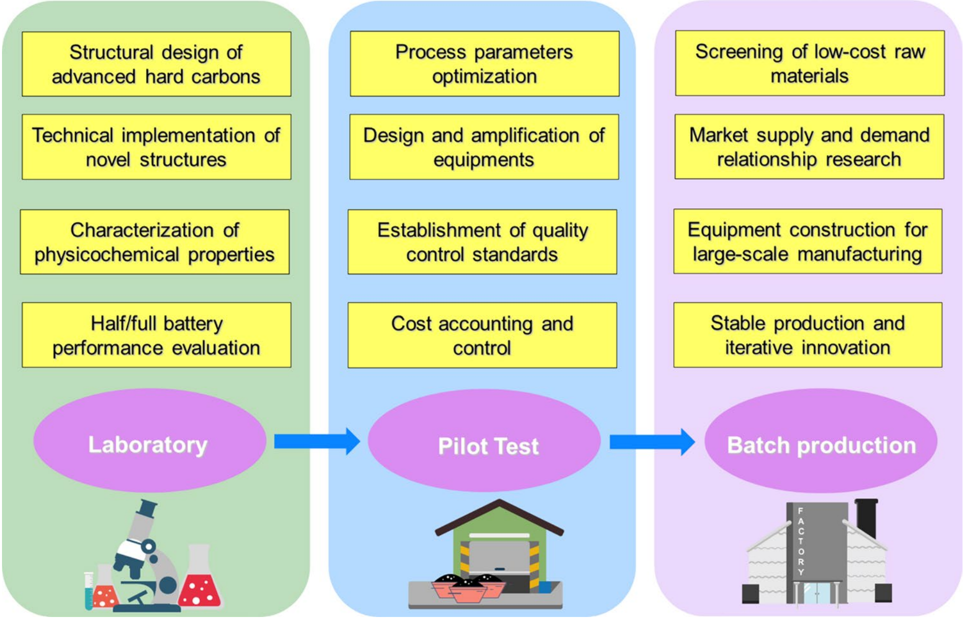

Fig. 21 Outlook on hard carbon moving from laboratory to factory

This approach minimizes uncontrollable factors during the evolution of hard carbon, promoting our understanding of structural evolution during pyrolysis and enabling precise design of hard carbon structures by leveraging the properties of certain structures that do not collapse upon carbonization. Future research should focus on rational precursor design to reduce uncontrollable factors in hard carbon synthesis, leading to more regular and uniform hard carbon materials.

In terms of the practical applications of hard carbon, significant advancements are still required (Fig. 21). Beyond optimizing hard carbon structures and performance, future considerations will also include the actual production and practical utilization of these materials. The lithium-ion battery system based on graphite cannot be fully applicable to hard carbon. Further development is needed for emerging energy technologies, such as SIBs and PIBs. Future research in hard carbon should prioritize enhancing performance and expanding its use across various energy storage systems.

In summary, advancing hard carbon involves not only exploring and refining its structural design but also transitioning from laboratory-scale synthesis to industrial production. For successful commercialization, it is crucial to balance the development of high-performance synthesis methods with considerations of cost and practical implementation. This includes focusing on cost-effective structural regulation strategies, utilizing low-cost precursors such as anthracite and asphalt, and developing low-cost resin-based and biomass-based materials to achieve widespread commercialization of hard carbon.

Acknowledgements This work was supported by the National Natural Science Foundation of China (Grant Nos. 92372101, 52122211, 52072323 and 21875155), the Fundamental Research Funds for the Central Universities (No. 20720220010), the National Key Research and Development Program of China (No. 2021YFA1201502), the Frontier Exploration Projects of Longmen Laboratory (grant No. LMQYTSKT008) and the Shenzhen Technical Plan Project (No. JCYJ20220818101003008). L. Zhang and Q. B. Zhang acknowledge the support of Nanqiang Young Top-notch Talent Fellowship in Xiamen University. We also thank Prof. Zhaowu Tian in Department of Chemistry, Xiamen University for his helpful guidance.

Declarations

Conflict of interest The authors declare no competing interests.

References

1. Franklin, R.E.: Crystallite growth in graphitizing and non-graphitizing carbons. Proc. R. Soc. Lond. A **209**, 196–218 (1951). https://doi.org/10.1098/rspa.1951.0197
2. Tang, Z., Zhou, S.Y., Huang, Y.C., et al.: Improving the initial coulombic efficiency of carbonaceous materials for Li/Na-ion batteries: origins, solutions, and perspectives. Electrochem. Energy Rev. **6**, 8 (2023). https://doi.org/10.1007/s41918-022-00178-y
3. Harris, P.J.F.: Rosalind Franklin's work on coal, carbon, and graphite. Interdiscip. Sci. Rev. **26**, 204–210 (2001). https://doi.org/10.1179/030801801679467
4. Franklin, R.E.: The interpretation of diffuse X-ray diagrams of carbon. Acta Crystallogr. **3**, 107–121 (1950). https://doi.org/10.1107/s0365110x50000264
5. Xie, L.J., Tang, C., Bi, Z.H., et al.: Hard carbon anodes for next-generation Li-ion batteries: review and perspective. Adv. Energy Mater. **11**, 2101650 (2021). https://doi.org/10.1002/aenm.202101650
6. Dou, X.W., Hasa, I., Saurel, D., et al.: Hard carbons for sodium-ion batteries: structure, analysis, sustainability, and electrochemistry. Mater. Today **23**, 87–104 (2019). https://doi.org/10.1016/j.mattod.2018.12.040
7. Mauger, A., Julien, C.M., Goodenough, J.B., et al.: Tribute to Michel armand: from rocking chair–Li-ion to solid-state lithium batteries. J. Electrochem. Soc. **167**, 070507 (2020). https://doi.org/10.1149/2.0072007jes
8. Zhang, H., Li, C.M., Eshetu, G.G., et al.: From solid-solution electrodes and the rocking-chair concept to today's batteries. Angew. Chem. Int. Ed. **59**, 534–538 (2020). https://doi.org/10.1002/anie.201913923
9. Xie, J., Lu, Y.C.: A retrospective on lithium-ion batteries. Nat. Commun. **11**, 2499 (2020). https://doi.org/10.1038/s41467-020-16259-9
10. Yao, Y.X., Yan, C., Zhang, Q.: Emerging interfacial chemistry of graphite anodes in lithium-ion batteries. Chem. Commun. **56**, 14570–14584 (2020). https://doi.org/10.1039/d0cc05084a
11. Megahed, S., Ebner, W.: Lithium-ion battery for electronic applications. J. Power Sources **54**, 155–162 (1995). https://doi.org/10.1016/0378-7753(94)02059-c
12. Cao, W.J., Zheng, J.S., Adams, D., et al.: Comparative study of the power performance for advanced Li-ion capacitors with various carbon anodes. ECS Trans. **61**, 37–48 (2014). https://doi.org/10.1149/06118.0037ecst
13. Bashir, T., Zhou, S.W., Yang, S.Q., et al.: Progress in 3D-MXene electrodes for lithium/sodium/potassium/magnesium/zinc/aluminum-ion batteries. Electrochem. Energy Rev. **6**, 5 (2023). https://doi.org/10.1007/s41918-022-00174-2
14. Stevens, D.A., Dahn, J.R.: The mechanisms of lithium and sodium insertion in carbon materials. J. Electrochem. Soc. **148**, A803 (2001). https://doi.org/10.1149/1.1379565
15. Ge, P., Fouletier, M.: Electrochemical intercalation of sodium in graphite. Solid State Ion. **28–30**, 1172–1175 (1988). https://doi.org/10.1016/0167-2738(88)90351-7
16. Vaalma, C., Buchholz, D., Weil, M., et al.: A cost and resource analysis of sodium-ion batteries. Nat. Rev. Mater. **3**, 18013 (2018)
17. Dubois, M., Billaud, D.: Solid state electrochemical intercalation of lithium and sodium ions into polyparaphenylene. J. Solid State Chem. **127**, 123–125 (1996). https://doi.org/10.1006/jssc.1996.0365
18. Stevens, D.A., Dahn, J.R.: High capacity anode materials for rechargeable sodium-ion batteries. J. Electrochem. Soc. **147**, 1271 (2000). https://doi.org/10.1149/1.1393348
19. Chen, D.Q., Zhang, W., Luo, K.Y., et al.: Hard carbon for sodium storage: mechanism and optimization strategies toward commercialization. Energy Environ. Sci. **14**, 2244–2262 (2021). https://doi.org/10.1039/d0ee03916k
20. Chu, Y., Zhang, J., Zhang, Y.B., et al.: Reconfiguring hard carbons with emerging sodium-ion batteries: a perspective. Adv. Mater. **35**, 2212186 (2023). https://doi.org/10.1002/adma.202212186
21. He, H.N., He, J., Yu, H.B., et al.: Dual-interfering chemistry for soft-hard carbon translation toward fast and durable sodium

storage. Adv. Energy Mater. **13**, 2300357 (2023). https://doi.org/10.1002/aenm.202300357
22. Guo, Z.Y., Xu, Z., Xie, F., et al.: Investigating the superior performance of hard carbon anodes in sodium-ion compared with lithium- and potassium-ion batteries. Adv. Mater. **35**, 2304091 (2023). https://doi.org/10.1002/adma.202304091
23. Yu, Z.L., Chen, C.S., Liu, Q., et al.: Discovering the pore-filling of potassium ions in hard carbon anodes: revisit the low-voltage region. Energy Storage Mater. **60**, 102805 (2023). https://doi.org/10.1016/j.ensm.2023.102805
24. Lu, Z.X., Wang, J., Feng, W.L., et al.: Zinc single-atom-regulated hard carbons for high-rate and low-temperature sodium-ion batteries. Adv. Mater. **35**, 2211461 (2023). https://doi.org/10.1002/adma.202211461
25. Jian, Z.L., Xing, Z.Y., Bommier, C., et al.: Hard carbon microspheres: potassium-ion anode versus sodium-ion anode. Adv. Energy Mater. **6**, 1501874 (2016). https://doi.org/10.1002/aenm.201501874
26. Kim, H., Hyun, J.C., Jung, J.I., et al.: Potassium-ion storage behavior of microstructure-engineered hard carbons. J. Mater. Chem. A **10**, 2055–2063 (2022). https://doi.org/10.1039/d1ta08981a
27. Zhong, L., Zhang, W.L., Sun, S.R., et al.: Engineering of the crystalline lattice of hard carbon anodes toward practical potassium-ion batteries. Adv. Funct. Mater. **33**, 2211872 (2022). https://doi.org/10.1002/adfm.202211872
28. Lei, H., Li, J.L., Zhang, X.Y., et al.: A review of hard carbon anode: rational design and advanced characterization in potassium ion batteries. InfoMat **4**, e12272 (2022). https://doi.org/10.1002/inf2.12272
29. Feng, X., Li, Y., Li, Y., et al.: Unlocking the local structure of hard carbon to grasp sodium-ion diffusion behavior for advanced sodium-ion batteries. Energy Environ. Sci. **17**, 1387–1396 (2024). https://doi.org/10.1039/d3ee03347c
30. Li, Y.M., Hu, Y.S., Titirici, M.M., et al.: Hard carbon microtubes made from renewable cotton as high-performance anode material for sodium-ion batteries. Adv. Energy Mater. **6**, 1600659 (2016). https://doi.org/10.1002/aenm.201600659
31. Huang, Y.J., Zhong, X., Hu, X.Y., et al.: Rationally designing closed pore structure by carbon dots to evoke sodium storage sites of hard carbon in low-potential region. Adv. Funct. Mater. **34**, 2308392 (2023). https://doi.org/10.1002/adfm.202308392
32. Tennison, S: Book review: Harry Marsh, Francisco Rodríguez Reinoso, 2006. Activated Carbon. Elseiver. 554 p., price GBP 115, $195 USD, EUR 175. Carbon **46**, 1626–1626 (2008). https://doi.org/10.1016/j.carbon.2008.06.024
33. Piotrowska, A., Kierzek, K., Rutkowski, P., et al.: Properties and lithium insertion behavior of hard carbons produced by pyrolysis of various polymers at 1000 °C. J. Anal. Appl. Pyrolysis **102**, 1–6 (2013). https://doi.org/10.1016/j.jaap.2013.04.011
34. Barr, J.B., Lewis, I.C.: Chemical changes during the mild air oxidation of pitch. Carbon **16**, 439–444 (1978). https://doi.org/10.1016/0008-6223(78)90090-8
35. Fromm, O., Heckmann, A., Rodehorst, U.C., et al.: Carbons from biomass precursors as anode materials for lithium ion batteries: new insights into carbonization and graphitization behavior and into their correlation to electrochemical performance. Carbon **128**, 147–163 (2018). https://doi.org/10.1016/j.carbon.2017.11.065
36. Wahid, M., Gawli, Y., Puthusseri, D., et al.: Nutty carbon: morphology replicating hard carbon from walnut shell for Na ion battery anode. ACS Omega **2**, 3601–3609 (2017). https://doi.org/10.1021/acsomega.7b00633
37. Li, H.B., Shen, F., Luo, W., et al.: Carbonized-leaf membrane with anisotropic surfaces for sodium-ion battery. ACS Appl. Mater. Interfaces **8**, 2204–2210 (2016). https://doi.org/10.1021/acsami.5b10875
38. Tang, Z., Zhang, R., Wang, H.Y., et al.: Revealing the closed pore formation of waste wood-derived hard carbon for advanced sodium-ion battery. Nat. Commun. **14**, 6024 (2023). https://doi.org/10.1038/s41467-023-39637-5
39. Du, Y.F., Sun, G.H., Li, Y., et al.: Pre-oxidation of lignin precursors for hard carbon anode with boosted lithium-ion storage capacity. Carbon **178**, 243–255 (2021). https://doi.org/10.1016/j.carbon.2021.03.016
40. Yin, X.P., Zhao, Y.F., Wang, X., et al.: Modulating the graphitic domains of hard carbons derived from mixed pitch and resin to achieve high rate and stable sodium storage. Small **18**, 2105568 (2022). https://doi.org/10.1002/smll.202105568
41. Xie, L.J., Tang, C., Song, M.X., et al.: Molecular-scale controllable conversion of biopolymers into hard carbons towards lithium and sodium ion batteries: a review. J. Energy Chem. **72**, 554–569 (2022). https://doi.org/10.1016/j.jechem.2022.05.006
42. Saurel, D., Orayech, B., Xiao, B.W., et al.: From charge storage mechanism to performance: a roadmap toward high specific energy sodium-ion batteries through carbon anode optimization. Adv. Energy Mater. **8**, 1703268 (2018). https://doi.org/10.1002/aenm.201703268
43. Zhang, B., Zhang, R.W., Yin, X.Q., et al.: Inhibitory activities of some traditional Chinese herbs against testosterone 5α-reductase and effects of Cacumen platycladi on hair re-growth in testosterone-treated mice. J. Ethnopharmacol. **177**, 1–9 (2016). https://doi.org/10.1016/j.jep.2015.11.012
44. Xing, W.B., Xue, J.S., Zheng, T., et al.: Correlation between lithium intercalation capacity and microstructure in hard carbons. J. Electrochem. Soc. **143**, 3482–3491 (1996). https://doi.org/10.1149/1.1837241
45. He, X.X., Lai, W.H., Liang, Y.R., et al.: Achieving all-plateau and high-capacity sodium insertion in topological graphitized carbon. Adv. Mater. **35**, 2302613 (2023). https://doi.org/10.1002/adma.202302613
46. Xu, T.Y., Qiu, X., Zhang, X., et al.: Regulation of surface oxygen functional groups and pore structure of bamboo-derived hard carbon for enhanced sodium storage performance. Chem. Eng. J. **452**, 139514 (2023). https://doi.org/10.1016/j.cej.2022.139514
47. Nazri, G.A., Pistoia, G.: Lithium Batteries: Science and Technology. Springer Science & Business Media, Berlin (2008)
48. Edwards, I.A., Marsh, H., Menendez, R.: Introduction to Carbon Science. Butterworth-Heinemann, Oxford (2013)
49. Surta, T.W., Koh, E., Li, Z.F., et al.: Combining experimental and theoretical techniques to gain an atomic level understanding of the defect binding mechanism in hard carbon anodes for sodium ion batteries. Adv. Energy Mater. **12**, 2200647 (2022). https://doi.org/10.1002/aenm.202200647
50. Yang, Y.R., Wu, C., He, X.X., et al.: Boosting the development of hard carbon for sodium-ion batteries: strategies to optimize the initial coulombic efficiency. Adv. Funct. Mater. **34**, 2302277 (2023). https://doi.org/10.1002/adfm.202302277
51. Raccichini, R., Varzi, A., Passerini, S., et al.: The role of graphene for electrochemical energy storage. Nat. Mater. **14**, 271–279 (2015). https://doi.org/10.1038/nmat4170
52. Olsson, E., Cottom, J., Cai, Q.: Defects in hard carbon: where are they located and how does the location affect alkaline metal storage? Small **17**, 2007652 (2021). https://doi.org/10.1002/smll.202007652
53. Lu, Z.Y., Yang, H.J., Guo, Y., et al.: Consummating ion desolvation in hard carbon anodes for reversible sodium storage. Nat. Commun. **15**, 3497 (2024). https://doi.org/10.1038/s41467-024-47522-y

54. Vijaya Kumar Saroja, A.P., Wang, Z.P., Tinker, H.R., et al.: Enabling intercalation-type $TiNb_{24}O_{62}$ anode for sodium- and potassium-ion batteries via a synergetic strategy of oxygen vacancy and carbon incorporation. Sus. Mat. **3**, 222–234 (2023). https://doi.org/10.1002/sus2.113
55. Saju, S.K., Chattopadhyay, S., Xu, J.N., et al.: Hard carbon anode for lithium-, sodium-, and potassium-ion batteries: advancement and future perspective. Cell Rep. Phys. Sci. **5**, 101851 (2024). https://doi.org/10.1016/j.xcrp.2024.101851
56. Harris, P.J.F.: New perspectives on the structure of graphitic carbons. Crit. Rev. Solid State Mater. Sci. **30**, 235–253 (2005). https://doi.org/10.1080/10408430500406265
57. Dahn, J.R., Zheng, T., Liu, Y.H., et al.: Mechanisms for lithium insertion in carbonaceous materials. Science **270**, 590–593 (1995). https://doi.org/10.1126/science.270.5236.590
58. Cai, C.C., Chen, Y.A., Hu, P., et al.: Regulating the interlayer spacings of hard carbon nanofibers enables enhanced pore filling sodium storage. Small **18**, 2105303 (2022). https://doi.org/10.1002/smll.202105303
59. Qiu, S., Xiao, L.F., Sushko, M.L., et al.: Manipulating adsorption–insertion mechanisms in nanostructured carbon materials for high-efficiency sodium ion storage. Adv. Energy Mater. **7**, 1700403 (2017). https://doi.org/10.1002/aenm.201700403
60. Sun, N., Guan, Z., Liu, Y.W., et al.: Sodium storage mechanism: extended "adsorption–insertion" model: a new insight into the sodium storage mechanism of hard carbons. Adv. Energy Mater. **9**, 1970125 (2019). https://doi.org/10.1002/aenm.201970125
61. Zhao, L.F., Hu, Z., Lai, W.H., et al.: Hard carbon anodes: fundamental understanding and commercial perspectives for Na-ion batteries beyond Li-ion and K-ion counterparts. Adv. Energy Mater. **11**, 2002704 (2020). https://doi.org/10.1002/aenm.202002704
62. Buiel, E.R., George, A.E., Dahn, J.R.: Model of micropore closure in hard carbon prepared from sucrose. Carbon **37**, 1399–1407 (1999). https://doi.org/10.1016/s0008-6223(98)00335-2
63. Au, H., Alptekin, H., Jensen, A.C.S., et al.: A revised mechanistic model for sodium insertion in hard carbons. Energy Environ. Sci. **13**, 3469–3479 (2020). https://doi.org/10.1039/d0ee01363c
64. Li, Q., Zhang, J., Zhong, L.X., et al.: Unraveling the key atomic interactions in determining the varying Li/Na/K storage mechanism of hard carbon anodes. Adv. Energy Mater. **12**, 2201734 (2022). https://doi.org/10.1002/aenm.202201734
65. Zheng, Z., Hu, S.J., Yin, W.J., et al.: CO_2-etching creates abundant closed pores in hard carbon for high-plateau-capacity sodium storage. Adv. Energy Mater. **14**, 2303064 (2024). https://doi.org/10.1002/aenm.202303064
66. Ji, W.J., Yi, Z.L., Song, M.X., et al.: Free radicals trigger the closure of open pores in lignin-derived hard carbons toward improved sodium-storage capacity. J. Energy Chem. **94**, 551–559 (2024). https://doi.org/10.1016/j.jechem.2024.02.048
67. Jia, X.B., Wang, J.Q., Liu, Y.F., et al.: Facilitating layered oxide cathodes based on orbital hybridization for sodium-ion batteries: marvelous air stability, controllable high voltage, and anion redox chemistry. Adv. Mater. **36**, 2307938 (2024). https://doi.org/10.1002/adma.202307938
68. Su, Y., Johannessen, B., Zhang, S.L., et al.: Soft-rigid heterostructures with functional cation vacancies for fast-charging and high-capacity sodium storage. Adv. Mater. **35**, 2305149 (2023). https://doi.org/10.1002/adma.202305149
69. Wang, J.Q., Zhu, Y.F., Su, Y., et al.: Routes to high-performance layered oxide cathodes for sodium-ion batteries. Chem. Soc. Rev. **53**, 4230–4301 (2024). https://doi.org/10.1039/d3cs00929g
70. Chen, X.Y., Tian, J.Y., Li, P., et al.: An overall understanding of sodium storage behaviors in hard carbons by an "adsorption-intercalation/filling" hybrid mechanism. Adv. Energy Mater. **12**, 2200886 (2022). https://doi.org/10.1002/aenm.202200886
71. Wu, J.B., Lin, M.L., Cong, X., et al.: Raman spectroscopy of graphene-based materials and its applications in related devices. Chem. Soc. Rev. **47**, 1822–1873 (2018). https://doi.org/10.1039/c6cs00915h
72. He, X.X., Zhao, J.H., Lai, W.H., et al.: Soft-carbon-coated, free-standing, low-defect, hard-carbon anode to achieve a 94% initial coulombic efficiency for sodium-ion batteries. ACS Appl. Mater. Interfaces **13**, 44358–44368 (2021). https://doi.org/10.1021/acsami.1c12171
73. Li, D.H., Jia, Y., Chang, G.J., et al.: A defect-driven metal-free electrocatalyst for oxygen reduction in acidic electrolyte. Chem **4**, 2345–2356 (2018). https://doi.org/10.1016/j.chempr.2018.07.005
74. Jia, Y., Zhang, L.Z., Zhuang, L.Z., et al.: Identification of active sites for acidic oxygen reduction on carbon catalysts with and without nitrogen doping. Nat. Catal. **2**, 688–695 (2019). https://doi.org/10.1038/s41929-019-0297-4
75. Kubota, K., Shimadzu, S., Yabuuchi, N., et al.: Structural analysis of sucrose-derived hard carbon and correlation with the electrochemical properties for lithium, sodium, and potassium insertion. Chem. Mater. **32**, 2961–2977 (2020). https://doi.org/10.1021/acs.chemmater.9b05235
76. Daiyan, R., Tan, X., Chen, R., et al.: Electroreduction of CO_2 to CO on a mesoporous carbon catalyst with progressively removed nitrogen moieties. ACS Energy Lett. **3**, 2292–2298 (2018). https://doi.org/10.1021/acsenergylett.8b01409
77. Wang, B., Yao, Y.Z., Wang, W.L., et al.: Identifying the plateau sodium storage behavior of hard carbon through the spin state. Chem. Eng. J. **488**, 151055 (2024). https://doi.org/10.1016/j.cej.2024.151055
78. Wang, B., Fitzpatrick, J.R., Brookfield, A., et al.: Electron paramagnetic resonance as a tool to determine the sodium charge storage mechanism of hard carbon. Nat. Commun. **15**, 3013 (2024). https://doi.org/10.1038/s41467-024-45460-3
79. Bommier, C., Mitlin, D., Ji, X.L.: Internal structure–Na storage mechanisms–electrochemical performance relations in carbons. Prog. Mater. Sci. **97**, 170–203 (2018). https://doi.org/10.1016/j.pmatsci.2018.04.006
80. Zhang, T., Mao, J., Liu, X.L., et al.: Pinecone biomass-derived hard carbon anodes for high-performance sodium-ion batteries. RSC Adv. **7**, 41504–41511 (2017). https://doi.org/10.1039/c7ra07231g
81. Liu, Y.D., Watanasiri, S.: Representation of liquid-liquid equilibrium of mixed-solvent electrolyte systems using the extended electrolyte NRTL model. Fluid Phase Equilib. **116**, 193–200 (1996). https://doi.org/10.1016/0378-3812(95)02887-0
82. Stratford, J.M., Kleppe, A.K., Keeble, D.S., et al.: Correlating local structure and sodium storage in hard carbon anodes: Insights from pair distribution function analysis and solid-state NMR. J. Am. Chem. Soc. **143**, 14274–14286 (2021). https://doi.org/10.1021/jacs.1c06058
83. Sun, N., Qiu, J.S., Xu, B.: Understanding of sodium storage mechanism in hard carbons: ongoing development under debate. Adv. Energy Mater. **12**, 2200715 (2022). https://doi.org/10.1002/aenm.202200715
84. Chen, C., Huang, Y., Zhu, Y.D., et al.: Nonignorable influence of oxygen in hard carbon for sodium ion storage. ACS Sustain. Chem. Eng. **8**, 1497–1506 (2020). https://doi.org/10.1021/acssuschemeng.9b05948
85. Lotfabad, E.M., Ding, J., Cui, K., et al.: High-density sodium and lithium ion battery anodes from banana peels. ACS Nano **8**, 7115–7129 (2014). https://doi.org/10.1021/nn502045y

86. Shi, L., Liu, W., Zhao, F.J., et al.: Tailoring the dual precursors coupled hard carbon by embedding the pitch-derived graphitic domains to achieve high-performance sodium storage. J. Power Sources **596**, 234093 (2024). https://doi.org/10.1016/j.jpowsour.2024.234093
87. Saurel, D., Segalini, J., Jauregui, M., et al.: A SAXS outlook on disordered carbonaceous materials for electrochemical energy storage. Energy Storage Mater. **21**, 162–173 (2019). https://doi.org/10.1016/j.ensm.2019.05.007
88. Kaskhedikar, N.A., Maier, J.: Lithium storage in carbon nanostructures. Adv. Mater. **21**, 2664–2680 (2009). https://doi.org/10.1002/adma.200901079
89. Hou, H.S., Qiu, X.Q., Wei, W.F., et al.: Carbon anode materials for advanced sodium-ion batteries. Adv. Energy Mater. **7**, 1602898 (2017). https://doi.org/10.1002/aenm.201602898
90. Huang, S.F., Li, Z.P., Wang, B., et al.: N-doping and defective nanographitic domain coupled hard carbon nanoshells for high performance lithium/sodium storage. Adv. Funct. Mater. **28**, 1706294 (2018). https://doi.org/10.1002/adfm.201706294
91. Alvin, S., Cahyadi, H.S., Hwang, J., et al.: Revealing the intercalation mechanisms of lithium, sodium, and potassium in hard carbon. Adv. Energy Mater. **10**, 2000283 (2020). https://doi.org/10.1002/aenm.202000283
92. Li, W.B., Chen, M.M., Wang, C.Y.: Spherical hard carbon prepared from potato starch using as anode material for Li-ion batteries. Mater. Lett. **65**, 3368–3370 (2011). https://doi.org/10.1016/j.matlet.2011.07.072
93. Fujimoto, H., Tokumitsu, K., Mabuchi, A., et al.: The anode performance of the hard carbon for the lithium ion battery derived from the oxygen-containing aromatic precursors. J. Power Sources **195**, 7452–7456 (2010). https://doi.org/10.1016/j.jpowsour.2010.05.041
94. Han, Y.J., Chung, D., Nakabayashi, K., et al.: Effect of heat pretreatment conditions on the electrochemical properties of mangrove wood-derived hard carbon as an effective anode material for lithium-ion batteries. Electrochim. Acta **213**, 432–438 (2016). https://doi.org/10.1016/j.electacta.2016.07.138
95. Chang, Z.Z., Yu, B.J., Wang, C.Y.: Influence of H_2 reduction on lignin-based hard carbon performance in lithium ion batteries. Electrochim. Acta **176**, 1352–1357 (2015). https://doi.org/10.1016/j.electacta.2015.07.076
96. Xing, W.B., Dahn, J.R.: Study of irreversible capacities for Li insertion in hard and graphitic carbons. J. Electrochem. Soc. **144**, 1195–1201 (1997). https://doi.org/10.1149/1.1837572
97. Hu, L.F., Cheng, G., Ren, J.R., et al.: Conformal carbon coating on hard carbon anode derived from propionaldehyde for exellent performance of lithium-ion batteries. Int. J. Electrochem. Sci. **14**, 2804–2814 (2019). https://doi.org/10.20964/2019.03.75
98. Ni, J.F., Huang, Y.Y., Gao, L.J.: A high-performance hard carbon for Li-ion batteries and supercapacitors application. J. Power Sources **223**, 306–311 (2013). https://doi.org/10.1016/j.jpowsour.2012.09.047
99. Li, L.F., Fan, C.L., Zeng, B., et al.: Effect of pyrolysis temperature on lithium storage performance of pyrolitic-PVDF coated hard carbon derived from cellulose. Mater. Chem. Phys. **242**, 122380 (2020). https://doi.org/10.1016/j.matchemphys.2019.122380
100. Väli, R., Jänes, A., Thomberg, T., et al.: Synthesis and characterization of d-glucose derived nanospheric hard carbon negative electrodes for lithium- and sodium-ion batteries. Electrochim. Acta **253**, 536–544 (2017). https://doi.org/10.1016/j.electacta.2017.09.094
101. Tai, C.W., Jao, W.Y., Tseng, L.C., et al.: Lithium-ion storage mechanism in closed pore-rich hard carbon with ultrahigh extra plateau capacity. J. Mater. Chem. A **11**, 19669–19684 (2023). https://doi.org/10.1039/d3ta03855f
102. Wang, K., Xu, Y.B., Wu, H., et al.: A hybrid lithium storage mechanism of hard carbon enhances its performance as anodes for lithium-ion batteries. Carbon **178**, 443–450 (2021). https://doi.org/10.1016/j.carbon.2020.11.095
103. Kim, Y.J., Yang, H., Yoon, S.H., et al.: Anthracite as a candidate for lithium ion battery anode. J. Power Sources **113**, 157–165 (2003). https://doi.org/10.1016/s0378-7753(02)00528-1
104. Balasubramaniam, S., Mohanty, A., Balasingam, S.K., et al.: Comprehensive insight into the mechanism, material selection and performance evaluation of supercapatteries. Nano Micro Lett. **12**, 85 (2020). https://doi.org/10.1007/s40820-020-0413-7
105. Song, H.B., Na, R., Hong, C.Y., et al.: In situ measurement and mechanism analysis of the lithium storage behavior of graphene electrodes. Carbon **188**, 146–154 (2022). https://doi.org/10.1016/j.carbon.2021.11.066
106. Yang, G.J., Li, X.Y., Guan, Z., et al.: Insights into lithium and sodium storage in porous carbon. Nano Lett. **20**, 3836–3843 (2020). https://doi.org/10.1021/acs.nanolett.0c00943
107. Kandambeth, S., Jia, J.T., Wu, H., et al.: Covalent organic frameworks as negative electrodes for high-performance asymmetric supercapacitors. Adv. Energy Mater. **10**, 2001673 (2020). https://doi.org/10.1002/aenm.202001673
108. Zhang, X.X., Qu, H.N., Ji, W.X., et al.: Fast and controllable prelithiation of hard carbon anodes for lithium-ion batteries. ACS Appl. Mater. Interfaces **12**, 11589–11599 (2020). https://doi.org/10.1021/acsami.9b21417
109. Zheng, T., McKinnon, W.R., Dahn, J.R.: Hysteresis during lithium insertion in hydrogen-containing carbons. J. Electrochem. Soc. **143**, 2137–2145 (1996). https://doi.org/10.1149/1.1836972
110. Wang, N., Liu, Q.L., Sun, B.Y., et al.: N-doped catalytic graphitized hard carbon for high-performance lithium/sodium-ion batteries. Sci. Rep. **8**, 9934 (2018). https://doi.org/10.1038/s41598-018-28310-3
111. Sole, C., Drewett, N.E., Hardwick, L.J.: In situ Raman study of lithium-ion intercalation into microcrystalline graphite. Faraday Discuss. **172**, 223–237 (2014). https://doi.org/10.1039/c4fd00079j
112. Andersen, H.L., Djuandhi, L., Mittal, U., et al.: Strategies for the analysis of graphite electrode function. Adv. Energy Mater. **11**, 2102693 (2021). https://doi.org/10.1002/aenm.202102693
113. Sato, K., Noguchi, M., Demachi, A., et al.: A mechanism of lithium storage in disordered carbons. Science **264**, 556–558 (1994). https://doi.org/10.1126/science.264.5158.556
114. Winter, M., Besenhard, J.O., Spahr, M.E., et al.: Insertion electrode materials for rechargeable lithium batteries. Adv. Mater. **10**, 725–763 (1998). https://doi.org/10.1002/(sici)1521-4095(199807)10:10725:aid-adma725%3e3.0.co;2-z
115. Gotoh, K., Yamakami, T., Nishimura, I., et al.: Mechanisms for overcharging of carbon electrodes in lithium-ion/sodium-ion batteries analysed by operando solid-state NMR. J. Mater. Chem. A **8**, 14472–14481 (2020). https://doi.org/10.1039/d0ta04005c
116. Tatsumi, K., Conard, J., Nakahara, M., et al.: ^{7}Li NMR studies on a lithiated non-graphitizable carbon fibre at low temperatures. Chem. Commun., 687–688 (1997). https://doi.org/10.1039/a700221a
117. Kudo, H.: The nature of bonding of hyperlithiated molecules beyond the octet rule. J. Nucl. Radiochem. Sci. **2**, R13–R21 (2001). https://doi.org/10.14494/jnrs2000.2.r13
118. Bommier, C., Surta, T.W., Dolgos, M., et al.: New mechanistic insights on Na-ion storage in nongraphitizable carbon. Nano Lett. **15**, 5888–5892 (2015). https://doi.org/10.1021/acs.nanolett.5b01969
119. Li, Y.Q., Vasileiadis, A., Zhou, Q., et al.: Origin of fast charging in hard carbon anodes. Nat. Energy **9**, 134–142 (2024). https://doi.org/10.1038/s41560-023-01414-5

120. Kumaresan, T.K., Masilamani, S.A., Raman, K., et al.: High performance sodium-ion battery anode using biomass derived hard carbon with engineered defective sites. Electrochim. Acta **368**, 137574 (2021). https://doi.org/10.1016/j.electacta.2020.137574
121. Zhang, N., Liu, Q., Chen, W.L., et al.: High capacity hard carbon derived from lotus stem as anode for sodium ion batteries. J. Power Sources **378**, 331–337 (2018). https://doi.org/10.1016/j.jpowsour.2017.12.054
122. Qin, D.C., Zhang, F., Dong, S.Y., et al.: Analogous graphite carbon sheets derived from corn stalks as high performance sodium-ion battery anodes. RSC Adv. **6**, 106218–106224 (2016). https://doi.org/10.1039/c6ra22769d
123. Wang, K., Jin, Y., Sun, S.X., et al.: Low-cost and high-performance hard carbon anode materials for sodium-ion batteries. ACS Omega **2**, 1687–1695 (2017). https://doi.org/10.1021/acsomega.7b00259
124. Wang, C.W., Huang, J.F., Qi, H., et al.: Controlling pseudographtic domain dimension of dandelion derived biomass carbon for excellent sodium-ion storage. J. Power Sources **358**, 85–92 (2017). https://doi.org/10.1016/j.jpowsour.2017.05.011
125. Zhu, Y.E., Gu, H.C., Chen, Y.N., et al.: Hard carbon derived from corn straw piths as anode materials for sodium ion batteries. Ionics **24**, 1075–1081 (2018)
126. Wang, P.Z., Zhu, X.S., Wang, Q.Q., et al.: Kelp-derived hard carbons as advanced anode materials for sodium-ion batteries. J. Mater. Chem. A **5**, 5761–5769 (2017). https://doi.org/10.1039/c7ta00639j
127. Wu, F., Liu, L., Yuan, Y.F., et al.: Expanding interlayer spacing of hard carbon by natural K^+ doping to boost Na-ion storage. ACS Appl. Mater. Interfaces **10**, 27030–27038 (2018). https://doi.org/10.1021/acsami.8b08380
128. Yang, B., Wang, J., Zhu, Y.Y., et al.: Engineering hard carbon with high initial coulomb efficiency for practical sodium-ion batteries. J. Power Sources **492**, 229656 (2021). https://doi.org/10.1016/j.jpowsour.2021.229656
129. Nita, C., Zhang, B., Dentzer, J., et al.: Hard carbon derived from coconut shells, walnut shells, and corn silk biomass waste exhibiting high capacity for Na-ion batteries. J. Energy Chem. **58**, 207–218 (2021). https://doi.org/10.1016/j.jechem.2020.08.065
130. Guo, S., Chen, Y.M., Tong, L.P., et al.: Biomass hard carbon of high initial coulombic efficiency for sodium-ion batteries: preparation and application. Electrochim. Acta **410**, 140017 (2022). https://doi.org/10.1016/j.electacta.2022.140017
131. Wang, J., Yan, L., Ren, Q.J., et al.: Facile hydrothermal treatment route of reed straw-derived hard carbon for high performance sodium ion battery. Electrochim. Acta **291**, 188–196 (2018). https://doi.org/10.1016/j.electacta.2018.08.136
132. Wang, Q.Q., Zhu, X.S., Liu, Y.H., et al.: Rice husk-derived hard carbons as high-performance anode materials for sodium-ion batteries. Carbon **127**, 658–666 (2018). https://doi.org/10.1016/j.carbon.2017.11.054
133. Wang, Y.S., Feng, Z.M., Zhu, W., et al.: High capacity and high efficiency maple tree-biomass-derived hard carbon as an anode material for sodium-ion batteries. Materials **11**, 1294 (2018). https://doi.org/10.3390/ma11081294
134. Zhu, X.M., Li, Q., Qiu, S., et al.: Hard carbon fibers pyrolyzed from wool as high-performance anode for sodium-ion batteries. JOM **68**, 2579–2584 (2016). https://doi.org/10.1007/s11837-016-2064-1
135. Kamiyama, A., Kubota, K., Igarashi, D., et al.: MgO-template synthesis of extremely high capacity hard carbon for Na-ion battery. Angew. Chem. Int. Ed. **60**, 5114–5120 (2021). https://doi.org/10.1002/anie.202013951
136. Igarashi, D., Tanaka, Y., Kubota, K., et al.: New template synthesis of anomalously large capacity hard carbon for Na- and K-ion batteries. Adv. Energy Mater. **13**, 2302647 (2023). https://doi.org/10.1002/aenm.202302647
137. Chen, R., Li, X.Y., Cai, C.C., et al.: Amine–aldehyde condensation-derived N-doped hard carbon microspheres for high-capacity and robust sodium storage. Small **19**, 2303790 (2023). https://doi.org/10.1002/smll.202303790
138. Lu, Y.X., Zhao, C.L., Qi, X.G., et al.: Pre-oxidation-tuned microstructures of carbon anodes derived from pitch for enhancing Na storage performance. Adv. Energy Mater. **8**, 1800108 (2018). https://doi.org/10.1002/aenm.201800108
139. Zhang, M., Li, Y., Wu, F., et al.: Boost sodium-ion batteries to commercialization: strategies to enhance initial coulombic efficiency of hard carbon anode. Nano Energy **82**, 105738 (2020). https://doi.org/10.1016/j.nanoen.2020.105738
140. Komaba, S., Murata, W., Ishikawa, T., et al.: Electrochemical Na insertion and solid electrolyte interphase for hard-carbon electrodes and application to Na-ion batteries. Adv. Funct. Mater. **21**, 3859–3867 (2011). https://doi.org/10.1002/adfm.201100854
141. Lu, Y., Lu, Y.Y., Niu, Z.Q., et al.: Graphene-based nanomaterials for sodium-ion batteries. Adv. Energy Mater. **8**, 1702469 (2018). https://doi.org/10.1002/aenm.201702469
142. Anji Reddy, M., Helen, M., Groß, A., et al.: Insight into sodium insertion and the storage mechanism in hard carbon. ACS Energy Lett. **3**, 2851–2857 (2018). https://doi.org/10.1021/acsenergylett.8b01761
143. Zhang, P., Shu, Y.R., Wang, Y., et al.: Simple and efficient synthesis methods for fabricating anode materials of sodium-ion batteries and their sodium-ion storage mechanism study. J. Mater. Chem. A **11**, 2920–2932 (2023). https://doi.org/10.1039/d2ta09051a
144. Li, Z.F., Bommier, C., Chong, Z.S., et al.: Mechanism of Na-ion storage in hard carbon anodes revealed by heteroatom doping. Adv. Energy Mater. **7**, 1602894 (2017). https://doi.org/10.1002/aenm.201602894
145. Li, Y.Q., Lu, Y.X., Adelhelm, P., et al.: Intercalation chemistry of graphite: alkali metal ions and beyond. Chem. Soc. Rev. **48**, 4655–4687 (2019). https://doi.org/10.1039/c9cs00162j
146. Chen, X.Y., Liu, C.Y., Fang, Y.J., et al.: Understanding of the sodium storage mechanism in hard carbon anodes. Carbon Energy **4**, 1133–1150 (2022). https://doi.org/10.1002/cey2.196
147. Wang, Z.H., Feng, X., Bai, Y., et al.: Sodium-ion batteries: probing the energy storage mechanism of quasi-metallic Na in hard carbon for sodium-ion batteries (adv. energy mater. 11/2021). Adv. Energy Mater. **11**, 2170041 (2021). https://doi.org/10.1002/aenm.202170041
148. Kitsu Iglesias, L., Antonio, E.N., Martinez, T.D., et al.: Revealing the sodium storage mechanisms in hard carbon pores. Adv. Energy Mater. **13**, 2302171 (2023). https://doi.org/10.1002/aenm.202302171
149. Morikawa, Y., Nishimura, S.I., Hashimoto, R.I., et al.: Mechanism of sodium storage in hard carbon: an X-ray scattering analysis. Adv. Energy Mater. **10**, 1903176 (2020). https://doi.org/10.1002/aenm.201903176
150. Zhang, K., He, Q., Xiong, F.Y., et al.: Active sites enriched hard carbon porous nanobelts for stable and high-capacity potassium-ion storage. Nano Energy **77**, 105018 (2020). https://doi.org/10.1016/j.nanoen.2020.105018
151. Xu, J., Fan, C.Y., Ou, M.Y., et al.: Correlation between potassium-ion storage mechanism and local structural evolution in hard carbon materials. Chem. Mater. **34**, 4202–4211 (2022). https://doi.org/10.1021/acs.chemmater.2c00646
152. Li, W.T., Li, Z.L., Zhang, C., et al.: Hard carbon derived from rice husk as anode material for high performance potassium-ion batteries. Solid State Ion. **351**, 115319 (2020). https://doi.org/10.1016/j.ssi.2020.115319

153. Yamamoto, H., Muratsubaki, S., Kubota, K., et al.: Synthesizing higher-capacity hard-carbons from cellulose for Na- and K-ion batteries. J. Mater. Chem. A **6**, 16844–16848 (2018). https://doi.org/10.1039/c8ta05203d
154. Kamiyama, A., Kubota, K., Nakano, T., et al.: High-capacity hard carbon synthesized from macroporous phenolic resin for sodium-ion and potassium-ion battery. ACS Appl. Energy Mater. **3**, 135–140 (2020). https://doi.org/10.1021/acsaem.9b01972
155. Zou, J.M., He, C.H., Bao, J.Z., et al.: Hard carbon derived from spent black tea as a high-stability anode for potassium-ion batteries. Ionics **29**, 3517–3523 (2023). https://doi.org/10.1007/s11581-023-05082-z
156. Huang, T., Peng, D.C., Chen, Z., et al.: Microstructures and electrochemical properties of coconut shell-based hard carbons as anode materials for potassium ion batteries. N. Carbon Mater. **37**, 1125–1132 (2022). https://doi.org/10.1016/s1872-5805(21)60069-0
157. He, X.D., Liao, J.Y., Tang, Z.F., et al.: Highly disordered hard carbon derived from skimmed cotton as a high-performance anode material for potassium-ion batteries. J. Power Sources **396**, 533–541 (2018). https://doi.org/10.1016/j.jpowsour.2018.06.073
158. Yang, M.M., Dai, J.Y., He, M.Y., et al.: Biomass-derived carbon from ganoderma lucidum spore as a promising anode material for rapid potassium-ion storage. J. Colloid Interface Sci. **567**, 256–263 (2020). https://doi.org/10.1016/j.jcis.2020.02.023
159. Richard Prabakar, S.J., Han, S.C., Park, C., et al.: Spontaneous formation of interwoven porous channels in hard-wood-based hard-carbon for high-performance anodes in potassium-ion batteries. J. Electrochem. Soc. **164**, A2012–A2016 (2017). https://doi.org/10.1149/2.1251709jes
160. Cao, W., Zhang, E.J., Wang, J., et al.: Potato derived biomass porous carbon as anode for potassium ion batteries. Electrochim. Acta **293**, 364–370 (2019). https://doi.org/10.1016/j.electacta.2018.10.036
161. Zhu, T., Mai, B., Hu, P., et al.: Bagasse-derived hard carbon anode with an adsorption–intercalation mechanism for high-rate potassium storage. ACS Appl. Energy Mater. **6**, 2370–2377 (2023). https://doi.org/10.1021/acsaem.2c03628
162. Gao, C., Wang, Q., Luo, S., et al.: High performance potassium-ion battery anode based on biomorphic N-doped carbon derived from walnut septum. J. Power Sources **415**, 165–171 (2019). https://doi.org/10.1016/j.jpowsour.2019.01.073
163. Katorova, N.S., Fedotov, S.S., Rupasov, D.P., et al.: Effect of concentrated diglyme-based electrolytes on the electrochemical performance of potassium-ion batteries. ACS Appl. Energy Mater. **2**, 6051–6059 (2019). https://doi.org/10.1021/acsaem.9b01173
164. Bin, D.S., Lin, X.J., Sun, Y.G., et al.: Engineering hollow carbon architecture for high-performance K-ion battery anode. J. Am. Chem. Soc. **140**, 7127–7134 (2018). https://doi.org/10.1021/jacs.8b02178
165. Chen, C., Wu, M.Q., Wang, Y.S., et al.: Insights into pseudographite-structured hard carbon with stabilized performance for high energy K-ion storage. J. Power Sources **444**, 227310 (2019). https://doi.org/10.1016/j.jpowsour.2019.227310
166. Vaalma, C., Giffin, G.A., Buchholz, D., et al.: Non-aqueous K-ion battery based on layered $K_{0.3}MnO_2$ and hard carbon/carbon black. J. Electrochem. Soc. **163**, A1295–A1299 (2016). https://doi.org/10.1149/2.0921607jes
167. Li, D.P., Ren, X.H., Ai, Q., et al.: Facile fabrication of nitrogen-doped porous carbon as superior anode material for potassium-ion batteries. Adv. Energy Mater. **8**, 1802386 (2018). https://doi.org/10.1002/aenm.201802386
168. Chang, X.Q., Zhou, X.L., Ou, X.W., et al.: Ultrahigh nitrogen doping of carbon nanosheets for high capacity and long cycling potassium ion storage. Adv. Energy Mater. **9**, 1902672 (2019). https://doi.org/10.1002/aenm.201902672
169. Xie, F., Xu, Z., Guo, Z.Y., et al.: Hard carbons for sodium-ion batteries and beyond. Prog. Energy **2**, 042002 (2020). https://doi.org/10.1088/2516-1083/aba5f5
170. Zhang, Y., Li, L., Xiang, Y.E., et al.: High sulfur-doped hard carbon with advanced potassium storage capacity via a molten salt method. ACS Appl. Mater. Interfaces **12**, 30431–30437 (2020). https://doi.org/10.1021/acsami.0c07616
171. Wu, X., Chen, Y.L., Xing, Z., et al.: Advanced carbon-based anodes for potassium-ion batteries. Adv. Energy Mater. **9**, 1900343 (2019). https://doi.org/10.1002/aenm.201900343
172. Yuan, F., Li, Y.N., Zhang, D., et al.: A comprehensive review of carbon anode materials for potassium-ion batteries based on specific optimization strategies. Inorg. Chem. Front. **10**, 2547–2573 (2023). https://doi.org/10.1039/d3qi00056g
173. Wu, Z.R., Zou, J., Shabanian, S., et al.: The roles of electrolyte chemistry in hard carbon anode for potassium-ion batteries. Chem. Eng. J. **427**, 130972 (2022). https://doi.org/10.1016/j.cej.2021.130972
174. Katorova, N.S., Luchkin, S.Y., Rupasov, D.P., et al.: Origins of irreversible capacity loss in hard carbon negative electrodes for potassium-ion batteries. J. Chem. Phys. **152**, 194704 (2020). https://doi.org/10.1063/5.0003257
175. Jian, Z.L., Luo, W., Ji, X.L.: Carbon electrodes for K-ion batteries. J. Am. Chem. Soc. **137**, 11566–11569 (2015). https://doi.org/10.1021/jacs.5b06809
176. Nagmani, Tyagi, A., Verma, P., et al.: Effect of pore morphology on the enhanced potassium storage in hard carbon derived from polyvinyl chloride for K-ion batteries. Electrochim. Acta **464**, 142903 (2023). https://doi.org/10.1016/j.electacta.2023.142903
177. Nagmani, Verma, P., Puravankara, S.: Jute-fiber precursor-derived low-cost sustainable hard carbon with varying micro/mesoporosity and distinct storage mechanisms for sodium-ion and potassium-ion batteries. Langmuir **38**, 15703–15713 (2022). https://doi.org/10.1021/acs.langmuir.2c02575
178. Kim, H., Hyun, J.C., Kim, D.H., et al.: Revisiting lithium- and sodium-ion storage in hard carbon anodes. Adv. Mater. **35**, 2209128 (2023). https://doi.org/10.1002/adma.202209128
179. Huang, C.Y., Yin, J.Y., Shi, W.C., et al.: Recent advances of tailoring defects and pores in hard carbon for sodium storage. Mater. Today Energy **40**, 101501 (2024). https://doi.org/10.1016/j.mtener.2024.101501
180. Memarzadeh Lotfabad, E., Kalisvaart, P., Kohandehghan, A., et al.: Origin of non-SEI related coulombic efficiency loss in carbons tested against Na and Li. J. Mater. Chem. A **2**, 19685–19695 (2014). https://doi.org/10.1039/c4ta04995k
181. Tang, Z., Zhou, S.Y., Wu, P.F., et al.: Engineering surface oxygenated functionalities on commercial hard carbon toward superior sodium storage. Chem. Eng. J. **441**, 135899 (2022). https://doi.org/10.1016/j.cej.2022.135899
182. Matei Ghimbeu, C., Górka, J., Simone, V., et al.: Insights on the Na^+ ion storage mechanism in hard carbon: discrimination between the porosity, surface functional groups and defects. Nano Energy **44**, 327–335 (2018). https://doi.org/10.1016/j.nanoen.2017.12.013
183. Fan, L.L., Zhang, X., Fan, L.P., et al.: Boosting the high capacitance-controlled capacity of hard carbon by using surface oxygen functional groups for fast and stable sodium storage. ACS Appl. Energy Mater. **4**, 11436–11446 (2021). https://doi.org/10.1021/acsaem.1c02214
184. Li, Z.F., Ma, L., Surta, T.W., et al.: High capacity of hard carbon anode in Na-ion batteries unlocked by PO_x doping. ACS

Energy Lett. **1**, 395–401 (2016). https://doi.org/10.1021/acsenergylett.6b00172

185. Dong, Y., Zhang, S., Du, X., et al.: Boosting the electrical double-layer capacitance of graphene by self-doped defects through ball-milling. Adv. Funct. Mater. **29**, 1901127 (2019). https://doi.org/10.1002/adfm.201901127
186. Li, N., Wang, Y., Liu, L.S., et al.: "Self-doping" defect engineering in SnP_3@gamma-irradiated hard carbon anode for rechargeable sodium storage. J. Colloid Interface Sci. **592**, 279–290 (2021). https://doi.org/10.1016/j.jcis.2021.02.060
187. Mu, S.C., Tang, H.L., Qian, S.H., et al.: Hydrogen storage in carbon nanotubes modified by microwave plasma etching and Pd decoration. Carbon **44**, 762–767 (2006). https://doi.org/10.1016/j.carbon.2005.09.010
188. Tao, L., Wang, Q., Dou, S., et al.: Edge-rich and dopant-free graphene as a highly efficient metal-free electrocatalyst for the oxygen reduction reaction. Chem. Commun. **52**, 2764–2767 (2016). https://doi.org/10.1039/c5cc09173j
189. Li, Z.F., Chen, Y.C., Jian, Z.L., et al.: Highly defective hard carbon anode for Na-ion batteries by microwave heating. Meet. Abstr. , 446 (2018). https://doi.org/10.1149/ma2018-01/3/446
190. Zhao, X., Ding, Y., Xu, Q., et al.: Low-temperature growth of hard carbon with graphite crystal for sodium-ion storage with high initial coulombic efficiency: a general method. Adv. Energy Mater. **9**, 1803648 (2019). https://doi.org/10.1002/aenm.201803648
191. Li, X.W., Sun, J.Y., Zhao, W.X., et al.: Intergrowth of graphite-like crystals in hard carbon for highly reversible Na-ion storage. Adv. Funct. Mater. **32**, 2106980 (2022). https://doi.org/10.1002/adfm.202106980
192. Yu, X., Xin, L., Li, X.W., et al.: Completely crystalline carbon containing graphite-like crystal enables 99.5% initial coulombic efficiency for Na-ion batteries. Mater. Today **59**, 25–35 (2022). https://doi.org/10.1016/j.mattod.2022.07.013
193. Zhang, H.M., Zhang, W.F., Huang, F.Q.: Graphene inducing graphitization: towards a hard carbon anode with ultrahigh initial coulombic efficiency for sodium storage. Chem. Eng. J. **434**, 134503 (2022). https://doi.org/10.1016/j.cej.2022.134503
194. Zhao, J.H., He, X.X., Lai, W.H., et al.: Catalytic defect-repairing using manganese ions for hard carbon anode with high-capacity and high-initial-coulombic-efficiency in sodium-ion batteries. Adv. Energy Mater. **13**, 2300444 (2023). https://doi.org/10.1002/aenm.202300444
195. Sun, D., Luo, B., Wang, H.Y., et al.: Engineering the trap effect of residual oxygen atoms and defects in hard carbon anode towards high initial coulombic efficiency. Nano Energy **64**, 103937 (2019). https://doi.org/10.1016/j.nanoen.2019.103937
196. Hunter, R.D., Ramírez-Rico, J., Schnepp, Z.: Iron-catalyzed graphitization for the synthesis of nanostructured graphitic carbons. J. Mater. Chem. A **10**, 4489–4516 (2022). https://doi.org/10.1039/d1ta09654k
197. Chen, J.F., Feng, J.M., Dong, L., et al.: Nanoporous coal via Ni-catalytic graphitization as anode materials for potassium ion battery. J. Electroanal. Chem. **862**, 113902 (2020). https://doi.org/10.1016/j.jelechem.2020.113902
198. Gomez-Martin, A., Schnepp, Z., Ramirez-Rico, J.: Structural evolution in iron-catalyzed graphitization of hard carbons. Chem. Mat. **33**, 3087–3097 (2021). https://doi.org/10.1021/acs.chemmater.0c04385
199. Deng, M.X., Dong, W.J., Huang, F.Q.: High initial coulombic efficiency hard carbon anodes enabled by facile surface annealing engineering. Chem. **18**, e202300210 (2023). https://doi.org/10.1002/asia.202300210
200. Zhang, X., Dong, X.L., Qiu, X., et al.: Extended low-voltage plateau capacity of hard carbon spheres anode for sodium ion batteries. J. Power Sources **476**, 228550 (2020). https://doi.org/10.1016/j.jpowsour.2020.228550
201. Roy Goswami, S., Sudhakaran Nair, S., Wang, S., et al.: Recent progress on starch maleate/polylactic acid blends for compostable food packaging applications. ACS Sustainable Chem. Eng. **10**, 3–15 (2022). https://doi.org/10.1021/acssuschemeng.1c04940
202. Wang, J., Yan, L., Liu, B.H., et al.: A solvothermal pre-oxidation strategy converting pitch from soft carbon to hard carbon for enhanced sodium storage. Chin. Chemical Lett. **34**, 107526 (2023). https://doi.org/10.1016/j.cclet.2022.05.040
203. Xu, R., Yi, Z.L., Song, M.X., et al.: Boosting sodium storage performance of hard carbons by regulating oxygen functionalities of the cross-linked asphalt precursor. Carbon **206**, 94–104 (2023). https://doi.org/10.1016/j.carbon.2023.02.004
204. Li, F.Y., Tao, H.C., Yang, X.L.: Adjusting the state of pitch anode for effective oxidation with suppressed graphitization and enhanced Na storage performances. Ionics **28**, 5141–5151 (2022). https://doi.org/10.1007/s11581-022-04734-w
205. Zhang, H.M., Ming, H., Zhang, W.F., et al.: Coupled carbonization strategy toward advanced hard carbon for high-energy sodium-ion battery. ACS Appl. Mater. Interfaces **9**, 23766–23774 (2017). https://doi.org/10.1021/acsami.7b05687
206. Xie, F., Xu, Z., Jensen, A.C.S., et al.: Hard-soft carbon composite anodes with synergistic sodium storage performance. Adv. Funct. Mater. **29**, 1901072 (2019). https://doi.org/10.1002/adfm.201970164
207. Zhao, C.L., Wang, Q.D., Lu, Y.X., et al.: High-temperature treatment induced carbon anode with ultrahigh Na storage capacity at low-voltage plateau. Sci. Bull. **63**, 1125–1129 (2018). https://doi.org/10.1016/j.scib.2018.07.018
208. Kano, A., Okano, T., Hojo, N., et al.: New carbon materials with large closed pore volume for the anode of high energy Na-ion batteries. Meet. Abstr. **MA2016–02**, 668 (2016). https://doi.org/10.1149/ma2016-02/5/668
209. Meng, Q.S., Lu, Y.X., Ding, F.X., et al.: Tuning the closed pore structure of hard carbons with the highest Na storage capacity. ACS Energy Lett. **4**, 2608–2612 (2019). https://doi.org/10.1021/acsenergylett.9b01900
210. Wang, K.F., Sun, F., Wang, H., et al.: Altering thermal transformation pathway to create closed pores in coal-derived hard carbon and boosting of Na^+ plateau storage for high-performance sodium-ion battery and sodium-ion capacitor. Adv. Funct. Mater. **32**, 2203725 (2022). https://doi.org/10.1002/adfm.202203725
211. Li, Q., Liu, X.S., Tao, Y., et al.: Sieving carbons promise practical anodes with extensible low-potential plateaus for sodium batteries. Natl. Sci. Rev. **9**, nwac084 (2022). https://doi.org/10.1093/nsr/nwac084
212. Zhang, S.H., Sun, N., Li, X., et al.: Closed pore engineering of activated carbon enabled by waste mask for superior sodium storage. Energy Storage Mater. **66**, 103183 (2024). https://doi.org/10.1016/j.ensm.2024.103183
213. Chen, X.Y., Sawut, N., Chen, K.A., et al.: Filling carbon: A microstructure-engineered hard carbon for efficient alkali metal ion storage. Energy Environ. Sci. **16**, 4041–4053 (2023). https://doi.org/10.1039/d3ee01154b
214. Wang, C.Y., Liu, H.Y., Duan, H.C., et al.: 3D atomic imaging of low-coordinated active sites in solid-state dealloyed hierarchical nanoporous gold. J. Mater. Chem. A **9**, 25513–25521 (2021). https://doi.org/10.1039/d1ta05942d
215. Zhen, Y.C., Chen, Y., Li, F., et al.: Ultrafast synthesis of hard carbon anodes for sodium-ion batteries. Proc. Natl. Acad. Sci. U.S.A. **118**, e2111119118 (2021). https://doi.org/10.1073/pnas.2111119118
216. Zhang, F., Yao, Y.G., Wan, J.Y., et al.: High temperature carbonized grass as a high performance sodium ion battery anode. ACS

Appl. Mater. Interfaces **9**, 391–397 (2017). https://doi.org/10.1021/acsami.6b12542

217. Zhang, B., Deschamps, M., Ammar, M.R., et al.: Laser synthesis of hard carbon for anodes in Na-ion battery. Adv. Mater. Technol. **2**, 1600227 (2017). https://doi.org/10.1002/admt.201600227
218. Ji, T.Y., Liu, X.X., Sheng, D.W., et al.: Machine learning-assisted thermomechanical coupling fabrication of hard carbon for sodium-ion batteries. Energy Storage Mater. **71**, 103563 (2024). https://doi.org/10.1016/j.ensm.2024.103563
219. Song, Z.Q., Di, M.X., Zhang, X.Y., et al.: Nanoconfined strategy optimizing hard carbon for robust sodium storage. Adv. Energy Mater., 2401763 (2024). https://doi.org/10.1002/aenm.202401763
220. Sun, D., Zhao, L., Sun, P.L., et al.: Rationally regulating closed pore structures by pitch coating to boost sodium storage performance of hard carbon in low-voltage platforms. Adv. Funct. Mater., 2403642 (2024). https://doi.org/10.1002/adfm.202403642
221. Zhao, X.B., Shi, P., Wang, H.B., et al.: Unlocking plateau capacity with versatile precursor crosslinking for carbon anodes in Na-ion batteries. Energy Storage Mater. **70**, 103543 (2024). https://doi.org/10.1016/j.ensm.2024.103543
222. Qiu, C., Li, A., Qiu, D.P., et al.: One-step construction of closed pores enabling high plateau capacity hard carbon anodes for sodium-ion batteries: closed-pore formation and energy storage mechanisms. ACS Nano **18**, 11941–11954 (2024). https://doi.org/10.1021/acsnano.4c02046

Junjie Liu is now studying for the master's degree at Xiamen University, China, under the supervision of Prof. Jinbao Zhao and Prof. Li Zhang. His research interests focus on advanced carbon materials for sodium-ion batteries.

Ling Huang is now studying for the master's degree at Xiamen University of Chemistry and Chemical Engineering, China, under the supervision of Prof. Li Zhang. Her research interests focus on modifications of carbon materials for lithium-ion batteries.

Huiqun Wang is now studying for the master's degree at Xiamen University, China, under the supervision of Prof. Li Zhang. Her research interests focus on improving high specific energy anode materials for lithium batteries.

Liyuan Sha is now studying for the master's degree at Xiamen University, China, under the supervision of Prof. Li Zhang. His research interests focus on carbon-based anode material for lithium-/sodium-ion batteries.

Miao Liu is currently working as Postdoctoral Associate in the Department of Chemistry and Chemical Engineering at Xiamen University. She received B.S. degree and M.S. degree from the Xi'an Technological University and the South China Normal University in 2016 and 2019, respectively. She obtained Ph.D. degree from Hunan university in 2023. Her research interests lie in the development and design of novel materials and novel electrolytes in energy storage and conversion devices, such as low-temperature sodium-ion batteries and potassium-ion batteries.

Zhefei Sun received his Bachelor's degree at the College of Materials Science and Engineering from Nanjing Tech University in 2020. He is currently a Ph.D. candidate in the State Key Laboratory of Physical Chemistry of Solid Surfaces, College of Materials, at Xiamen University, under the supervision of Prof. Qiaobao Zhang. His research interests focus on in situ TEM characterization of high-capacity electrode materials and solid-state electrolytes for alkali metal-ion batteries and solid-state batteries.

Jiawei Gu is now studying for the master's degree at Xiamen University of Chemistry and Chemical Engineering, China, under the supervision of Prof. Li Zhang. His research interests focus on high-performance anode materials for sodium/potassium-ion batteries.

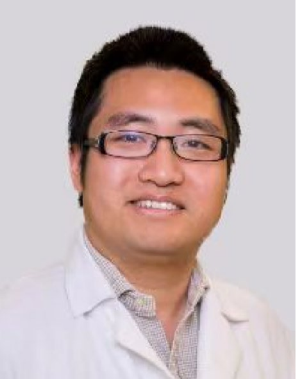

Haodong Liu worked as a project scientist at UC San Diego, where he earned his Ph.D. degree in Nanoengineering. He is an expert in a variety of electrochemical systems and in the design, synthesis, processing, and characterization of advanced electrode materials for Li-ion batteries and novel electrolytes for Li-metal batteries. He has more than 120 papers with an *H*-index of 53 and been recognized as a highly cited researcher from 2023 by Clarivate.

Jinbao Zhao is currently a professor in the State Key Laboratory of Physical Chemistry of Solid Surfaces, College of Chemistry and Chemical Engineering, at Xiamen University, China. He obtained his Ph.D. degree from the Kyoto University in 1996. His current research focuses on high-performance lithium-ion batteries, green and efficient fuel cells and other chemical energy storage system related research work from the foundation and application of both sides.

Qiaobao Zhang is currently a professor in the State Key Laboratory of Physical Chemistry of Solid Surfaces, College of Materials, at Xiamen University, China. He obtained his Ph.D. degree from the City University of Hong Kong in 2016. His current research focuses on the fundamental issues relevant to energy storage systems including Li/Na/K/Zn-ion batteries and solid-state batteries, especially on pivotal electrode materials, interfacial properties, and the development of in situ characterization techniques. He has published one authored book and more than 200 papers with an *H*-index of 66 and been recognized as a highly cited researcher from 2022 by Clarivate.

Li Zhang is currently a professor in the State Key Laboratory of Physical Chemistry of Solid Surfaces, College of Chemistry and Chemical Engineering, at Xiamen University, China. He obtained his B.S. and Ph.D. degrees from Xiamen University in 2003 and 2008, respectively. His current research focuses on the mass production technology of advanced battery materials, organic electrode materials, all-solid-state electrolytes and transient thermal synthesis. He has published more than 80 papers as a corresponding author.